UC San Diego

UC San Diego Electronic Theses and Dissertations

Title

Molecular and Cellular Engineering to Guide CAR T Cell Therapy through the Immunosuppressive Tumor Microenvironment

Permalink

https://escholarship.org/uc/item/2v29x1p9

Author

Man, Chi-Wei

Publication Date

2022

Peer reviewed|Thesis/dissertation

eScholarship.org Powered by the California Digital Library
University of California

UNIVERSITY OF CALIFORNIA SAN DIEGO

Molecular and Cellular Engineering to Guide CAR T Cell Therapy through the Immunosuppressive Tumor Microenvironment

A Dissertation submitted in partial satisfaction of the requirements
for the degree Doctor of Philosophy

in

Biochemistry and Molecular Biophysics

by

Chi-Wei Man

Committee in charge:

Professor Yingxiao Wang, Chair
Professor Brian Zid, Co-chair
Professor Andrew Kummel
Professor Wei Wang
Professor Jin Zhang

2022

Copyright

Chi-Wei Man, 2022

All rights reserved.

The Dissertation of Chi-Wei Man is approved, and it is acceptable in quality and form for publication on microfilm and electronically.

University of California San Diego

2022

DEDICATION

To my beloved family and friends

TABLE OF CONTENTS

LIST OF FIGURES

ACKNOWLEDGEMENTS

First and foremost, I would like to acknowledge my advisor, Professor Yingxiao (Peter) Wang who has provided unwavering support throughout my graduate school journey. Without Professor Wang's unshakable optimism, the projects described in this dissertation certainly would not have come to fruition. Despite his busy schedule, Professor Wang always makes time for his students, which is a trait that I greatly admire and appreciate. I would also like to acknowledge my committee members Drs. Andrew Kummel, Wei Wang, Jin Zhang, and Brian Zid for their advice and feedback.

During my graduate school tenure, I was incredibly fortunate to have worked alongside an inspirational group of colleagues. To my mentees Anthony Mamaril and Matthew Hashimoto, thanks so much for choosing to work with me throughout your entire undergraduate studies. Your aptitude, maturity, and positivity were advanced far beyond your years. I would like to thank Dr. Shaoying (Kathy) Lu for her kind help and suggestions. I would like to thank Drs. Qin Peng, Praopim Limsakul, and Pengzhi Wang for being my mentors and teaching me fundamental lab techniques when I first joined the lab. I would like to thank Linshan Zhu for being a great friend, mentee, and mentor all at the same time. To my past labmates Dr. Charlotte Hepples, Ali Zamat, Jeyan Thangaraj, Dr. Reed Harrison, Dr. Yijia Pan, Ya Gong, Jiaming Wei, Xin Wang, Yiwen Shi, and many others, thank you for being great friends and for creating such a positive environment in the lab. To my current labmates Dr. Chi Woo Yoon, Dr. Ziliang Huang, Dr. Yiqian Wu, Dr. Longwei Liu, Dr. Yuan Zhou, Phuong Ho, Jenny Qu, Katie Cui, and Tianze Guo, I wish you all the best of luck for your new adventure in Los Angeles.

Last but not least, I would like to thank my family and friends for supporting me through everything. Specifically, I would like to thank my wife and beset friend Lia Chan-Man for her unconditional support, especially all those late nights and weekends of driving me to and from the lab. Finally, I would also like to thank the ARCS foundation and Interfaces training grant for their financial support.

Because portions of this dissertation have been published or will be published in various journals, I would like to acknowledge each of the authors for their contributions.

Chapter 2, in part has been submitted for publication of the material as it may appear in ACS Central Science. Man, Chi-Wei; Zhu, Linshan; Harrison, Reed; Peng, Qin; Limsakul, Praopim; Hashimoto, Matthew; Mamaril, Anthony; Xu, Hongquan; Wang, Yingxiao. "Engineering a PD-L1-targeting Monobody via Directed Evolution for SynNotch-Gated Cancer Immunotherapy". The dissertation author was the primary researcher and author of this paper.

Chapter 3, in part has been submitted for publication of the material as it may appear in ACS Central Science. Man, Chi-Wei; Zhu, Linshan; Harrison, Reed; Peng, Qin; Limsakul, Praopim; Hashimoto, Matthew; Mamaril, Anthony; Xu, Hongquan; Wang, Yingxiao. "Engineering a PD-L1-targeting Monobody via Directed Evolution for SynNotch-Gated Cancer Immunotherapy". The dissertation author was the primary researcher and author of this paper.

Chapter 4, in full is currently being prepared for submission of the material. Man, Chi-Wei; Wu, Yiqian; Liu, Longwei; Hashimoto, Matthew; Mamaril, Anthony; Wang, Yingxiao. "Inducible Cis Activation Drives CAR T Cell Function Against Heterogeneous and Antigen

Negative Tumors". The dissertation author was the primary researcher and author of this paper.

Chi-Wei Man

La Jolla, CA

November 2022

VITA

2015 Bachelor of Arts in Biological Chemistry, University of Pennsylvania

Bachelor of Science and Engineering in Chemical and Biomolecular Engineering, University of Pennsylvania

2017 Master of Science in Chemistry, University of California San Diego

2022 Doctor of Philosophy in Biochemistry and Molecular Biophysics, University of California San Diego

ABSTRACT OF THE DISSERTATION

Molecular and Cellular Engineering to Guide CAR T Cell Therapy through the Immunosuppressive Tumor Microenvironment

by

Chi-Wei Man

Doctor of Philosophy in Biochemistry and Molecular Biophysics

University of California San Diego, 2022

Professor Yingxiao Wang, Chair

Chimeric Antigen Receptor (CAR) T cell therapy is a revolutionary treatment option for cancer therapy, demonstrating widespread clinical success in treating hematological malignancies such as acute lymphoblastic leukemia and certain lymphomas. Despite its widespread success treating hematological malignancies, CAR T cells still struggle to treat

solid tumors. One reason for this is the immunosuppressive tumor microenvironment. Expressed in certain tumors, Programmed Death-Ligand 1 (PD-L1) actively suppresses T cell activation and function. To both neutralize this immunoinhibitory effect and eliminate tumor cells, I used yeast display mediated directed evolution to engineer PDbody, derived from the monobody scaffold, to bind to PD-L1. I then employed PDbody as a SynNotch-gated CAR receptor to eliminate a triple-negative breast cancer model *in vitro* and slow tumor growth *in vivo*. CAR T cell therapy can also fail when tumors do not homogenously express the CAR target antigen. To combat this problem, I developed heat-inducible Cis-activated CAR (CisCAR) to allow CAR T cells to self-present their target antigen. I then used CisCAR to eliminate antigen-negative leukemic and breast cancer cells *in vitro*, demonstrating the universal applicability of this treatment strategy. Overall, this dissertation presents new methods that enhance CAR T cell therapy, enabling them to more effectively target a wider range of diseases.

CHAPTER 1

INTRODUCTION

1.1: CAR T CELLS: A PARADIGM SHIFT FOR CANCER TREATMENT

Cancer is one of the top causes of death worldwide and accordingly, needs no lengthy introduction. The most common treatment methods for cancer are chemotherapy, surgery, and radiation therapy. While these methods have demonstrated efficacy and are still widely used, a vastly different type of treatment demonstrated clinical success in the early 2010's and would later give rise to a whole new field of translational medicine; this was Chimeric Antigen Receptor T (CAR T) cell therapy. Starting from 2010, CAR T cell therapy was first used to treat patients with B cell malignancies to promising success[1–4]. Impressively in one clinical trial of 30 patients with acute lymphoblastic leukemia, CAR T cell therapy caused complete remission in 90% of patients[5]. Due to the early success of these clinical trials and others like them, the FDA was quick to approve the first CAR T cell therapy in 2017[6–8]. Interest in the potential of CAR T cell therapy has since risen dramatically. As of 2021, there are over 500 ongoing worldwide clinical trials involving CAR T cell therapy for the treatment of cancer[9].

CAR T cell therapy is a "living" therapy and the first gene therapy to be FDA-approved. It is autologous, which means that it is derived from the patient's own cells to avoid problems associated with allogeneic transplantation such as graft versus host disease (Figure 1.1). After removal of a portion of the patient's peripheral blood cells, T cells are isolated through the process of leukapheresis. After extraction, T cells are genetically modified to express CAR with either viral or non-viral methods. CAR T cells are then expanded *ex vivo* through CD3/CD28 stimulation. Finally, these CAR T cells are then infused back into the patient for disease treatment[10]. Overall, this manufacturing process operates in the timescale of days to weeks.

Research is actively being performed to shorten the turnaround time for CAR T cell manufacturing[11].

1.2: PARTS AND FUNCTIONS OF CAR RECEPTOR

While there are many active areas of research within the CAR field, this dissertation focuses on the engineering of CAR itself. CAR is composed of five domains: (1) an extracellular ligand-binding domain, (2) a hinge domain, (3) a transmembrane domain, (4) a co-stimulatory domain(s), and (5) a CD3ζ signaling domain (Figure 1.2). The number of co-stimulatory domains determines the CAR generation. First generation CARs have no co-stimulatory domain, second generation CARs have exactly one co-stimulatory domain, and third generation CARs have more than one co-stimulatory domain. First generation CARs lacked efficacy, but future generations were able to demonstrate higher levels of cytotoxicity.

The extracellular ligand-binding domain directs the CAR T cell to kill tumor cells expressing a specific target antigen. For their ligand-binding domains, clinically-approved CARs all contain variable light (V_L) and variable heavy (V_H) domains derived from antibodies (scFvs) targeting either the CD19 or B cell maturation antigen (BCMA)[12]. While scFvs are widely used as the ligand-binding domain, structural and aggregation events have been known to occur[13–15], which is why research has focused on replacing these with alternative single-domain regions[16–18]. Target antigen selection is an especially important decision because non-uniform target antigen expression on tumor cells can lead to incomplete killing, and target antigen expression on healthy tissue can lead to off-target cytotoxicity.

Moving intracellularly along the CAR, the hinge region connects the ligand-binding domain to the transmembrane region of the CAR. Typically, this region is derived from either

CD8 or CD28. The hinge provides flexibility to the extracellular ligand-binding domain, allowing it to bind to its epitope. Varying the hinge domain can affect cytokine production levels and alter activation-induced cell death[19]. The transmembrane domain, in addition to connecting the intracellular and extracellular regions of CAR, can also affect whether CAR dimerizes or trimerizes[20,21]. Similar to the hinge region, the transmembrane domain is usually derived from either CD8 or CD28.

The co-stimulation domain provides additional activation power to the CAR T cell, enhancing its killing capabilities. As mentioned previously, first generation CARs lacked this domain and were ineffective in the clinic. Thus, every FDA-approved CAR product to date, has at least one co-stimulatory domain. Although CD28[22] and 4-1BB[23] are the most commonly used, OX40[24], CD27[25], and inducible T cell co-stimulator (ICOS)[26] domains have also been used in CARs as co-stimulators. Interchanging these co-stimulation domains can change expansion rates and durability of CAR T cells, as well as alter their differentiation into different T cell subtypes[27–29].

Lastly, the CD3ζ signaling domain is the most intracellular component of the CAR and responsible for activating canonical T cell killing pathways upon receptor engagement[30]. Containing three immunoreceptor tyrosine-based activation motifs (ITAMs), the CD3ζ domain becomes phosphorylated when CAR recognizes its target antigen[31]. Phosphorylation of CD3ζ recruits Zeta-chain Associated Protein kinase 70 (ZAP70), which then initiates downstream signaling events that trigger the T cell effector response. This response includes increased proliferation, cytokine release, and cytotoxic killing through the release of granzyme and perforin. Thus, CAR is a highly modular protein with interchangeable and modifiable domains.

Indeed, the modularity of CAR provides a tunable platform to treat different disease types even beyond cancer[32].

1.3: OBSTACLES AND LIMITATIONS OF CAR T CELL THERAPY

Despite the remarkable success of CAR T cell therapy with B cell malignancies, it has struggled to translate this success to other cancer types, especially solid tumor cancers. Currently, all FDA-approved CAR T cell therapies target either CD19 or BCMA, both of which are expressed on B cells. Due to their intrinsic design, CAR T cells indiscriminately target and kill cells expressing their target antigen, whether they be tumor or bystander cells. As such, B cell aplasia is an unavoidable side effect of CAR T cell treatment. Fortunately, this is clinically manageable with immunoglobulin transfusion[33]. Unfortunately, this does point to a worrying trend. Tumor cells are essentially "haywire" healthy cells. In an ideal scenario, all tumor cells should homogenously express the CAR target antigen while healthy cells should completely lack target antigen expression; however, since tumor cells are derived from healthy cells, it is unlikely that these antigen targets exist. Thus, off-target toxicity from CAR T cell therapy is quite difficult to avoid.

The two class toxicities of CAR T cell therapy are Cytokine Release Syndrome (CRS) and neurotoxicity, both of which can be lethal if too extreme. CRS is caused by an overactive immune response in which CAR T cells and other immune cells secrete dangerous levels of cytokines[34]. Symptoms of CRS usually include fever, hypotension, and respiratory insufficiency. CRS is typically treated with anti-IL-6 receptor-α (IL-6Rα) antibody (tocilizumab), Tumor Necrosis Factor (TNF) inhibitor (etanercept), or corticosteroids[34]. The cause of neurotoxicity is still largely unknown; however, similar with CRS, symptoms include elevated levels of

inflammatory cytokines[35]. Symptoms of neurotoxicity include seizures, delirium, temporary working memory loss, and in worst case scenarios, cerebral edema[36]. In one study, it was suggested that neurotoxicity was due to target antigen presence in the brain[37].

Accordingly, selection of target antigen seems to be the largest hindrance to the expansion of CAR T cell therapy to other types of cancers. Expression of target antigen by healthy tissue can lead to on-target off-tumor toxicity (Figure 1.3 Top Right). In patients treated with melanoma antigen recognized by T cells 1 (MART1)-targeting T cells, patients experienced on-target off-tumor toxicity of healthy melanocytes, resulting in damage to the skin, eyes and ears[38]. If the ligand-binding domain of CAR is non-specific, patient death can even occur. In patients treated with MAGE-A3-targeting cells, MAGE-A12 expression in the brain, and titin expression in the myocardium caused patient fatalities[39,40]. On the other end of the spectrum, if tumor cells do not uniformly express the target antigen, antigen-negative tumor cells are spared from CAR T cell killing. Even in the case of tumors that uniformly express the target antigen, their rapid mutation rate can in some cases eliminate expression of the target antigen, a phenomenon known as tumor antigen escape[41] (Figure 1.3 Bottom Left). Antigen escape has been observed in T cell therapies with various antigen targets[5,42].

The local immunosuppressive tumor microenvironment is another obstacle to the expansion of CAR T cell therapy (Figure 1.3 Bottom Right), especially when targeting solid tumors. Immunosuppression is a necessary feature for a healthy immune system because it acts as a negative feedback regulator to keep immune response mediated inflammation in check; however, tumors with increased immunosuppression possess a survival advantage, which is why oftentimes the local tumor microenvironment is populated with highly suppressive immune cells like regulatory T cells (T_{reg} cells), myeloid-derived suppressor cells (MDSCs), and tumor-

associated macrophages (TAMs)[43]. In addition, tumors often upregulate immune checkpoint inhibitors which cause T cell exhaustion, a hypofunctional T cell state usually caused by overstimulation[44]. Of these immune checkpoint inhibitors, programmed-death (PD-1) receptor and its target ligand programmed death-ligand 1 (PD-L1)[45] have received tremendous attention as therapeutic targets. Upon activation, T cells express PD-1 which then binds to PD-L1, causing T cell exhaustion. Thus, researchers have found that targeting of the PD-1/PD-L1 axis, for example through antibody administration, can restore immune cell function[46]. One promising strategy is to use immune checkpoint in conjunction with CD19 CAR T cell therapy, a strategy known as combination therapy. This is already being explored in several clinical trials[47–50].

1.4: SCOPE OF DISSERTATION

CARs are a revolutionary new treatment paradigm, demonstrating efficacy even against relapsed and refractory cancers. While CAR T cell therapy has had great success against hematological malignancies, it has struggled against other cancer types, especially solid tumors. Two major reasons for this are (1) the local immunosuppressive tumor microenvironment and (2) the selection of a suitable antigen target. The ideal antigen target needs to meet two criteria: (1) it needs to be uniformly expressed across the whole tumor population and (2) it needs to be absent from healthy tissue. Even if these criteria are met, tumors can still evade immune detection through a process called antigen escape. Fortunately, the CAR platform is extremely tunable, so it can be modified to overcome these obstacles. Accordingly, this dissertation seeks to engineer CAR to overcome resistance to treatment, which should help to expand CAR T cell treatment to other cancer types.

In chapter one (Directed evolution of PDbody, a PD-L1-targeting monobody), I utilized yeast-display mediated directed evolution to engineer the monobody scaffold to bind to the immune checkpoint inhibitor PD-L1. I used site-saturated mutagenesis to generate DNA libraries of the FG and BC binding loop regions then used multiple rounds of Fluorescence Activated Cell Sorting (FACS) to screen for the strongest PD-L1 binders. This screening process yielded PDbody, an enhanced PD-L1 binding monobody.

In chapter two (Application of CD19-SynNotch PDbody-CAR to target tumor cells), I applied PDbody as the extracellular ligand-binding domain of CAR to target tumor cells overexpressing PD-L1. Not only does PDbody-CAR eradicate tumor cells, but it suppresses immune checkpoint inhibition by acting as a dominant negative receptor. One particular problem of targeting PD-L1 is that it is expressed at low levels in healthy tissues. To mitigate on-target off-tumor toxicity, the expression of PDbody-CAR was controlled by CD19-SynNotch. This provided an AND-gate to T cell cytotoxicity to limit CAR T cell killing to just the tumor site. Efficacy of CD19-SynNotch PDbody-CAR was demonstrated *in vitro* and *in vivo*.

In chapter three (Inducible CisCAR to overcome antigen escape), I developed a controllable universal method to trigger CAR T cell activation and killing. During CD19-CAR treatment, tumors can acquire mutations that cause target antigen loss, a phenomenon known as antigen escape, which is why cancers have been observed to relapse without detectable CD19. Thus, I engineered CD19-CAR T cells with a heat shock inducible CD19 ligand, which allowed them to self-activate when heat shocked, a cell therapy I named ‘CisCAR”. I then demonstrated that CisCAR can significantly improve *in vitro* killing in antigen escape models of multiple tumor types.

1.5: FIGURES

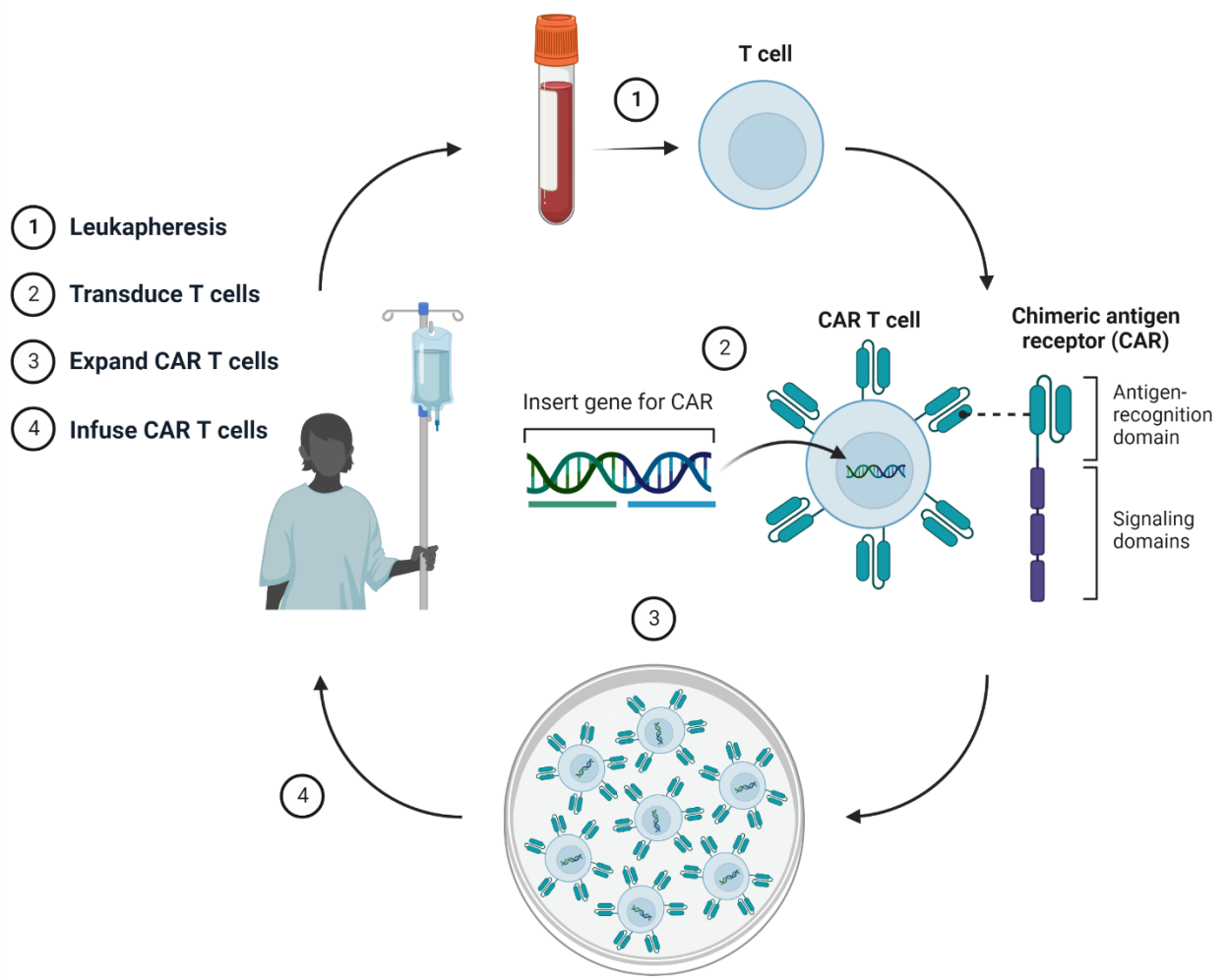

Figure 1.1: Manufacturing process for CAR T cell therapy

Workflow for CAR T cell treatment. Peripheral blood is extracted from the patient then (1) T cells are separated from the blood through the process of leukapheresis. (2) T cells are then genetically modified to express CAR. (3) T cells are then expanded through the process of *ex vivo* culture. (4) T cells are finally reintroduced into the patient for disease treatment.

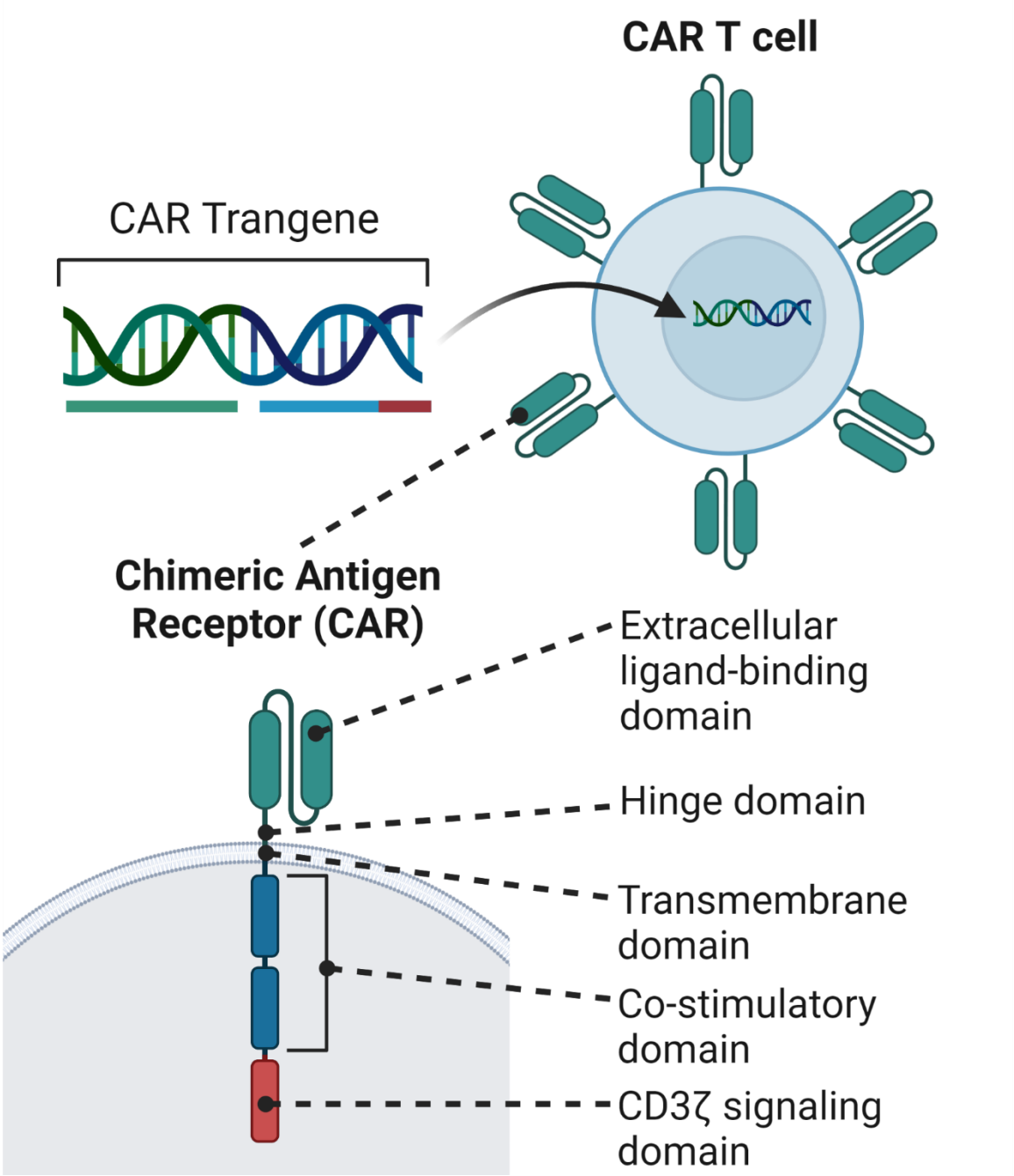

Figure 1.2: CAR parts and function

CAR is introduced through genetic modification of T cells. This can occur through viral or non-viral methods. The domains of standard CAR are shown above. From proximal to distal, the domains are as follows: (1) Extracellular ligand-binding domain, (2) Hinge domain, (3) Transmembrane domain, (4) Co-stimulatory domain, and (5) CD3ζ signaling domain.

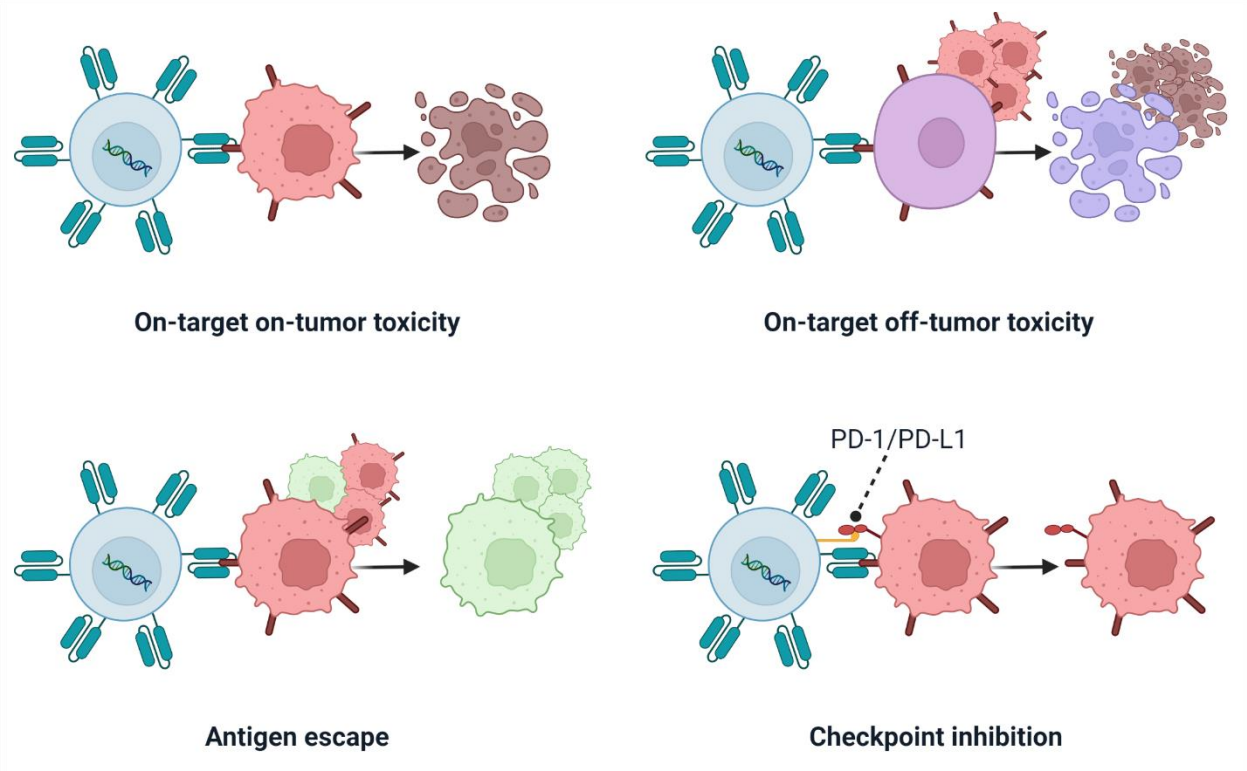

Figure 1.3: Resistance to CAR T cell therapy

A few obstacles to the intended application of CAR T cell therapy (Top Left) are shown above. On-target off-tumor toxicity occurs when the target antigen is present in healthy cells (Top Right). This leads to unintended collateral damage of healthy tissues. Antigen escape occurs when tumor cells lose expression of the target antigen (Bottom Left). This can lead to antigen-negative cancer relapse. Checkpoint inhibition occurs when T cells' immunosuppressive signaling pathways are triggered, for example through PD-1/PD-L1 signaling (Bottom Right). This can lead to T cell exhaustion.

ACKNOWLEDGEMENTS

The figures in this chapter were created using BioRender. Figure 1.1 was adapted from "CAR T Cell Therapy Overview", by BioRender.com (2022). Figure 1.2 was adapted from "Chimeric Antigen Receptor (CAR)", by BioRender.com (2022). Figure 1.1 and 1.2 were retrieved from https://app.biorender.com/biorender-templates. Figure 1.3 was also created with Biorender.com

REFERENCES

1. Kochenderfer, J. N., Wilson, W. H., Janik, J. E., Dudley, M. E., Stetler-Stevenson, M., Feldman, S. A., Maric, I., Raffeld, M., Nathan, D. A. N., Lanier, B. J., Morgan, R. A. & Rosenberg, S. A. Eradication of B-lineage cells and regression of lymphoma in a patient treated with autologous T cells genetically engineered to recognize CD19. *Blood* **116**, 4099–4102 (2010).

2. Porter, D. L., Levine, B. L., Kalos, M., Bagg, A. & June, C. H. Chimeric Antigen Receptor–Modified T Cells in Chronic Lymphoid Leukemia. *New England Journal of Medicine* vol. 365 725–733 at https://doi.org/10.1056/nejmoa1103849 (2011).

3. Brentjens, R. J., Davila, M. L., Riviere, I., Park, J., Wang, X., Cowell, L. G., Bartido, S., Stefanski, J., Taylor, C., Olszewska, M., Borquez-Ojeda, O., Qu, J., Wasielewska, T., He, Q., Bernal, Y., Rijo, I. V., Hedvat, C., Kobos, R., Curran, K., *et al.* CD19-targeted T cells rapidly induce molecular remissions in adults with chemotherapy-refractory acute lymphoblastic leukemia. *Sci. Transl. Med.* **5**, (2013).

4. Grupp, S. A., Kalos, M., Barrett, D., Aplenc, R., Porter, D. L., Rheingold, S. R., Teachey, D. T., Chew, A., Hauck, B., Wright, J. F., Milone, M. C., Levine, B. L. & June, C. H. Chimeric Antigen Receptor–Modified T Cells for Acute Lymphoid Leukemia. *N. Engl. J. Med.* **368**, 1509–1518 (2013).

5. Maude, S. L., Frey, N., Shaw, P. A., Aplenc, R., Barrett, D. M., Bunin, N. J., Chew, A., Gonzalez, V. E., Zheng, Z., Lacey, S. F., Mahnke, Y. D., Melenhorst, J. J., Rheingold, S. R., Shen, A., Teachey, D. T., Levine, B. L., June, C. H., Porter, D. L. & Grupp, S. A. Chimeric Antigen Receptor T Cells for Sustained Remissions in Leukemia. *N. Engl. J. Med.* **371**, 1507–1517 (2014).

6. Mullard, A. FDA approves first CAR T therapy. *Nat. Rev. Drug Discov.* **16**, 669 (2017).

7. Maude, S. L., Laetsch, T. W., Buechner, J., Rives, S., Boyer, M., Bittencourt, H., Bader, P., Verneris, M. R., Stefanski, H. E., Myers, G. D., Qayed, M., De Moerloose, B.,

Hiramatsu, H., Schlis, K., Davis, K. L., Martin, P. L., Nemecek, E. R., Yanik, G. A., Peters, C., *et al.* Tisagenlecleucel in Children and Young Adults with B-Cell Lymphoblastic Leukemia. *N. Engl. J. Med.* **378**, 439–448 (2018).

8. Neelapu, S. S., Locke, F. L., Bartlett, N. L., Lekakis, L. J., Miklos, D. B., Jacobson, C. A., Braunschweig, I., Oluwole, O. O., Siddiqi, T., Lin, Y., Timmerman, J. M., Stiff, P. J., Friedberg, J. W., Flinn, I. W., Goy, A., Hill, B. T., Smith, M. R., Deol, A., Farooq, U., *et al.* Axicabtagene Ciloleucel CAR T-Cell Therapy in Refractory Large B-Cell Lymphoma. *New England Journal of Medicine* vol. 377 2531–2544 at https://doi.org/10.1056/nejmoa1707447 (2017).

9. Albinger, N., Hartmann, J. & Ullrich, E. Current status and perspective of CAR-T and CAR-NK cell therapy trials in Germany. *Gene Ther.* **28**, 513–527 (2021).

10. Larson, R. C. & Maus, M. V. Recent advances and discoveries in the mechanisms and functions of CAR T cells. *Nature Reviews Cancer* vol. 21 145–161 at https://doi.org/10.1038/s41568-020-00323-z (2021).

11. Ghassemi, S., Durgin, J. S., Nunez-Cruz, S., Patel, J., Leferovich, J., Pinzone, M., Shen, F., Cummins, K. D., Plesa, G., Cantu, V. A., Reddy, S., Bushman, F. D., Gill, S. I., O'Doherty, U., O'Connor, R. S. & Milone, M. C. Rapid manufacturing of non-activated potent CAR T cells. *Nat. Biomed. Eng.* **6**, 118–128 (2022).

12. OHSU Knight Cancer Institute. CAR T-Cell Therapy for Cancer | OHSU. https://www.ohsu.edu/knight-cancer-institute/car-t-cell-therapy-cancer (2021).

13. Schrum, D. G. and A. G. Strategies to stabilize compact folding and minimize aggregation of antibody-based fragments. *Adv Biosci Biotechnol* **23**, 1–7 (2012).

14. Long, A. H., Haso, W. M., Shern, J. F., Wanhainen, K. M., Murgai, M., Ingaramo, M., Smith, J. P., Walker, A. J., Kohler, M. E., Venkateshwara, V. R., Kaplan, R. N., Patterson, G. H., Fry, T. J., Orentas, R. J. & Mackall, C. L. 4-1BB costimulation ameliorates T cell exhaustion induced by tonic signaling of chimeric antigen receptors. *Nat. Med.* **21**, 581–590 (2015).

15. Ajina, A. & Maher, J. *Strategies to address chimeric antigen receptor tonic signalling*. vol. 17 (2019).

16. Rajabzadeh, A., Rahbarizadeh, F., Ahmadvand, D., Salmani, M. K. & Hamidieh, A. A VHH-Based Anti-MUC1 Chimeric Antigen Receptor for Specific Retargeting of Human Primary T Cells to MUC1-Positive Cancer Cells Citation: Rajabzadeh A, Rahbarizadeh F, Ahmadvand D, Kabir Salmani M, Hamidieh AA. A VHH-based anti-MUC1 chimeric antigen recep. *Cell Journal(Yakhteh)* **22**, 502–513 (2019).

17. Lee, L., Draper, B., Chaplin, N., Philip, B., Chin, M., Galas-Filipowicz, D., Onuoha, S., Thomas, S., Baldan, V., Bughda, R., Maciocia, P., Kokalaki, E., Neves, M. P., Patel, D., Rodriguez-Justo, M., Francis, J., Yong, K. & Pule, M. An APRIL-based chimeric antigen receptor for dual targeting of BCMA and TACI in multiple myeloma. *Blood* **131**, 746–758

(2018).

18. Balakrishnan, A., Rajan, A., Salter, A. I., Kosasih, P. L., Wu, Q., Voutsinas, J., Jensen, M. C., Pluckthun, A. & Riddell, S. R. Multispecific targeting with synthetic ankyrin repeat motif chimeric antigen receptors. *Clin. Cancer Res.* **25**, 7506–7516 (2019).

19. Alabanza, L., Pegues, M., Geldres, C., Shi, V., Wiltzius, J. J. W., Sievers, S. A., Yang, S. & Kochenderfer, J. N. Function of Novel Anti-CD19 Chimeric Antigen Receptors with Human Variable Regions Is Affected by Hinge and Transmembrane Domains. *Mol. Ther.* **25**, 2452–2465 (2017).

20. Schmidts, A., Ormhøj, M., Choi, B. D., Taylor, A. O., Bouffard, A. A., Scarfò, I., Larson, R. C., Frigault, M. J., Gallagher, K., Castano, A. P., Riley, L. S., Cabral, M. L., Boroughs, A. C., Velasco Cárdenas, R. M. H., Schamel, W., Zhou, J., Mackay, S., Tai, Y. T., Anderson, K. C., *et al.* Rational design of a trimeric April-based CAR-binding domain enables efficient targeting of multiple myeloma. *Blood Adv.* **3**, 3248–3260 (2019).

21. Bridgeman, J. S., Hawkins, R. E., Bagley, S., Blaylock, M., Holland, M. & Gilham, D. E. The Optimal Antigen Response of Chimeric Antigen Receptors Harboring the CD3ζ Transmembrane Domain Is Dependent upon Incorporation of the Receptor into the Endogenous TCR/CD3 Complex. *J. Immunol.* **184**, 6938–6949 (2010).

22. Maher, J., Brentjens, R. J., Gunset, G., Rivière, I. & Sadelain, M. Human T-lymphocyte cytotoxicity and proliferation directed by a single chimeric TCRζ/CD28 receptor. *Nat. Biotechnol.* **20**, 70–75 (2002).

23. Imai, C., Mihara, K., Andreansky, M., Nicholson, I. C., Pui, C. H., Geiger, T. L. & Campana, D. Chimeric receptors with 4-1BB signaling capacity provoke potent cytotoxicity against acute lymphoblastic leukemia. *Leukemia* **18**, 676–684 (2004).

24. Pulè, M. A., Straathof, K. C., Dotti, G., Heslop, H. E., Rooney, C. M. & Brenner, M. K. A chimeric T cell antigen receptor that augments cytokine release and supports clonal expansion of primary human T cells. *Mol. Ther.* **12**, 933–941 (2005).

25. Song, D. G., Ye, Q., Poussin, M., Harms, G. M., Figini, M. & Powell, D. J. CD27 costimulation augments the survival and antitumor activity of redirected human T cells in vivo. *Blood* **119**, 696–706 (2012).

26. Guedan, S., Chen, X., Madar, A., Carpenito, C., McGettigan, S. E., Frigault, M. J., Lee, J., Posey, A. D., Scholler, J., Scholler, N., Bonneau, R. & June, C. H. ICOS-based chimeric antigen receptors program bipolar TH17/ TH1 cells. *Blood* **124**, 1070–1080 (2014).

27. Van Der Stegen, S. J. C., Hamieh, M. & Sadelain, M. The pharmacology of second-generation chimeric antigen receptors. *Nat. Rev. Drug Discov.* **14**, 499–509 (2015).

28. Porter, D. L., Hwang, W. T., Frey, N. V., Lacey, S. F., Shaw, P. A., Loren, A. W., Bagg, A., Marcucci, K. T., Shen, A., Gonzalez, V., Ambrose, D., Grupp, S. A., Chew, A., Zheng, Z., Milone, M. C., Levine, B. L., Melenhorst, J. J. & June, C. H. Chimeric antigen

receptor T cells persist and induce sustained remissions in relapsed refractory chronic lymphocytic leukemia. *Sci. Transl. Med.* **7**, 1–13 (2015).

29. Kawalekar, O. U., O'Connor, R. S., Fraietta, J. A., Guo, L., McGettigan, S. E., Posey, A. D., Patel, P. R., Guedan, S., Scholler, J., Keith, B., Snyder, N., Blair, I., Milone, M. C. & June, C. H. Distinct Signaling of Coreceptors Regulates Specific Metabolism Pathways and Impacts Memory Development in CAR T Cells. *Immunity* **44**, 380–390 (2016).

30. Ramello, M. C., Benzaïd, I., Kuenzi, B. M., Lienlaf-Moreno, M., Kandell, W. M., Santiago, D. N., Pabón-Saldaña, M., Darville, L., Fang, B., Rix, U., Yoder, S., Berglund, A., Koomen, J. M., Haura, E. B. & Abate-Daga, D. An immunoproteomic approach to characterize the CAR interactome and signalosome. *Sci. Signal.* **12**, 1–16 (2019).

31. Feucht, J., Sun, J., Eyquem, J., Ho, Y. J., Zhao, Z., Leibold, J., Dobrin, A., Cabriolu, A., Hamieh, M. & Sadelain, M. Calibration of CAR activation potential directs alternative T cell fates and therapeutic potency. *Nat. Med.* **25**, 82–88 (2019).

32. Mu, W., Carrillo, M. A. & Kitchen, S. G. Engineering CAR T Cells to Target the HIV Reservoir. *Frontiers in Cellular and Infection Microbiology* vol. 10 at https://doi.org/10.3389/fcimb.2020.00410 (2020).

33. Sadelain, M., Brentjens, R., Rivière, I. & Park, J. CD19 CAR Therapy for Acute Lymphoblastic Leukemia. *Am. Soc. Clin. Oncol. Educ. B.* e360–e363 (2015) doi:10.14694/edbook_am.2015.35.e360.

34. Lee, D. W., Gardner, R., Porter, D. L., Louis, C. U., Ahmed, N., Jensen, M., Grupp, S. A. & Mackall, C. L. Current concepts in the diagnosis and management of cytokine release syndrome. *Blood* **124**, 188–195 (2014).

35. Santomasso, B. D., Park, J. H., Salloum, D., Riviere, I., Flynn, J., Mead, E., Halton, E., Wang, X., Senechal, B., Purdon, T., Cross, J. R., Liu, H., Vachha, B., Chen, X., Deangelis, L. M., Li, D., Bernal, Y., Gonen, M., Wendel, H. G., *et al.* Clinical and biological correlates of neurotoxicity associated with car t-cell therapy in patients with B-cell acute lymphoblastic leukemia. *Cancer Discov.* **8**, 958–971 (2018).

36. Gust, J., Taraseviciute, A. & Turtle, C. J. Neurotoxicity Associated with CD19-Targeted CAR-T Cell Therapies. *CNS Drugs* **32**, 1091–1101 (2018).

37. Parker, K. R., Migliorini, D., Perkey, E., Yost, K. E., Bhaduri, A., Bagga, P., Haris, M., Wilson, N. E., Liu, F., Gabunia, K., Scholler, J., Montine, T. J., Bhoj, V. G., Reddy, R., Mohan, S., Maillard, I., Kriegstein, A. R., June, C. H., Chang, H. Y., *et al.* Single-Cell Analyses Identify Brain Mural Cells Expressing CD19 as Potential Off-Tumor Targets for CAR-T Immunotherapies. *Cell* **183**, 126-142.e17 (2020).

38. Johnson, L. A., Morgan, R. A., Dudley, M. E., Cassard, L., Yang, J. C., Hughes, M. S., Kammula, U. S., Royal, R. E., Sherry, R. M., Wunderlich, J. R., Lee, C. C. R., Restifo, N. P., Schwarz, S. L., Cogdill, A. P., Bishop, R. J., Kim, H., Brewer, C. C., Rudy, S. F., VanWaes, C., *et al.* Gene therapy with human and mouse T-cell receptors mediates cancer

regression and targets normal tissues expressing cognate antigen. *Blood* **114**, 535–546 (2009).

39. Tcr, A., Morgan, R. A., Chinnasamy, N., Abate-daga, D. D., Gros, A., Robbins, F., Zheng, Z., Feldman, S. A., Yang, J. C., Sherry, R. M., Phan, Q., Hughes, M. S., Kammula, U. S., Miller, A. D., Hessman, C. J., Stewart, A. A., Restifo, N. P., Quezado, M. M., Alimchandani, M., *et al.* Cancer regression and neurologic toxicity following anti-MAGE-A3 TCR gene therapy Richard. *J Immunother.* **36**, 133–151 (2014).

40. Linette, G. P., Stadtmauer, E. A., Maus, M. V., Rapoport, A. P., Levine, B. L., Emery, L., Litzky, L., Bagg, A., Carreno, B. M., Cimino, P. J., Binder-Scholl, G. K., Smethurst, D. P., Gerry, A. B., Pumphrey, N. J., Bennett, A. D., Brewer, J. E., Dukes, J., Harper, J., Tayton-Martin, H. K., *et al.* Cardiovascular toxicity and titin cross-reactivity of affinity-enhanced T cells in myeloma and melanoma. *Blood* **122**, 863–871 (2013).

41. Majzner, R. G. & Mackall, C. L. Tumor antigen escape from car t-cell therapy. *Cancer Discov.* **8**, 1219–26 (2018).

42. Rapoport, A. P., Stadtmauer, E. A., Binder-Scholl, G. K., Goloubeva, O., Vogl, D. T., Lacey, S. F., Badros, A. Z., Garfall, A., Weiss, B., Finklestein, J., Kulikovskaya, I., Sinha, S. K., Kronsberg, S., Gupta, M., Bond, S., Melchiori, L., Brewer, J. E., Bennett, A. D., Gerry, A. B., *et al.* NY-ESO-1-specific TCR-engineered T cells mediate sustained antigen-specific antitumor effects in myeloma. *Nat. Med.* **21**, 914–921 (2015).

43. Binnewies, M., Roberts, E. W., Kersten, K., Chan, V., Fearon, D. F., Merad, M., Coussens, L. M., Gabrilovich, D. I., Ostrand-Rosenberg, S., Hedrick, C. C., Vonderheide, R. H., Pittet, M. J., Jain, R. K., Zou, W., Howcroft, T. K., Woodhouse, E. C., Weinberg, R. A. & Krummel, M. F. Understanding the tumor immune microenvironment (TIME) for effective therapy. *Nat. Med.* **24**, 541–550 (2018).

44. Ahmadzadeh, M., Johnson, L. A., Heemskerk, B., Wunderlich, J. R., Dudley, M. E., White, D. E. & Rosenberg, S. A. Tumor antigen-specific CD8 T cells infiltrating the tumor express high levels of PD-1 and are functionally impaired. *Blood* **114**, 1537–1544 (2009).

45. Sun, C., Mezzadra, R. & Schumacher, T. N. Regulation and Function of the PD-L1 Checkpoint. *Immunity* **48**, 434–452 (2018).

46. Topalian, S. L., Drake, C. G. & Pardoll, D. M. Targeting the PD-1/B7-H1(PD-L1) pathway to activate anti-tumor immunity. *Curr. Opin. Immunol.* **24**, 207–212 (2012).

47. Chong, E. A., Svoboda, J., Dwivedy Nasta, S., Landsburg, D. J., Winchell, N., Napier, E., Mato, A. R., Melenhorst, J. J., Ruella, M., Lacey, S. F., June, C. H. & Schuster, S. J. Sequential Anti-CD19 Directed Chimeric Antigen Receptor Modified T-Cell Therapy (CART19) and PD-1 Blockade with Pembrolizumab in Patients with Relapsed or Refractory B-Cell Non-Hodgkin Lymphomas. *Blood* **132**, 4198 (2018).

48. Hirayama, A. V., Gauthier, J., Hay, K. A., Sheih, A., Cherian, S., Chen, X., Pender, B. S.,

Hawkins, R. M., Vakil, A., Steinmetz, R. N., Phi, T.-D., Chapuis, A. G., Till, B. G., Kiem, H.-P., Shadman, M., Cassaday, R. D., Acharya, U. H., Riddell, S. R., Maloney, D. G., *et al.* Efficacy and Toxicity of JCAR014 in Combination with Durvalumab for the Treatment of Patients with Relapsed/Refractory Aggressive B-Cell Non-Hodgkin Lymphoma. *Blood* **132**, 1680–1680 (2018).

49. Jacobson, C. A., Locke, F. L., Miklos, D. B., Herrera, A. F., Westin, J. R., Lee, J., Rossi, J. M., Zheng, L., Avanzi, M. P., Roberts, Z. J. & Sun, J. End of Phase 1 Results from Zuma-6: Axicabtagene Ciloleucel (Axi-Cel) in Combination with Atezolizumab for the Treatment of Patients with Refractory Diffuse Large B Cell Lymphoma. *Blood* **132**, 4192 (2018).

50. A Safety and Efficacy Trial of JCAR017 Combinations in Subjects With Relapsed/Refractory B-cell Malignancies - Full Text View - ClinicalTrials.gov. https://clinicaltrials.gov/ct2/show/NCT03310619.

CHAPTER 2

DIRECTED EVOLUTION OF PDBODY, A PROGRAMMED DEATH-LIGAND 1-TARGETING MONOBODY

2.1: INTRODUCTION

In this chapter, yeast-display mediated directed evolution was used to generate PDbody, a PD-L1-binding monobody. Mimicking natural selection, directed evolution is a powerful method to drive proteins towards a desired phenotype. Indeed, the Royal Swedish Academy of Sciences recognized the broad versatility and usefulness of this technique and accordingly awarded it the Nobel Prize in Chemistry in 2018[1]. Quite broadly, this technique works by first generating a DNA library of a protein of interest, which creates a diverse population of members with varying levels of desirability for the target phenotype. Next, the library is screened for the desired phenotype through either positive or negative selection. For the former, population members with high levels of the desired phenotype are selected for further rounds of selection, and for the latter, population members with low levels of the desired phenotype are removed from the population. These processes of library diversification and screening are then iteratively repeated until the desired target protein(s) are acquired.

More specifically, I utilized directed evolution to affinity mature the monobody scaffold to bind to PD-L1. The monobody is a low molecular weight (~11 kDa), single domain Ig-like protein scaffold derived from the 10th repeat of human fibronectin III[2–4]. As an Ig-like protein scaffold, the monobody shares similar tertiary structure to that of PD-1[5], the natural binding partner of PD-L1. Thus, it is a suitable starting point for directed evolution. For its intended use in immunotherapy, the monobody possesses several advantages as a protein scaffold: (1) its small size makes it easier to package into lentiviruses[6], (2) its human origin reduces the risk of immunogenicity[7,8], and (3) its lack of disulfide bonds renders it capable of being produced in

both the reducing environment of bacteria and the oxidizing endoplasmic reticulum of eukaryotic cells, compared to only the latter for disulfide bond-containing proteins[9]. Typically, the most common areas to engineer the monobody are on the BC and FG loops[4]. Thus, I generated a site-saturated library[10] on both of these loops for directed evolution screening.

I used yeast-surface display to screen the monobody library[11,12]. Yeast surface display is an advantageous screening platform for directed evolution for a variety of reasons: (1) it possesses a mutational space of 10^8 library members, (2) it is compatible with fluorescence activated cell sorting (FACS)[13], and (3) its codon-optimization and post-translational modification pathways (e.g. N-linked glycosylation and oxidative protein folding) are more similar to those of humans[14]. Specifically in our case with monobody engineering, the monobody library was cloned into the pYD1 vector[15] and then transformed into EBY100 yeast cells[16] such that the majority of cells contained either one or zero copies of the monobody construct. The purpose of this is to eliminate the confounding variable of one cell displaying multiple library members. Yeast cells were cultured in galactose-containing media to induce library expression on their surface via their α-agglutinin adhesion receptors, then they were stained with biotinylated PD-L1 and streptavidin-phycoerythrin (SA-PE) dye. Library members with the strongest PD-L1 binding should accordingly bind to the most SA-PE dye, appearing brighter than other library members. Bright yeast cells were then sorted via FACS. Through repetitive iterations of this cycle, monobody variants with the strongest binding affinity to PD-L1 were positively selected for, resulting in PDbody, a PD-L1 binding monobody.

2.2: MATERIALS AND METHODS

2.2.1: Molecular cloning

Plasmids were generated using Gibson Assembly (NEB, E2611L), T4 ligation (NEB, M0202L), and golden gate assembly (Thermo Scientific, FERER0452). PCR was performed using Q5 DNA polymerase (NEB, M0491) and synthesized primers (Integrated DNA Technologies). Constructs were verified by Sanger sequencing (Azenta).

2.2.2: Protein purification of recombinant PD-L1

An expression vector pEF-Bos containing PD-L1 was transfected into HEK 293T Lenti-X^{TM} 293T cells with Lipofectamine 3000 (Life Technologies, L3000). Cells were cultured in Advanced DMEM (ThermoFisher, 124291015) with 1x Penicillin/Streptomycin (Fisher Scientific, 15140122) and 2x Glutamax (Fisher Scientific, 35050061). Media was collected after 2 days of culture. Protease cocktail inhibitors were added (Millipore Sigma, 11697498001), and proteins were extracted and concentrated using 3-kDa Amicon centrifugal units (Millipore Sigma, UFC800396) through 5 successive 25 min spindowns at 4˚C and 7830 RPM. PD-L1 was then purified via its coupled 6xHis tag with Ni-NTA beads (Qiagen, 30210) nickel column and biotinylated using BirA biotin-protein ligase standard reaction kit (Avidity, BirA500). Buffer exchange to PBS was performed using 10 kDa snakeskin dialysis tubing for 24 hrs with 2 L of PBS (500 mL for 3 hrs, 500 mL for 5 hrs, and 1 L for 16 hrs). Total protein concentration was determined using Bio-Rad Protein Assay Dye Reagent Concentrate (Bio-Rad, #5000006). Anti PD-L1 antibody was used in Western blot to verify protein identity (eBioscience, 14-5983-82). Streptavidin Alexa Fluor 488 (Invitrogen, S11223) immunoblot staining was used to verify biotinylation.

2.2.3: Protein purification of biotinylated monobodies

Monobody constructs with biotin targeting site were cloned into the pRSET vector then transformed into BL21 (DE3) cells. Cells were cultured in LB Amp then induced in 0.5mM IPTG overnight at 16 degrees. Cells were lysed in B-PER (ThermoFisher, 78243) with one cOmplete^{TM}, EDTA-free Protease Inhibitor Cocktail tablet (Millipore Sigma, 04693132001) and 100 µM PMSF. Supernatant was filtered and then monobody proteins were purified using nickel column purification (Qiagen, 30210). Biotinylation was performed using BirA biotin-protein ligase standard reaction kit (Avidity, BirA500). Buffer exchange to PBS was performed using 3 kDa snakeskin dialysis tubing for 24 hrs with 2 L of PBS (500 mL for 3 hrs, 500 mL for 5 hrs, and 1 L for 16 hrs). Total protein concentration was determined using Bradford Assay. Streptavidin Alexa Fluor 488 immunoblot staining was used to verify protein identity and biotinylation.

2.2.4: Yeast culture

Saccharomyces cerevisiae EBY100 (a GAL1-AGA1::URA3 ura3-52 trp1 leu2Δ1 his3Δ200 pep4::HIS2 prbΔ1 .6R can1 GAL) was used for the yeast surface display. EBY100 were cultured in rich media (YPD) until transformation with yeast display plasmid pYD1 (ThermoFisher, V835-01). For selection, yeast cells were grown in synthetic complete medium minus tryptophan (SC-Trp with 2% (w/v) glucose). To induce monobody expression, yeast cells were induced in galactose media (SC-Trp with 2% (w/v) galactose.

2.2.5: K_D measurement via flow cytometry

The protein-protein dissociation constant K_D of monobody was measured using yeast surface display as described[17]. Antigen concentrations ranged from 10 pM to 5 µM were applied to label $1*10^7$ induced yeast cells. Biotinylated PD-L1 was incubated with yeast cells for 45 min,

then the resulting cells were stained with streptavidin-PE for 15 min. Nonlinear least-squares regression was used to calculate the K_D to be 47 nM. Flow cytometry data was analyzed using Flowjo Software (Flowjo, LLC).

2.2.6: K_D measurement via bio-layer interferometry

Binding kinetics of biotinylated monobody and PD-L1 were measured using Bio-Layer Interferometry. 9 μM biotinylated monobody was loaded onto the streptavidin biosensor for 2 min, PD-L1 association was then measured for 2 min, followed by dissociation observed for another 2 min. Data was exported into Matlab and nonlinear regression was used to determine k_{on}, k_{off}, and K_D values according to the procedures as reported earlier[18].

2.2.7: Simulations of molecular dynamics for monobody optimization

Starting from the G9 Mb (PDB: 1ttg), we grafted the CDR3 loop of known PDL1-binder (PDB: 5jds) into the FG loop of the Mb while preserving the CDR3-PDL1 interface. The resulting G9NbFG was solvated in a water box with 1nm padding with 150mM NaCl. Counterions were added to neutralize the net charge of the system. All molecular dynamics simulations were performed with OpenMM using a Langevin integrator with a friction coefficient of 1.0/ps, the Amber ff14SB forcefield, and the TIP3P water model[19]. The system was minimized twice with 1000 max iterations and 5 kJ/mol tolerance. In the first run, 1 kJ/Å^2 harmonic restraints were applied to non-hydrogen atoms in G9NbFG and all backbone atoms in PDL1. In the second minimization, 1 kJ/Å^2 harmonic restraints were applied to all backbone atoms. After minimization, the system was gradually heated to 300K from 25K in increments of 25K using an integration time step of 2fs/step and 50,000 steps with protein restrained with 1 kJ/Å^2 harmonic restraints. Following heating, the system was equilibrated for 50,000 steps with backbone restrained before a final equilibration of 500,000 steps with no restraints. After system

preparation and equilibration, we performed a 2 μs production simulation with the Geodesic BAOAB integrator from OpenMM tools[20]. The resulting trajectory was superposed onto the first frame and conformations were clustered into 3 conformational states using spectral clustering of atomic coordinates. Hydrogen bonding and atomic contacts (radius of 3.5Å) were calculated for each frame.

2.2.8: Library construction

Site saturated libraries were constructed in the BC loop (residues 26-30) and KN035 insertion into the FG loop regions of the monobody. To prepare plasmids for Golden Gate Assembly, ESP3I sites were cloned into the pYD1 vector. To create regions of genetic variance, DNA library synthesis via primer annealing was performed using NNK primers, where N represents an equimolar mixture of A, T, G, and C nucleotides, and K represents an equimolar ratio of T and G nucleotides. Golden Gate Assembly was performed, transformed into MegaX DH10B Electrocomp cells (ThermoFisher C640003), and then purified with Qiagen HiSpeed Plasmid Maxi kit. Purified DNA was transformed into EBY100 cells according to the following protocol as previously reported[21].

2.2.9: FACS screening of monobody library

BC and FG loop libraries were sorted using the BD FACSAria. To induce monobody expression, yeast cells were cultured in 2% galactose-containing synthetic complete media minus tryptophan. Cells were induced at 20˚C and shaken at 250 RPM for 48 hrs. After induction, $5*10^7$ cells were stained with 1 μM biotinylated PD-L1, αV5 Alexa Fluor 647 (ThermoFisher, 451098) at 1:100 v/v, and Propidium Iodide (ThermoFisher, P1304MP) at 1:750 v/v for 90 min. After primary staining, cells were stained with PE-SA (BD Biosciences, 554061) for 30 min at a concentration of 1:100 v/v for the FG loop library and 1:1000 v/v for the BC loop

library. Washing and staining was performed in PBS buffer with 0.1% bovine serum albumin at pH 7.4 for FG loop library, and PBS buffer with 0.1% bovine serum albumin at pH 6.5 titrated with 10M HCl. Buffers were filtered with 0.22 μm filters for sterility.

2.2.10: Statistical analysis

Statistical analysis was performed using the Prism software. One Way ANOVA was utilized to calculate P-values. Error bars were displayed as SEM's.

2.3: RESULTS

2.3.1: Monobody scaffold binds PD-L1 in low pH

The G9 monobody (Mb-G9) was originally engineered to bind to the SH3 domain of Fyn tyrosine protein kinase[22]. As a member of the immunoglobulin-like domain family, its secondary structure is similar to that of human Programmed Death Receptor-1 (PD-1)[5] (Figure 2.1A). Thus, it was chosen as a starting scaffold for further engineering to increase its affinity towards PD-L1. To engineer the monobody scaffold to bind to PD-L1, monobody libraries were generated using site-saturated mutagenesis, displayed on the yeast surface then stained by biotinylated PD-L1 (PD-L1 BTN) (Figure S2.1) which was then detected by the dye PhycoErythrin (PE) conjugated to streptavidin (SA-PE). Clones with the brightest PE signals were sorted via Fluorescence Activated Cell Sorting (FACS) (Figure 2.1B). In our design, we plan to improve the initial binding affinity by grafting a PD-L1 binding peptide sequence into the Mb-G9 scaffold (Mb-035). A site saturated FG-loop library, guided by rational design, will then be created on top of Mb-035. The clone that resulted from FG-loop library screening will be dubbed Mb-FG-EVO. Finally, a BC loop library will then be generated on top of Mb-FG-EVO, which will be screened

through another round of directed evolution, and the PDbody sequence will then be determined (Figure 2.1C).

To set up the yeast display system, Mb-G9 and human (PD-1) as a reference were transformed into EBY100 yeast cells. As the natural binding partner of PD-L1, PD-1 was included as a positive control; however, PD-1 showed no apparent binding to PD-L1 when stained in PBS buffer (Figure S2.2), suggesting a weak physiological binding affinity of PD-1 towards PD-L1 as previously reported[23]. PD-L1 binding of PD-1 was only observed after changing the buffer to pH 5.5 MES buffer (Figure 2A), which was earlier reported to boost PD-L1 binding[24]. Mb-G9 also showed PD-L1 binding in MES buffer at slightly higher levels than that of PD-1 (Figure 2.2A).

Further staining experiments showed that increased binding was significantly affected by the pH level of the buffers. Indeed, when MES buffer was titrated from pH 5.5 to pH 6.9, PD-L1 binding of Mb-G9 decreased. Likewise, when PBS buffer was titrated from pH 7.4 to pH 6.0, PD-L1 binding slightly increased (Figure S2.3). Interestingly, PD-L1 binding towards Mb-G9 in pH 6.9 MES buffer was stronger than binding in pH 6.0 PBS buffer, suggesting that buffer composition also plays an important role in regulating PD-L1 binding. Because PD-L1 binding was weak in PBS buffers, initial comparisons of binding between monobody variants were performed in MES buffer. Library screening was thereafter performed in PBS buffers to better mimic physiological conditions.

To measure binding affinity of Mb-G9 towards PD-L1, titrated amounts of PD-L1 were bound to yeast surface displayed Mb-G9 (Figure 2.2B). As can be seen in the flow cytometry graph, magnitude of binding correlated with added amount of PD-L1. Mean fluorescence intensities were extracted from flow cytometry plots, and non-linear squares regression[17] was

used to calculate the dissociation constant K_D of Mb-G9 to be 47 nM (Figure 2.2C) in pH 5.5 MES buffer. To cross check PD-L1 binding with a different method, Bio-Layer Interferometry (BLI) was used (Figure 2.2D). K_D, k_{on}, and k_{off} values were determined from kinetics measurements using non-linear squares regression. At 500 nM PD-L1, K_D value of purified biotinylated Mb-G9 (Figure S2.4) was measured to be 169 nM which is in the similar range of the Mb-G9 K_D measured by yeast display and flow cytometry. MES buffer was used here for both flow cytometry and BLI analysis.

Before starting the process of directed evolution, more information was desired on where Mb-G9 binds to PD-L1 and which amino acid residues might be key in its binding. In an inhibition assay, PD-1 was expressed via yeast surface display, and PD-L1 binding was examined with titrated Mb-G9. The group with added Mb-G9 showed less binding to PD-L1 (Figure S2.5). This suggests that Mb-G9 may compete against PD-1 in binding to PD-L1 via the same binding pocket and could thus act as a competitive inhibitor. To further probe which monobody residues may play an important role in PD-L1 binding, the BC and FG loop regions were mutated to see whether PD-L1 binding would be significantly affected following an earlier publication[25]. Results suggested that binding did not significantly change in MES buffer (Figure S2.6). Thus, a more systematic and high-throughput method of protein engineering was required to further improve monobody affinity toward PD-L1.

2.3.2: Affinity maturation of monobody towards PD-L1

Since the success of optimizing a protein binder via directed evolution is dependent on choosing a good starting point[26], KN-035 CDR loop[27] was grafted into the FG loop region of the monobody to create Mb-035 to increase the basal PD-L1 binding before directed evolution. The KN-035 loop was originally part of a PD-L1-binding nanobody, but the monobody is

advantageous to the nanobody because the monobody is human derived and hence potentially less immunogenic. In addition, CAR engineered by using PD-L1-binding nanobody has shown severe chronic activation and tonic signaling[28]. Yeast staining results showed no significant difference in PD-L1 binding between Mb-035 compared to that of Mb-G9 in physiological pH PBS buffer (Figure S2.7), but staining in pH 5.5 MES buffer showed a slightly higher PD-L1 binding in Mb-035 (Figure 2.3A). To further improve monobody affinity and identify which residues of the KN-035 loop to mutate for directed evolution, molecular dynamics simulations were performed between Mb-035 and PD-L1 (Figure 2.3B). Based on molecular dynamics simulations, residues were deemed suitable targets for mutation and optimization if they spent a long time in close proximity to PD-L1 but not directly interacting with PD-L1 (Figure S2.8). Accordingly, residues targeted for optimization are shown in cyan, with less optimizable residues shown in magenta (Figure 2.3C). Site saturated mutagenesis was performed on the identified target residues C82, T83, V85, T86, and T88.

After site saturated mutagenesis and directed evolution screening of the FG loop library of Mb-035 by PD-L1 staining and FACS sorting, Mb-FG-EVO was obtained and demonstrated to have improved affinity toward PD-L1. The FG loop sequence of this variant is PRLTPSP which is significantly different from the CTLTVSS of the original Mb-035 scaffold. Consistently, PD-L1 staining of monobody variant Mb-FG-EVO showed a significant improvement in PD-L1 binding compared to previous variants (Figure S2.9). While improvement of PD-L1 binding was noticeable, overall binding was still relatively moderate.

To further improve monobody affinity, site saturated mutagenesis was performed on the BC loop of Mb-FG-EVO (Residues 26-30). Screening was performed using MES buffer at pH 6.5 to have robust staining of clones. After four rounds of FACS screening, a number of higher

affinity mutants were isolated and gathered (Figure 2.4A). Four promising candidates with BC loop sequences VLRYG, KWLAP, SPRSP, and TARVT were tested. PD-L1 binding in MES buffer showed that the BC loop sequence TARVT (PDbody) displayed stronger PD-L1 binding (Figure 2.4B-C) than those of other monobody variants at similar expression levels (Figure S2.10). Binding affinity of purified PDbody (Figure S2.4) was further measured by BLI and quantified to be 4.75 μM (Figure 2.4D) in PBS buffer, which is stronger than the 8.2 μM K_D of wild-type PD-1[29]. . This measured binding affinity also suggests a significant improvement to that of Mb-G9 which was previously undetectable by BLI in PBS.

2.4: DISCUSSION

In this study, we integrated computational modeling-based rational design, together with directed evolution utilizing yeast display and high throughput screening of mutation libraries to develop PDbody, which recognizes a key immune checkpoint blockade ligand PD-L1. Based on a single domain monobody derived from human fibronectin[2–4]. PDbody was engineered through a combination of rational design and directed evolution to bind to PD-L1 with micromolar affinity. Interestingly, pH 7.4 PBS buffer was insufficient to detect PD-L1 binding for yeast staining during initial experiments. For this reason, pH 6.5 PBS buffer was used for directed evolution. A possible drawback of lower pH screening is that it can be a poor representation of physiological conditions. Taking this into consideration, the pH was kept above 6.5, which is around the pK_a of histidine. Below pH 6.0, histidine becomes biprotonated and positively charged which may change the overall charge state and conformation of the monobody, potentially causing misrepresentation of physiological conformation. Nonetheless, a benefit of

lower pH screening is that it can leverage the acidic nature of the tumor microenvironment to increase targeting specificity and minimize toxic targeting of healthy tissues at physiological pH.

2.5: FIGURES

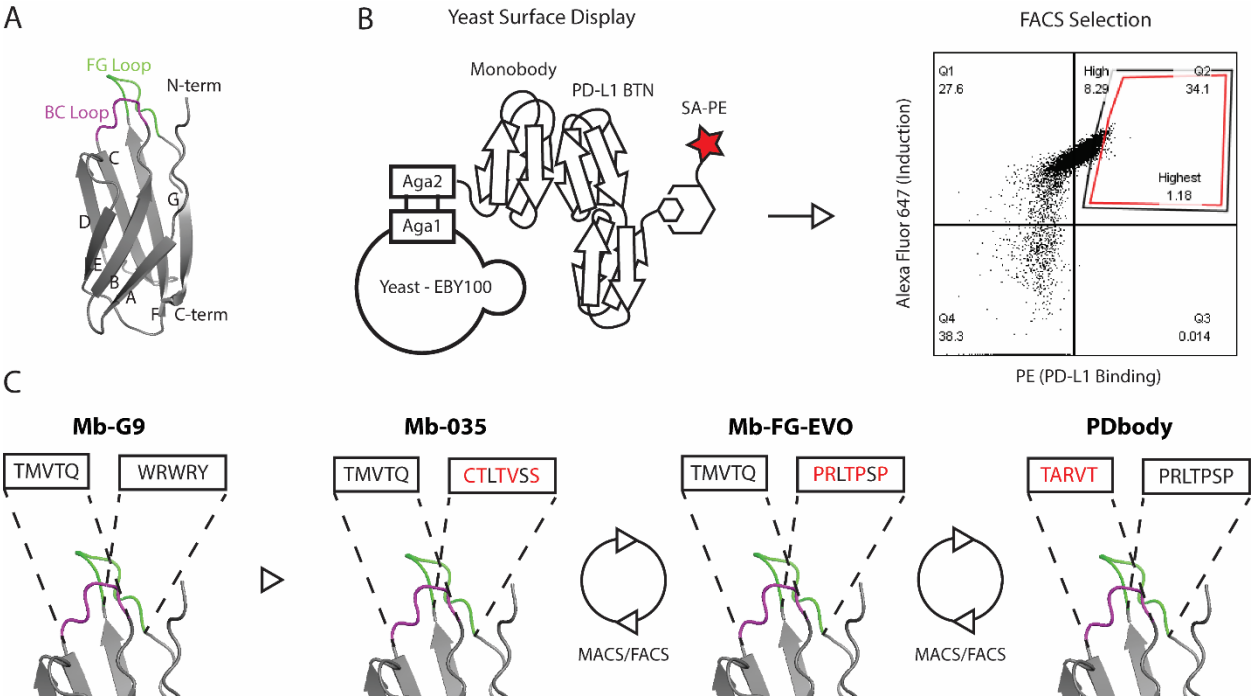

Figure 2.1: Protein engineering workflow: rational design guided directed evolution generated a PD-L1 binding monobody

(A) Crystal structure of monobody (ID: 1TTG) with loops and beta strands labeled. BC loop is shown in magenta, and FG loop in green. **(B)** Yeast-surface display sorting strategy. EBY100 yeast cells were induced to express monobody. Biotinylated PD-L1 and streptavidin-phycoerythrin were then used to quantify PD-L1 binding levels (Left). To enrich for higher affinity PD-L1 binders, FACS was used to sort out the top 1% of library populations (Right). **(C)** Monobody variants are sequentially obtained through a combination of rational design and directed evolution, and their BC and FG loop sequences are shown respectively in magenta and green. Mb-G9 represents the starting scaffold. Mb-035 is obtained after grafting KN-035 peptide into the FG loop. Rational design is used to guide the selection of amino acid residues to mutate for the FG loop library which resulted in the generation of Mb-FG-EVO. Ultimately, PDbody is obtained by creating a BC loop library of Mb-FG-EVO and undergoing another iteration of library screening.

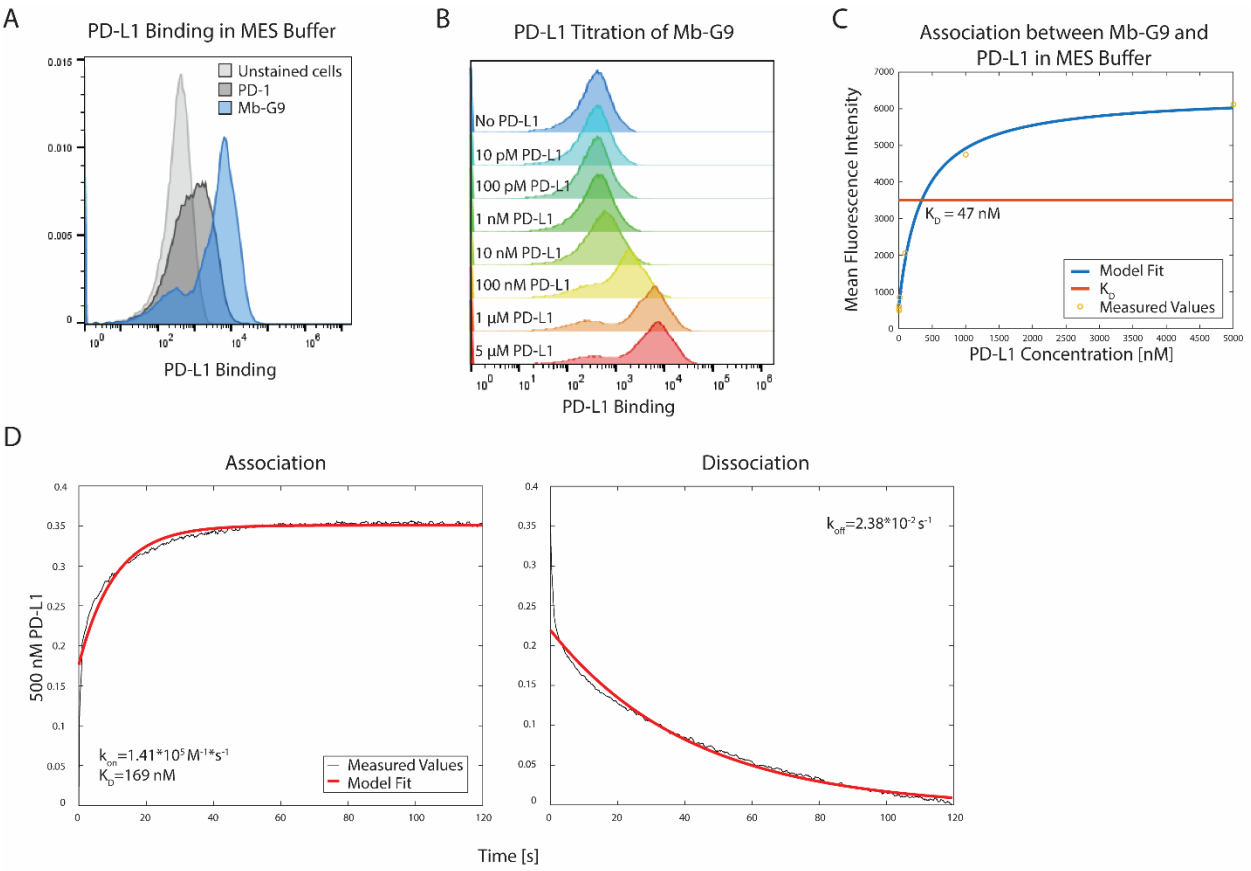

Figure 2.2: Mb-G9 binds to PD-L1 under acidic conditions
(A) PD-L1 binding of Mb-G9 in MES buffer. Mb-G9 was expressed on yeast cells and stained with biotinylated PD-L1 and streptavidin-phycoerythrin. PD-L1 binding of Mb-G9 and WT PD-1 are shown in blue and dark gray, respectively. Unstained cells are shown in light gray. **(B)** PD-L1 titration of Mb-G9. Biotinylated PD-L1 at varying concentrations was incubated to bind to yeast-displayed Mb-G9 and stained with streptavidin-phycoerythrin. **(C)** Mean fluorescence intensity values from Figure 2.2B were plotted, and nonlinear least-squares regression was fit to the data points to calculate a K_D of 47 nM. **(D)** BLI measurement of PD-L1 binding for Mb-G9 in MES buffer. Based on the kinetics data obtained, a K_D value of 169 nM was calculated.

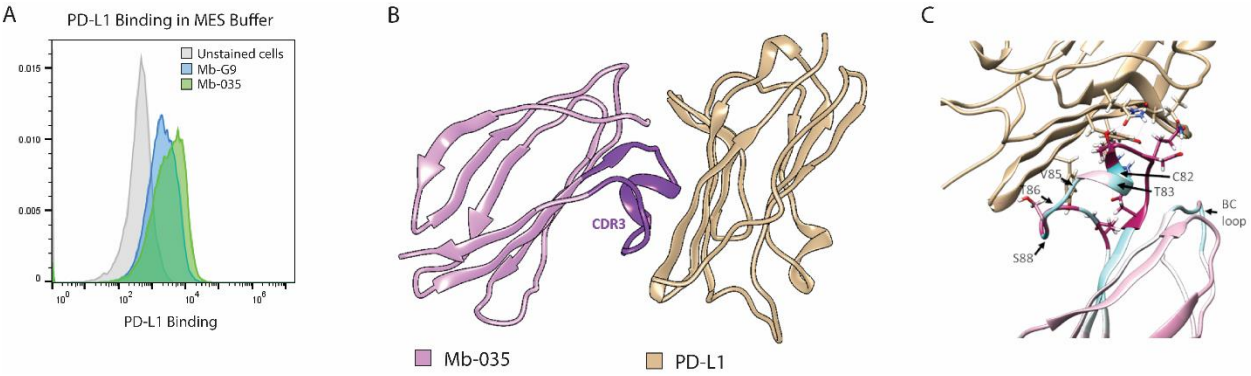

Figure 2.3: KN035 nanobody loop insertion in Mb-G9 improves PD-L1 binding

Molecular dynamics simulations predicted optimal amino acid residues of MB-035 to mutate. **(A)** PD-L1 binding of Mb-G9 (blue) and Mb-035 (green) in MES buffer. Yeast-displayed monobody variants were bound by biotinylated PD-L1 and stained with streptavidin-phycoerythrin. **(B)** Model of Mb-035 (magenta) binding to PD-L1 (light brown). Grafted KN-035 loop is shown in dark purple. **(C)** Molecular dynamics simulation of Mb-035 (magenta and cyan) binding to PD-L1 (light brown). Optimizable residues are labeled and shown in cyan.

A

Monobody Variant	BC Loop	FG Loop
Mb-G9	TMVTQ	WRWRY
Mb-035	TMVTQ	CTLTVSS
Mb-FG-EVO	TMVTQ	PRLTPSP
Mb-BC-1	VLRYG	PRLTPSP
Mb-BC-2	KWLAP	PRLTPSP
Mb-BC-3	SPRSP	PRLTPSP
PDbody	TARVT	PRLTPSP

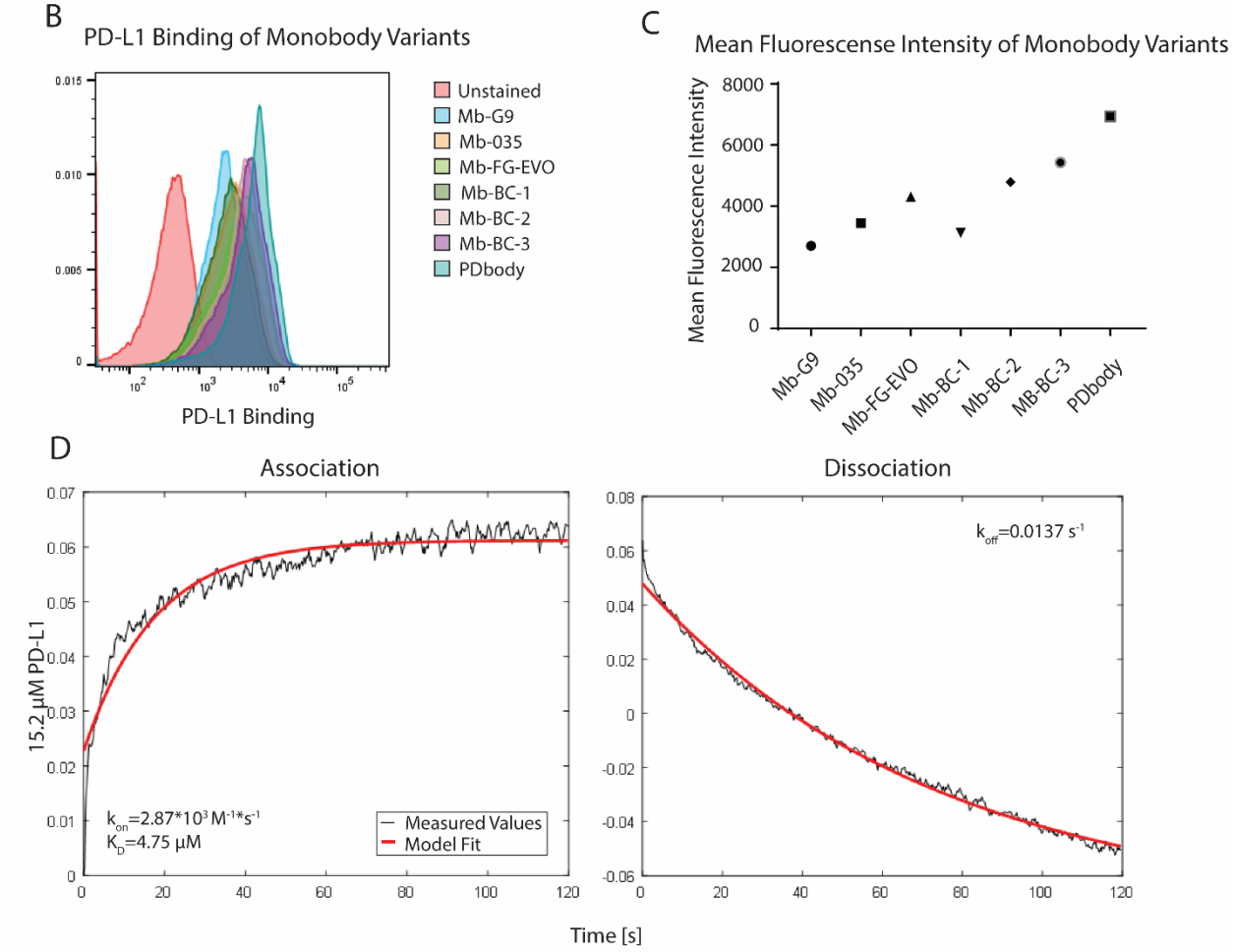

Figure 2.4: Directed evolution of the BC loop generated PDbody
(A) Table of monobody variants obtained through library screening and their amino acid sequences. **(B)** PD-L1 binding of monobody variants from Figure 2.4A. Yeast-displayed monobody variants were stained with 5µM biotinylated PD-L1 and streptavidin-phycoerythrin. **(C)** Mean fluorescence intensities from the graph in Figure 2.4B. **(D)** BLI measurement of PD-L1 binding for PDbody in pH 7.4 kinetics buffer. Based on the kinetics data obtained, a K_D value of 4.75 µM was calculated.

2.6: SUPPLEMENTARY FIGURES

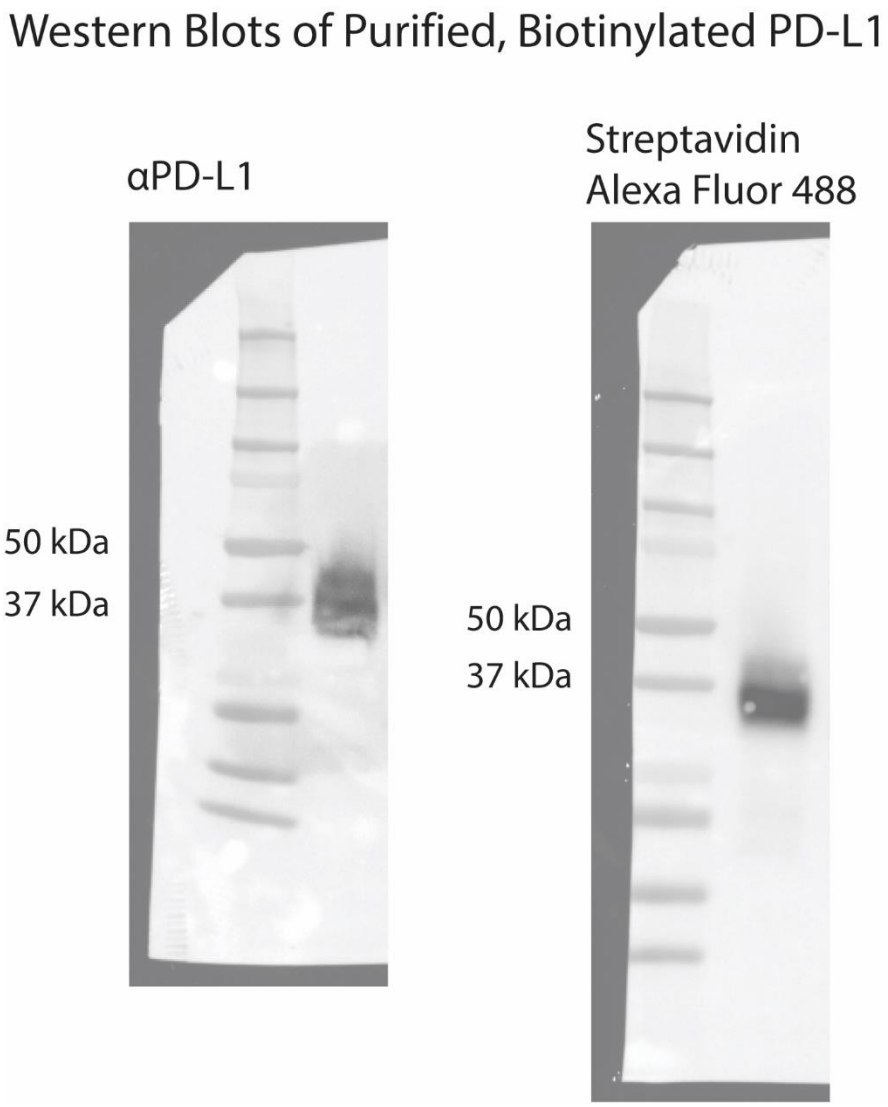

Figure S2.1: Western blot of purified and biotinylated PD-L1

The left image shows a Western blot of PD-L1 using αPD-L1 antibody which was visualized with goat αmouse HRP. The right shows the detection of biotinylated PD-L1 using streptavidin Alexa Fluor 488 conjugate.

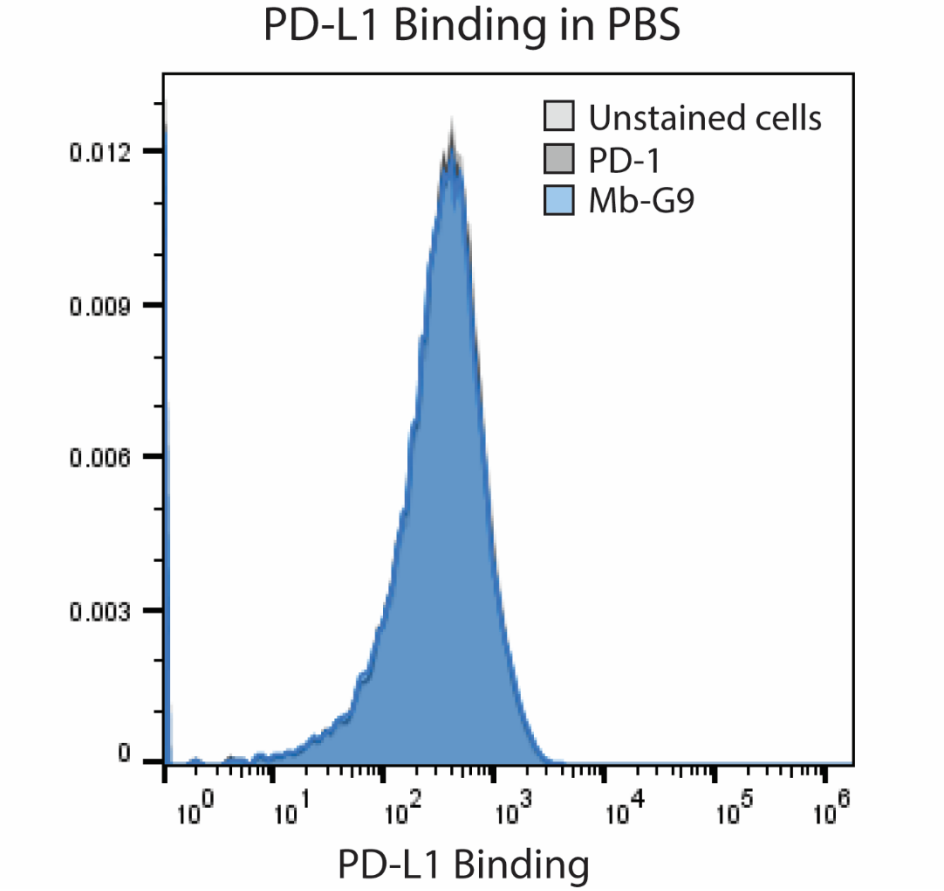

Figure S2.2: PD-L1 binding of Mb-G9 in PBS (0.5% w/v BSA)

Induced yeast cells expressing WT PD-1 or Mb-G9 were stained with 5 µM biotinylated PD-L1 and streptavidin-phycoerythrin. PD-L1 binding of Mb-G9 is shown in blue, PD-L1 binding of WT PD-1 is shown in dark gray, and PD-L1 binding of unstained cells is shown in light gray.

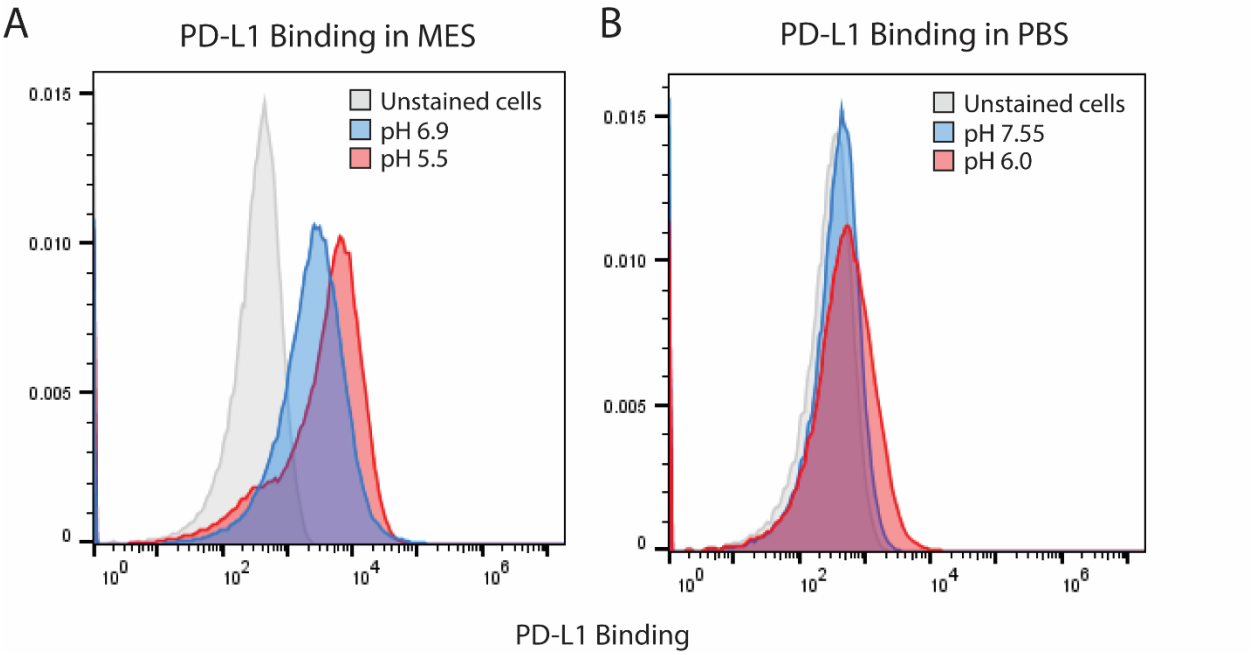

Figure S2.3: PD-L1 binding of Mb-G9 in different buffer conditions and pH's

Induced yeast cells expressing Mb-G9 were stained with 5 µM biotinylated PD-L1 and streptavidin-phycoerythrin. **(A)** PD-L1 binding in MES buffer (20 mM MES Sodium, 150 mM NaCl, 0.0005%Tween) at pH 5.5 (red) and pH 6.9 (blue). **(B)** PD-L1 binding in PBS buffer (0.5% w/v BSA) at pH 6.0 (red) and pH 7.55 (blue). Unstained cells are shown in light gray.

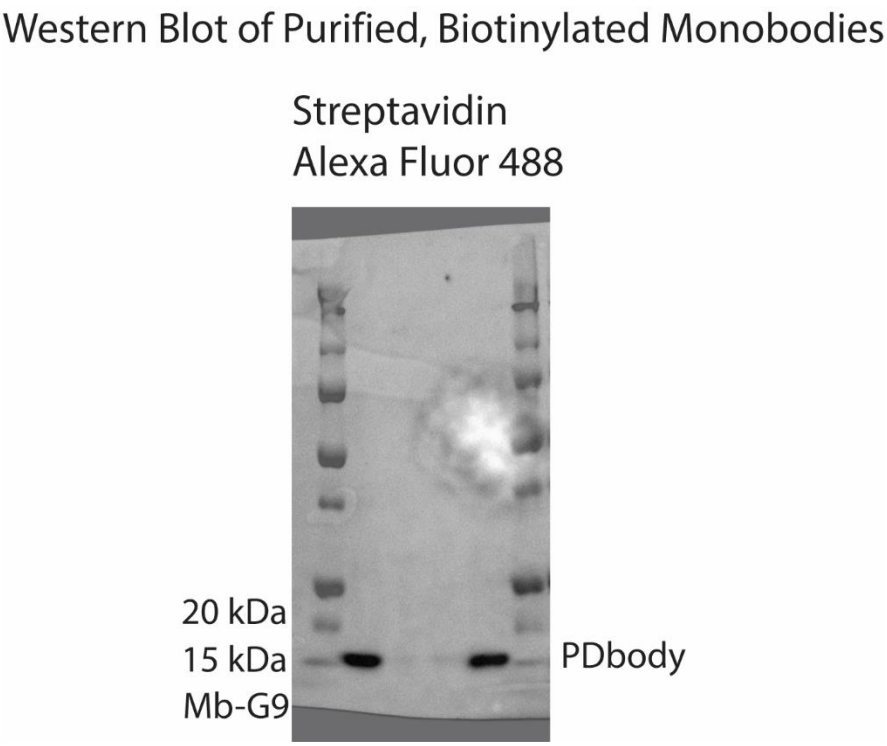

Figure S2.4: Western blot of purified and biotinylated monobodies
The left sample lane shows Mb-G9, and the right lane shows PDbody. Proteins were detected using streptavidin Alexa Fluor 488 conjugate.

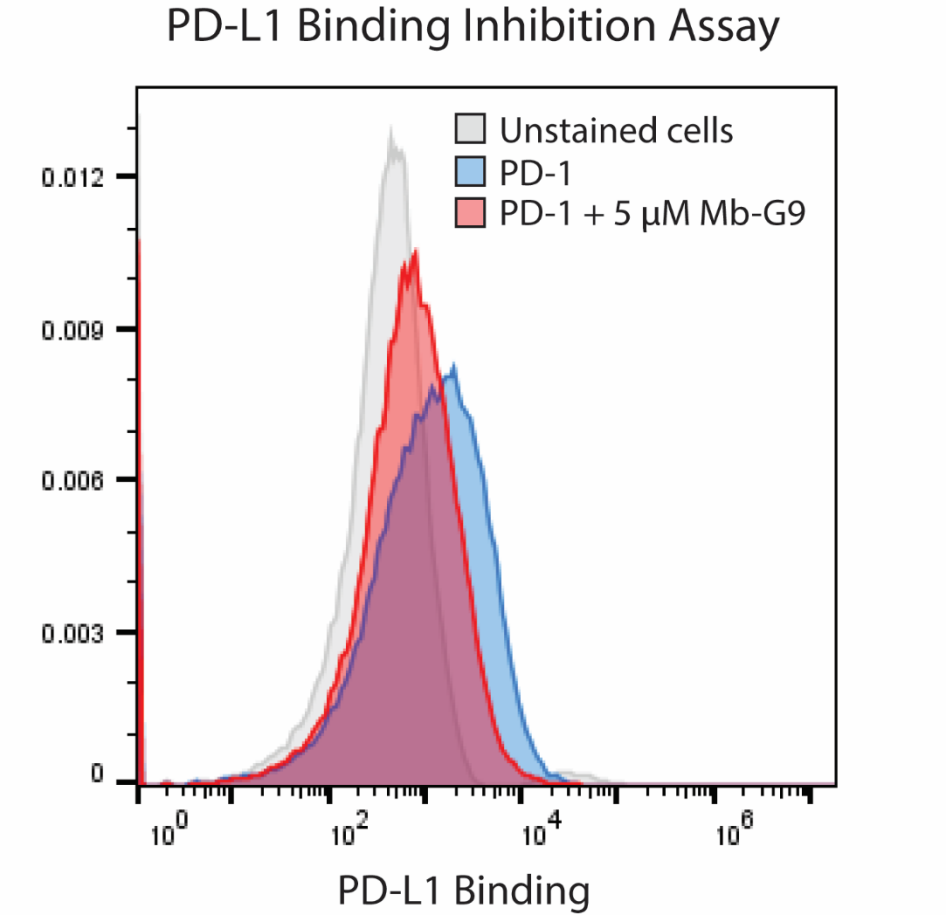

Figure S2.5: PD-L1 binding of PD-1 (WT)-expressing yeast cells in MES buffer
Mb-G9 was added to see whether it actively inhibited WT PD1 binding. Shown in blue is PD-L1 binding (5 µM) of WT PD-1, and shown in red is PD-L1 binding (5 µM) of WT PD-1 with 5 µM Mb-G9 added, and shown in gray is unstained cells.

Monobody Variant	BC Loop	FG Loop
Mb-G9 (WT)	TMVTQ	WRWRY
Mb-G9 (R83W)	TMVTQ	WRWWY
Mb-G9 (S4-W83R)	FINFK	WRWRY

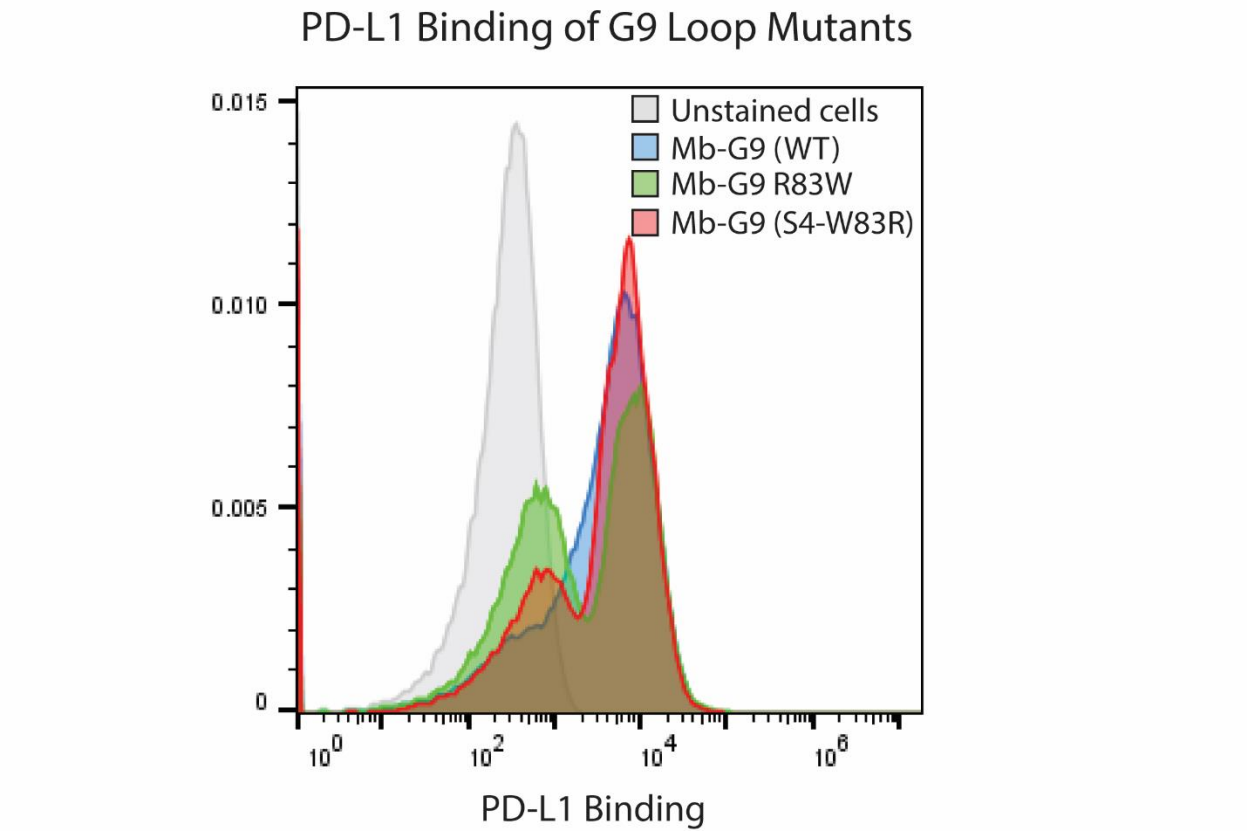

Figure S2.6: PD-L1 binding of monobody variants with different loop modifications
The modifications are shown in the table, and the staining results are shown in the figure: Monobody-G9 (WT) in blue, Monobody-G9 (R83W) in green, and Monobody-S4 (W83R) in red. PD-L1 binding was not significantly affected. The loop modifications seemed to play a larger role in monobody expression level. Gray is unstained cells.

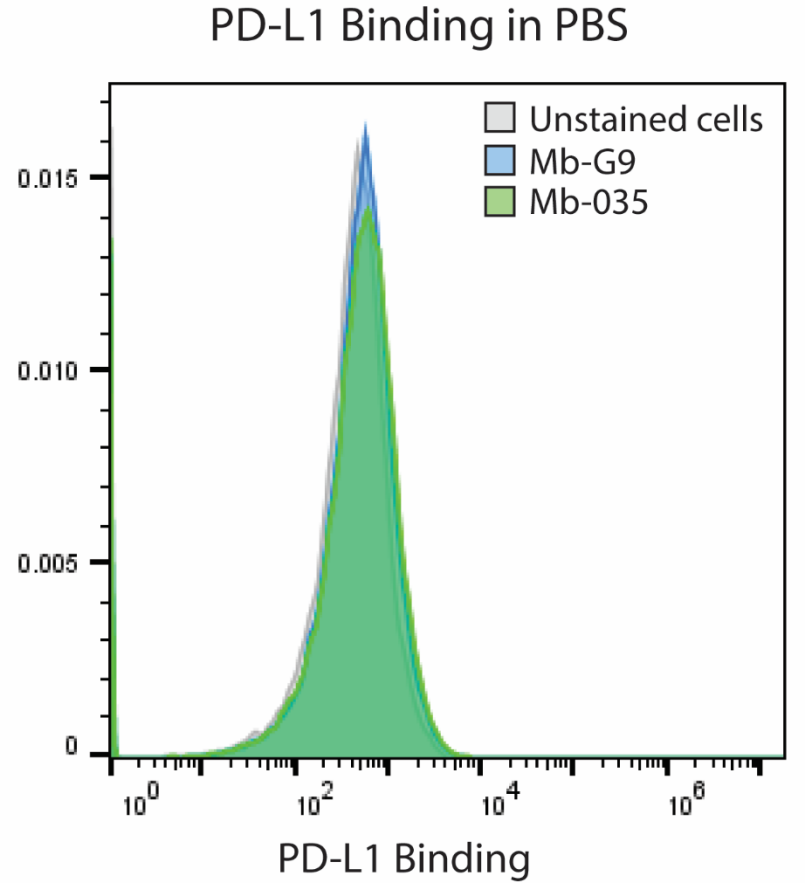

Figure S2.7: PD-L1 binding of Mb-035 in PBS (0.5% w/v BSA)
Induced yeast cells expressing Mb-G9 or Mb-035 were stained with 5 µM biotinylated PD-L1 and streptavidin-phycoerythrin. PD-L1 binding of Mb-G9 is shown in blue, PD-L1 binding of Mb-035 is shown in green, and PD-L1 binding of unstained cells is shown in light gray.

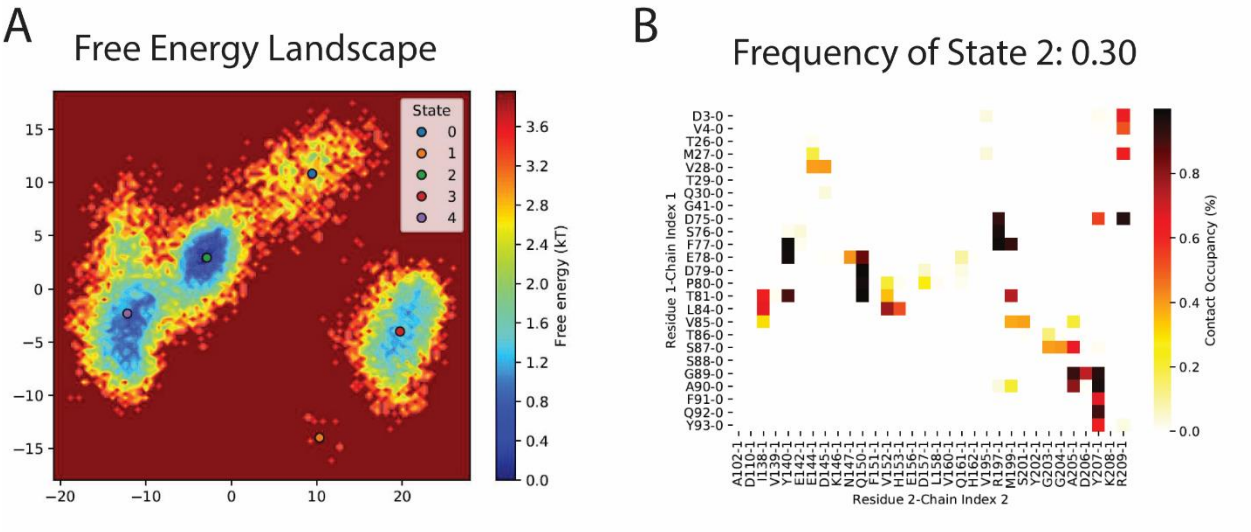

Figure S2.8: Molecular dynamics simulations of Mb-035/PD-L1 binding
(A) Energy landscape from a 2 μs simulation of Mb-035 bound to PD-L1 with 5 conformational states labeled. Because state 2 was one of the most energetically favorable, it was further analyzed. **(B)** Contact occupancies for interactions between Mb-035 and PD-L1. An occupancy of 1 indicates that the contact is observed in every instance of the conformational state.

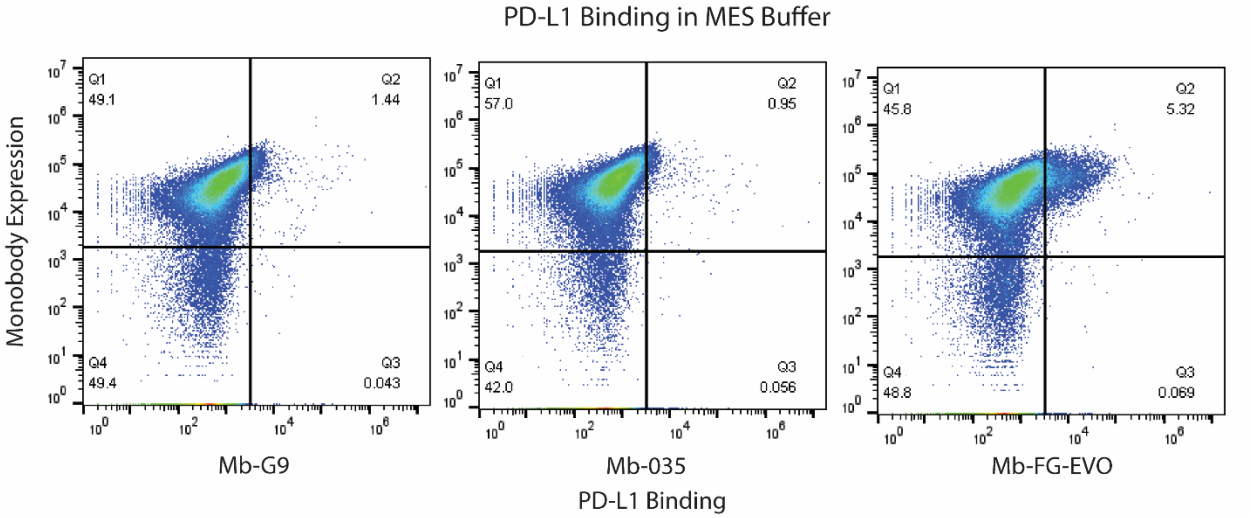

Figure S2.9: PD-L1 binding of engineered monobodies in pH 5.5 MES buffer
Induced yeast cells expressing Mb-G9 were stained with 5 µM biotinylated PD-L1 and streptavidin-phycoerythrin. Monobody expression was detected with anti-V5 Alexa-647 staining.

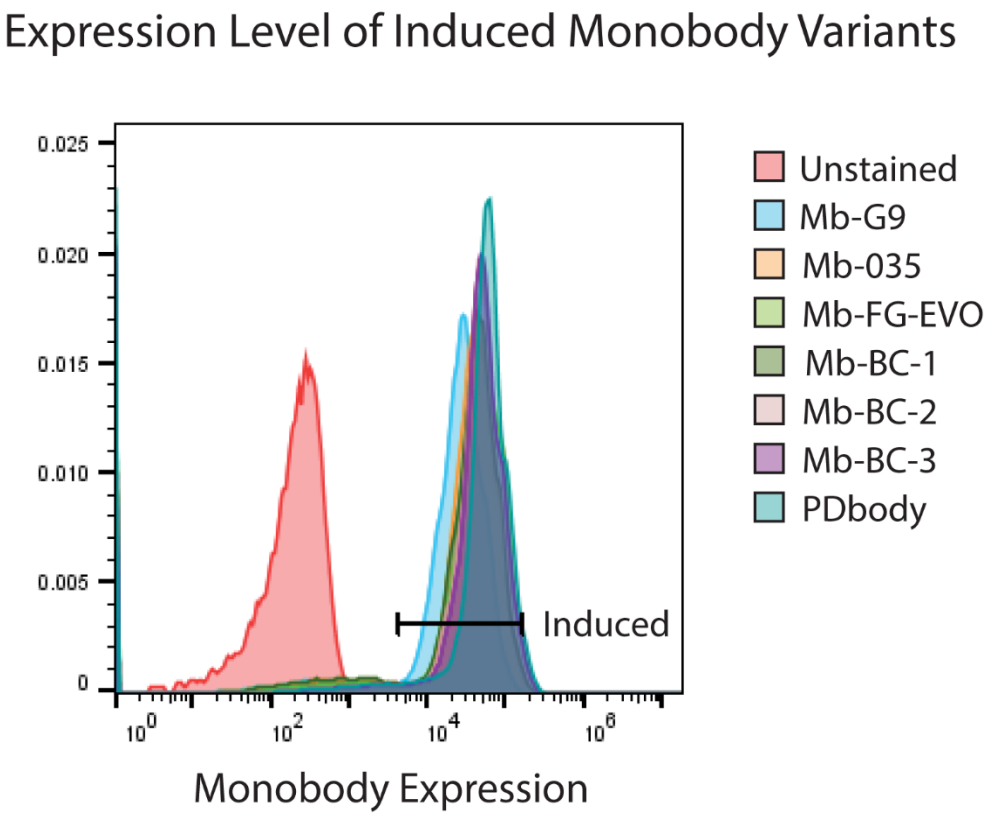

Figure S2.10: Expression levels of induced, yeast-displayed monobody variants

Induction levels were gated using the shown gate prior to measuring PD-L1 binding levels in Figure 2.4B.

ACKNOWLEDGEMENTS

Chapter 2, in part has been submitted for publication of the material as it may appear in ACS Central Science. Man, Chi-Wei; Zhu, Linshan; Harrison, Reed; Peng, Qin; Limsakul, Praopim; Hashimoto, Matthew; Mamaril, Anthony; Xu, Hongquan; Wang, Yingxiao. "Engineering a PD-L1-targeting Monobody via Directed Evolution for SynNotch-Gated Cancer Immunotherapy". The dissertation author was the primary researcher and author of this paper.

This work was supported in part by grants from NIH R01 CA262815, EB029122, R35 GM140929, R01 HL121365, and HD107206 (Y.W.).

REFERENCES

1. Arnold, F. H. Directed Evolution of Enzymes and Binding Proteins; Scientific Background on the Nobel Prize for Chemistry 2018. *R. Swedish Acad. Sci.* **50005**, 1–10 (2018).

2. Koide, S., Koide, A. & Lipovšek, D. Target-binding proteins based on the 10th human fibronectin type III domain (10 Fn3). *Methods Enzymol.* **503**, 135–156 (2012).

3. Koide, a, Bailey, C. W., Huang, X. & Koide, S. The fibronectin type III domain as a scaffold for novel binding proteins. *J. Mol. Biol.* **284**, 1141–51 (1998).

4. Koide, A., Wojcik, J., Gilbreth, R. N., Hoey, R. J. & Koide, S. Teaching an old scaffold new tricks: Monobodies constructed using alternative surfaces of the FN3 scaffold. *J. Mol. Biol.* **415**, 393–405 (2012).

5. Zak, K. M., Kitel, R., Przetocka, S., Golik, P., Guzik, K., Musielak, B., Dömling, A., Dubin, G. & Holak, T. A. Structure of the Complex of Human Programmed Death 1, PD-1, and Its Ligand PD-L1. *Structure* **23**, 2341–2348 (2015).

6. Bos, T. J., De Bruyne, E., Van Lint, S., Heirman, C. & Vanderkerken, K. Large double copy vectors are functional but show a size-dependent decline in transduction efficiency. *J. Biotechnol.* **150**, 37–40 (2010).

7. Lerner, R. A. Combinatorial antibody libraries: New advances, new immunological insights. *Nat. Rev. Immunol.* **16**, 498–508 (2016).

8. Wörn, A. & Plückthun, A. Stability engineering of antibody single-chain Fv fragments. *J. Mol. Biol.* **305**, 989–1010 (2001).

9. Wilcox, T. & Hirshkowitz, A. Native Disulfide Bond Formation in Proteins. *Curr. Opin.*

Chem. Biol. **4**, 533–539 (2000).

10. Siloto, R. M. P. & Weselake, R. J. Site saturation mutagenesis: Methods and applications in protein engineering. *Biocatal. Agric. Biotechnol.* **1**, 181–189 (2012).

11. Gera, N., Hussain, M. & Rao, B. M. Protein selection using yeast surface display. *Methods* **60**, 15–26 (2013).

12. Traxlmayr, M. W. & Obinger, C. Directed evolution of proteins for increased stability and expression using yeast display. *Arch. Biochem. Biophys.* **526**, 174–180 (2012).

13. Fulwyler, M. J. Electronic separation of biological cells by volume. *Science* **150**, 910–911 (1965).

14. Boder, E. T. & Wittrup, K. D. Yeast surface display for screening combinatorial polypeptide libraries. *Nat. Biotechnol.* **15**, 553–557 (1997).

15. Invitrogen. pYD1 Yeast Display Vector Kit. *Transformation* (2002).

16. Uchański, T., Zögg, T., Yin, J., Yuan, D., Wohlkönig, A., Fischer, B., Rosenbaum, D. M., Kobilka, B. K., Pardon, E. & Steyaert, J. An improved yeast surface display platform for the screening of nanobody immune libraries. *Sci. Rep.* **9**, 1–12 (2019).

17. Feldhaus, M. J., Siegel, R. W., Opresko, L. K., Coleman, J. R., Weaver Feldhaus, J. M., Yeung, Y. A., Cochran, J. R., Heinzelman, P., Colby, D., Swers, J., Graff, C., Steven Wiley, H. & Wittrup, K. D. Flow-cytometric isolation of human antibodies from a nonimmune Saccharomyces cerevisiae surface display library. *Nat. Biotechnol.* **21**, 163–170 (2003).

18. Dutta, S., Chen, T. S. & Keating, A. E. Peptide ligands for pro-survival protein Bfl-1 from computationally guided library screening. *ACS Chem. Biol.* **8**, 778–788 (2013).

19. Eastman, P., Swails, J., Chodera, J. D., McGibbon, R. T., Zhao, Y., Beauchamp, K. A., Wang, L. P., Simmonett, A. C., Harrigan, M. P., Stern, C. D., Wiewiora, R. P., Brooks, B. R. & Pande, V. S. OpenMM 7: Rapid development of high performance algorithms for molecular dynamics. *PLoS Comput. Biol.* **13**, 1–17 (2017).

20. Chodera, J. OpenMMTools — openmmtools documentation. https://openmmtools.readthedocs.io/en/stable/.

21. Gietz, R. D. & Schiestl, R. H. Large-scale high-efficiency yeast transformation using the LiAc/SS carrier DNA/PEG method. *Nat. Protoc.* **2**, 38–41 (2007).

22. Huang, R., Fang, P. & Kay, B. K. Isolation of monobodies that bind specifically to the SH3 domain of the Fyn tyrosine protein kinase. *N. Biotechnol.* **29**, 526–533 (2012).

23. Maute, R. L., Gordon, S. R., Mayer, A. T., McCracken, M. N., Natarajan, A., Ring, N. G., Kimura, R., Tsai, J. M., Manglik, A., Kruse, A. C., Gambhir, S. S., Weissman, I. L. & Ring, A. M. Engineering high-affinity PD-1 variants for optimized immunotherapy and immuno-PET imaging. *Proc. Natl. Acad. Sci. U. S. A.* **112**, E6506–E6514 (2015).

24. Pascolutti, R., Sun, X., Kao, J., Maute, R. L., Ring, A. M., Bowman, G. R. & Kruse, A. C. Structure and Dynamics of PD-L1 and an Ultra-High-Affinity PD-1 Receptor Mutant. *Structure* **24**, 1719–1728 (2016).

25. Limsakul, P., Peng, Q., Wu, Y., Allen, M. E., Liang, J., Remacle, A. G., Lopez, T., Ge, X., Kay, B. K., Zhao, H., Strongin, A. Y., Yang, X. L., Lu, S. & Wang, Y. Directed Evolution to Engineer Monobody for FRET Biosensor Assembly and Imaging at Live-Cell Surface. *Cell Chem. Biol.* 1–10 (2018) doi:10.1016/j.chembiol.2018.01.002.

26. Arnold, F. H. Design by Directed Evolution. *Acc. Chem. Res.* **31**, 125–131 (1998).

27. Zhang, F., Wei, H., Wang, X., Bai, Y., Wang, P., Wu, J., Jiang, X., Wang, Y., Cai, H., Xu, T. & Zhou, A. Structural basis of a novel PD-L1 nanobody for immune checkpoint blockade. *Cell Discov.* **3**, (2017).

28. Xie, Y. J., Dougan, M., Jailkhani, N., Ingram, J., Fang, T., Kummer, L., Momin, N., Pishesha, N., Rickelt, S., Hynes, R. O. & Ploegh, H. Nanobody-based CAR T cells that target the tumor microenvironment inhibit the growth of solid tumors in immunocompetent mice. *Proc. Natl. Acad. Sci. U. S. A.* **116**, 7624–7631 (2019).

29. Cheng, X., Veverka, V., Radhakrishnan, A., Waters, L. C., Muskett, F. W., Morgan, S. H., Huo, J., Yu, C., Evans, E. J., Leslie, A. J., Griffiths, M., Stubberfield, C., Griffin, R., Henry, A. J., Jansson, A., Ladbury, J. E., Ikemizu, S., Carr, M. D. & Davis, S. J. Structure and interactions of the human programmed cell death 1 receptor. *J. Biol. Chem.* **288**, 11771–11785 (2013).

CHAPTER 3

APPLICATION OF CD19-SYNNOTCH PDBODY-CAR FOR CANCER THERAPY

3.1: INTRODUCTION

Chimeric Antigen Receptor T (CAR T) cell therapy is a revolutionary treatment option for cancer therapy[1,2]. CAR consists of an extracellular antigen recognition domain (usually a scFv), a hinge, a transmembrane domain, and intracellular costimulatory and signaling domains[3,4]. Following the recognition of a specified antigen on the tumor cell surface, CAR T cells induce cytotoxicity by triggering endogenous T cell activation pathways[5,6]. CAR T cell therapy has demonstrated outstanding efficacy in treating hematological cancers, but solid tumors remain a challenge to treat[7]. Multiple factors contribute to this challenge, including the lack of tumor-specific antigens as well as the local immunosuppressive tumor microenvironment[8,9].

Immune checkpoint inhibition by PD-L1 provides negative regulatory feedback and suppresses T cell activation[10]. This negative regulatory function creates a survival advantage for tumor cells that upregulate PD-L1. Indeed, tumor cells with upregulated PD-L1 levels are found in many cancer types, including non-small cell lung cancer (NSCLC), head and neck squamous cell carcinoma (HNSCC), Hodgkin's lymphoma, and renal cell carcinoma[11]. Accordingly, immune checkpoint blockade (ICB) of the PD-1/PD-L1 axis is an effective treatment for a number of cancers[12,13]. ICB treatment usually involves the application of a PD-1 or PD-L1 blocking antibody in combination with one or more other treatments, a strategy referred to as combination therapy. The success of these strategies demonstrates the importance of the PD-1/PD-L1 axis in cancer therapy[14–16].

Thus, targeting PD-L1 as a CAR-T cell antigen is an exciting strategy. By targeting tumor cells overexpressing PD-L1, CAR T cells can not only be guided to attack tumor cells but also neutralize the immunosuppressive PD-1/PD-L1 axis and mitigate T cell exhaustion. Despite the promise of this approach, it is particularly risky because of potential on-target off-tumor effects. In fact, in addition to its upregulation in tumor cells, PD-L1 is expressed in various other cell types, including but not limited to T cells, B cells, dendritic cells, macrophages, and vascular endothelial cells[11]. Off-tumor CAR T cell attack can lead to cytokine release syndrome and in worst case scenario, even death[17–21]. For this reason, there is currently no FDA-approved CAR T cell developed to target PD-L1. Design strategies are particularly needed to avoid off-target toxicity when targeting PD-L1[22]. To avoid non-specific toxicity, two strategies were employed in our study: (1) the design of a CAR based on a PD-L1-recognizing monobody CAR with stronger affinity at relatively lower pH typical in the tumor microenvironment[23] and (2) the integration with SynNotch recognizing a clinically validated tumor-specific antigen (TSA) CD19 introduced into target tumors to form an AND gate with PD-L1 for high precision control.

The monobody is a low molecular weight (~11 kDa), single domain Ig-like protein scaffold derived from the 10th repeat of human fibronectin III[24–26]. Engineered to serve as a CAR receptor, the monobody provides a number of advantages compared to the standard scFv; (1) its small size makes it easier to package into lentiviruses[27], (2) its single domain nature prevents domain swapping which should reduce the risk of tonic signaling[28], (3) its human origin reduces the risk of immunogenicity[29,30], and (4) the monobody is more straightforward to engineer with three loops that are well studied and most frequently engineered, compared to the six binding loops and linker region of scFvs. These feature of the monobody should avoid the aggregation tendencies and inefficient folding typical of scFvs[31,32] as well as the chronic activation and tonic

signaling of a reported PD-L1 nanobody[22]. For this study, a combination of rational design and directed evolution was used to engineer the BC and FG loops of the monobody to bind to PD-L1. Studies have shown that CARs with moderate affinities are better suited to distinguish low versus high density of antigens on target cells, and hence designed for in some clinical treatments to specifically avoid off-tumor toxicity against healthy tissues/cells expressing low levels of target antigen[33–37]. Thus, the monobody CAR in this report was engineered to specifically target tumor cells with high PD-L1 density which tend to resist drug treatment[38] while sparing bystander cells expressing low levels of PD-L1.

To further address the issues associated with ubiquitous expression of PD-L1 in the body, an AND gate control SynNotch was added to the PD-L1-targeting system to provide localized targeting specificity[39,40]. SynNotch has already demonstrated a variety of uses in immunotherapy[41–45]. In our work, a clinically validated CD19 antigen was introduced to express on a subpopulation of MDA-MB-231 breast cancer cells, which served as "training centers" to engage SynNotch and induce PDbody-CAR production in engineered T cells. PDbody-CAR targeted PD-L1 which is universally expressed on MDA-MB-231 cells to eradicate the whole tumor population. Without the introduced CD19 SynNotch ligand, CAR was not produced to target PD-L1, demonstrating an added layer of safety against off-target toxicity. As such, our CD19-SynNotch-gated CAR with PD-L1 targeting monobody provides a safer method to target tumor cells with high PD-L1 expression.

3.2: MATERIALS AND METHODS

3.2.1: Molecular cloning

Plasmids were generated using Gibson Assembly (NEB, E2611L), T4 ligation (NEB, M0202L), and golden gate assembly (Thermo Scientific, FERER0452). PCR was performed

using Q5 DNA polymerase (NEB, M0491) and synthesized primers (Integrated DNA Technologies). Constructs were verified by Sanger sequencing (Azenta).

3.2.2: General mammalian cell culture

Human embryonic kidney (HEK293T) and MDA-MB-231 cells were cultured in Dulbecco's Modified Eagle Medium (DMEM) (Gibco, 11995115) with 10% fetal bovine serum (FBS) (Gibco, 10438026) and 1% penicillin-streptomycin (P/S) (Gibco, 15140122). Jurkat and K562 cells were cultured in Roswell Park Memorial Institute Medium (RPMI 1640) (Gibco, 22400105) with 10% FBS and 1% P/S. Primary human T cells were cultured in complete RPMI 1640 supplemented with 100 U mL^{-1} recombinant human IL-2 (PeproTech, 200-02). All cell types were cultured at 37˚C in a humidified 5% CO_2 incubator.

3.2.3: Isolation and transduction of primary human T cells

Human peripheral blood mononuclear cells were isolated from buffy coats from the San Diego Blood Bank with lymphocyte separation medium (Corning, 25-072-CV). Primary human T cells were isolated using a Pan T Cell Isolation Kit (Milteenyi, 130-096-535). Following isolation, T cells were stimulated with Dynabeads Human T-Expander CD3/CD28 (ThermoFisher, 11141D) at a ratio of 1:1 Dynabeads per T cell. 48 hrs after Dynabead stimulation, cells were transduced on Retronectin-coated (Takara, T100B) plates with concentrated Lentivirus at a multiplicity of infection 5 per construct. 6 days after infection Dynabeads were magnetically removed, T cells were stained with anti-myc Alexa Fluor 488 (Cell Signaling Technology, 9B11) and FACS sorted with a Sony SH800.

3.2.4: Cytotoxicity assay

MDA-MB-231 target cell lines were generated through Lentiviral transduction and subsequent sorting with Sony SH800. For cytotoxicity assays, $2.5*10^4$ CD19 positive and

$2.5*10^4$ CD19 negative MDA-MB-231 cells were co-cultured with $2.5*10^5$ CD19-SynNotch monobody-CAR T cells in 150 µL RPMI for 24 hrs. Bioluminescence measurements were taken using the Dual Glo Luciferase Assay kit (Promega, E2920). Cytotoxicity was measured by calculating the percent difference in luminescence of SynNotch T cells versus those of target tumor cells only.

3.2.5: In vivo bilateral tumor model

Animal experiments were performed in accordance with Protocol S15285 which was approved by the UCSD Institutional Animal Care and Use Committee (IACUC). All researchers involved in this study complied with animal-use guidelines and ethical regulations. 6-week old NOD scid gamma (NSG) mice, purchased from UCSD Animal Care Program (ACP), were used in the study. 5 mice were subcutaneously injected with $8*10^5$ CD19+ MDA-MB-231 cells in the right flank and $8*10^5$ CD19- MDA-MB-231 cells in the left flank. 10 days after tumor injection, $4*10^6$ CD19-SynNotch PDbody-CAR T cells were intravenously injected. Tumor volume was then measured twice a week via caliper measurement. Volume was calculated using the equation (l*w*w)/2, where l is the longest length of the tumor and w is the length of tumor perpendicular to l.

For the 50% CD19+/CD19- experiment, 6-week old NOD scid gamma (NSG) mice, purchased from UCSD Animal Care Program (ACP), were used in the study. 5 mice were subcutaneously injected with $2.5*10^5$ CD19+ MDA-MB-231 and $2.5*10^5$ CD19- MDA-MB-231 cells in the right flank and $5*10^5$ CD19- MDA-MB-231 cells in the left flank. 4 days after tumor injection, $4*10^6$ CD19-SynNotch PDbody-CAR T cells were intravenously injected. The growth of CD19- tumor cells on both sides was imaged using IVIS 10 min after Coelentarizine injection (GoldBio, CZ2.5) following the manufacturer's protocol.

3.2.6: Tumor extraction

Mice were sacrificed, and tumors were surgically removed. Tumors were manually chopped then digested with Collagenase P in RPMI (1 mg/mL working concentration) (Millipore Sigma, 11213857001) and DNAse I (1 mg/mL working concentration) (Millipore Sigma, 10104159001) for 1 hr at 37˚C. Cells suspensions were strained through 35 μm strainer tubes (Fisher Scientific, 352235) then red blood cells were lysed using RBC lysis buffer (BioLegend, 420301) following the manufacturer's instructions. Cells were then resuspended in 5 mL DMEM and counted.

3.2.7: Statistical analysis

Statistical analysis was performed using the Prism software. One Way ANOVA was utilized to calculate P-values. Error bars were displayed as SEM's. For in vivo studies, tumor volume was measured with the exponential growth law and its growth rate was computed at the time t as log(V(t)/V(0)), where V(t) was tumor volume at time t and V(0) was the tumor volume at time 0 before T cell treatment. For luminescence measurements, growth rate was calculated as log(Relative Luminescence). Regression analysis was performed on tumor growth rates with a randomized block design for each day separately, followed by residual analysis for checking model assumptions. Specifically, for each day a linear regression model was built, y = mouse + treatment + error, where the response y was the tumor growth rate for a mouse receiving one of the two treatments, and the error term represented the experimental error. Here each mouse formed a block of size two. The randomized block design was effective in eliminating the large mouse-to-mouse variation. Statistical tests were conducted using ANOVA (analysis of variance) and F tests. P values based on two-sided t tests were computed to determine the significance of the treatment effect. Residual analysis on the model confirmed the accuracy of the model

assumptions. Statistical analysis was performed using R (http://www.r-project.org/), a free software environment for statistical computing and graphics.

3.3: RESULTS

3.3.1: Monobody variants as CAR receptors

To be used for immunotherapy, monobody variants were tested as the tumor-recognition motifs in CAR receptors. Driven by PGK promoter, monobody variants were fused to CD28 transmembrane domain, CD28, and 4-1BB for the generation of CARs (Figure 3.1A). These monobody CARs were then expressed in Jurkat cells. To test for PD-L1 binding of monobody CARs at similar expression levels (Figure S3.1), PD-L1 staining was performed on each of the monobody variants. Results showed that PD-L1 binding of PDbody was higher than that of Mb-G9, Mb-035, and Mb-FG-EVO (Figure 3.1B). PD-L1 binding by PDbody-CAR was detected at 100 nM and 1 μM PD-L1 concentrations, which is consistent with the previously measured binding affinity of PDbody (Figure 2.4D). This affinity of PDbody should allow for the binding of tumor cells expressing high levels of PD-L1 while reducing on-target off-tumor toxicity of somatic cells and healthy tissues expressing low levels of PD-L1. Furthermore, an increase in PD-L1 binding was observed in lower pH, which should prove favorable and more specific for the acidic tumor microenvironment (Figure S3.2).

3.3.2: SynNotch-gated PDbody-CAR

As PD-L1 is expressed in a broad range of cell types, additional gating of PDbody should further improve the specificity of PDbody-based CAR T cell therapy. We reasoned that an AND gate integrating SynNotch and PDbody-CAR should minimize off-target toxicity and increase the safety of the PDbody-CAR system, as cytotoxicity will only occur when both a tumor specific antigen (TSA) and PD-L1 are expressed on the target cell (Figure 3.2). We first

examined and verified the SynNotch system. A CD19 scFv SynNotch receptor and cyan-orange fluorescent protein nanoluciferase (NC3) reporter[46] were lentivirally transduced in Jurkat cells. These cells were either cultured alone (added media) or co-cultured with CD19-negative K562 cells or CD19-positive Toledo cells in a 1:1 E:T ratio (Figure 3.3A). Luminescence measurements revealed that the SynNotch system was able to discern between CD19-negative and CD19-positive cells (Figure 3.3B).

Next, the NC3 reporter was replaced by Mb-G9, Mb-FG-EVO, and PDbody-CAR, and transduced into T cells isolated from Peripheral Blood Mononuclear Cells (PBMCs) along with CD19scFv SynNotch receptor (Figure 3.4A); FACS was used to sort and select T cells expressing similar levels of SynNotch among different groups (Figure S3.3). MDA-MB-231 cells, a highly aggressive, invasive and triple negative breast cancer (TNBC) cell line lacking estrogen receptor (ER), progesterone receptor (PR), and human epidermal growth factor receptor 2 (HER2)[47,48], but express high levels of endogenous PD-L1 (Figure S3.4), were used as target tumor cells in luminescence-based killing assays. These MDA-MB-231 cells were transduced with a gene cassette encoding a truncated CD19 (ectodomain and transmembrane domain only) connecting to self-cleaving peptide P2A and Firefly Luciferase (Figure S3.5) to create a CD19-positive cell line. MDA-MB-231 cells were also transduced with a myc-P2A-Renila Luciferase construct to serve as a CD19-negative control. The luciferase signals were measured in triplicate to verify a proportional correlation with cell number (Figure S3.6). To test killing specificity, CD19-SynNotch PDbody-CAR cells were first co-cultured with CD19-negative MDA-MB-231 cells (Figure 3.2, Left). No significant difference in killing was observed (Figure 3.4B). Similarly, SynNotch PDbody-CAR cells co-cultured with a CD19-positive but PD-L1-negative

K562 cell line (expressing CD19-P2A-Firefly Luciferase) (Figure 3.2, Middle) did not elicit non-specific cytotoxicity (Figure S3.7).

Having established these controls, we then mixed CD19 positive and negative MDA-MB-231 cells at a ratio of 1:1 to examine whether a subset of tumor cells can be introduced with the clinically validated CD19 to serve as "training centers" and trigger the production of PDbody-CARs in T cells for the eradication of the whole population of MDA-MB-231 cells which universally express a high level of PD-L1[45]. It is expected that the half CD19+ MDA-MB-231 cells will train and activate the CD19-SynNotch to induce monobody CAR production in T cells to target PD-L1 on both CD19+ and CD19- MDA-MB-231 cells. Indeed, both CD19+ and CD19- MDA-MB-231 cells were attacked in all the co-culture groups with PDbody-CAR demonstrating the highest level of killing (Figures 3.2, Right; 3.4C). PDbody-CAR can indeed eradicate both CD19+ and CD19- MDA-MB-231 cells in 24 hr with an E:T ratio of 3:1, whereas Mb-FG-EVO CAR and Mb-G9 CAR were unable to eradicate all of the tumor cells even after 48 hrs of co-culture, although Mb-FG-EVO CAR showed significantly higher cytotoxicity than that of Mb-G9 CAR (Figure S3.8).

Killing assays with varying E:T ratios verified that PDbody-CAR was effective in eradicating all of the MDA-MB-231 target cells with or without CD19 expression (Figure 3.4D). This result is exciting as PDbody-CAR integrated with CD19-SynNotch can produce CAR T cells to target solid tumor cells vaccinated to express clinically-validated antigen (e.g. CD19), albeit partially and heterogeneously. These CD19-expressing tumor cells can serve as "training centers" to induce PDbody-CAR which can attack the whole population of proximal tumor cells expressing PD-L1, which is not absolutely tumor specific. Furthermore, PDbody can neutralize

PD-L1 and its mediated immunosuppressive mechanism for the enhancement of cancer immunotherapy efficacy.

After verifying the function of the SynNotch PDbody-CAR system in vitro, it was tested in a bilateral tumor NSG mouse model. Equal numbers of CD19+ and CD19- MDA cells with high PD-L1 expression were injected into right and left flanks respectively of 5 mice, and tumor size was monitored via caliper measurement every 3-4 days (Figure 3.5A). After 10 days of tumor growth, CD19-SynNotch PDbody-CAR T cells were injected intravenously. Results indicated that tumor growth of CD19+ tumors was significantly slowed compared to that of CD19- tumors (Figure 3.5B). Results from all 5 individual mice also showed reduction in relative tumor size, indicating that the CD19-SynNotch PDbody-CAR T cells can robustly suppress tumor growth of CD19+ tumors *in vivo* (Figure S3.9).

To demonstrate that CD19-SynNotch PDbody-CAR can kill tumors partially vaccinated with the clinically validated CD19, another *in* vivo experiment was performed with only 50% of the target tumor cells express CD19 to serve as training centers to induce PDbody-CAR expression in T cells. Equal total numbers of CD19- MDA and a 1:1 CD19+/CD19- MDA mixture were injected into the left and right flanks, respectively. CD19-SynNotch PDbody-CAR T cells were intravenously (IV) injected 4 days after tumor implantation (Figure 3.5C). CD19- tumor growth was monitored via Renila luciferase luminescence and normalized to the first day of luminescence measurement. Results indicated that from Day 17 onward, growth of the CD19- tumor cells was significantly suppressed on the right side where there were 50% CD19+ tumor cells serving as training centers to induce PDbody-CAR production to target both CD19- and CD19+ tumor cells in the proximity (Figure 3.5D). These results were further validated by the individual tumor traces of each mouse and by *ex vivo* luminescence measurements of extracted

tumor cells the day of sacrifice (Figure S3.10). Overall, these results suggest that the integration of SynNotch and PDbody-CAR can be applied to add an additional level of control over cytotoxicity, allowing PDbody-CAR T cells to target *in vivo* tumors vaccinated to express clinically-validated antigens.

3.4: DISCUSSION

In this study, PDbody was utilized to generate PDbody-CAR which not only recognizes PD-L1 on the tumor cell surface for killing but also neutralizes an immunosuppressive checkpoint to further promote killing efficacy. Integrated with SynNotch recognizing an introduced and clinically validated antigen CD19 expressed on a subset of tumor cells as "training centers", PDbody-CAR was further applied to target the whole population of tumor cells expressing PD-L1. This AND gate integrating CD19-SynNotch and PDbody-CAR should enhance the specificity of T cell killing and potentially minimize on-target off-tumor toxicity in adoptive cell therapy, as PDbody-CAR is induced and maintained mainly at the proximity of "training centers" where SynNotch engages the vaccinated CD19 antigen.

PDbody was engineered from Mb-G9 with an affinity of 4.75 μM under physiological pH solutions, which is comparable to that of wild type PD-L1[49,50]. We hypothesized that this moderate affinity could protect against off-tumor toxicity, particularly against normal tissues/organs expressing low levels of PD-L1. From the killing assays performed in this study, complete killing was observed at 3:1 and 5:1 E:T ratios but was incomplete at 1:1 E:T ratio (Figure 3.4D). This suggests that PDbody-CAR T cells could be more locally cytotoxic at the tumor site and less cytotoxic if they migrated away to other locations where they would be scattered with decaying CAR expression[45], which should be beneficial to mitigate the off-tumor toxicity of standard CAR T cells. Nevertheless, PDbody-CAR was able to suppress tumor cells

in vitro and *in vivo*. This novel protein, in addition to its neutralization of immunosuppressive checkpoint to promote CAR killing efficacy, possesses several advantages afforded by the single domain monobody scaffold, such as ease of folding due to lack of disulfide bonds, small molecular weight, and human origin, thus adding another tool to the immunotherapeutic arsenal.

To add another layer of precise control to the PDbody-CAR, its expression was controlled by a CD19-SynNotch receptor. Without CD19 or PD-L1 expression on target tumor cells, cytotoxicity was not observed (Figures 3.4B and S3.7). Upon SynNotch engagement, CAR is produced at the proximity of tumor regions where the clinically validated antigen can be potentially introduced to express in a subset of tumor cells as "training centers" through vaccination. This high precision together with the flexible introduction of a synthetic antigen can pave the road for combination therapies integrating CAR and tumor vaccination with a clinically-validated antigen such as CD19 for which the known side effect of B-cell aplasia was demonstrated manageable[51,52].

3.5: FIGURES

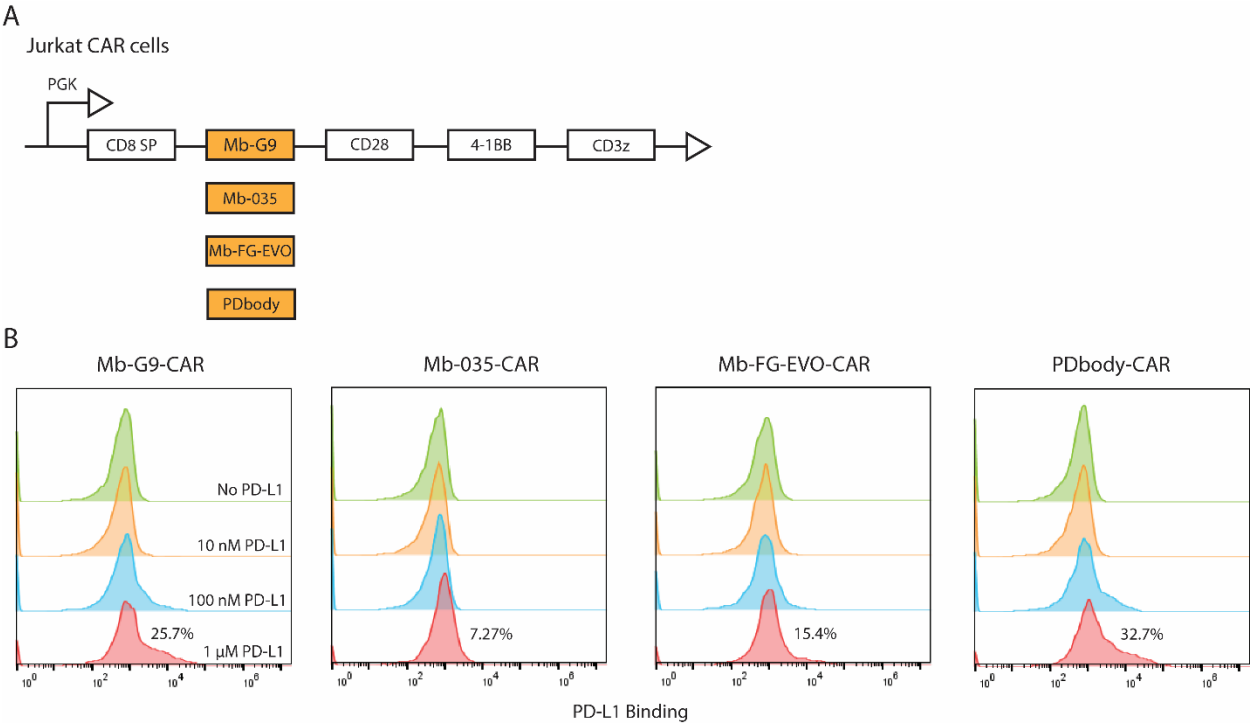

Figure 3.1: PD-L1 binding of monobody CAR variants

(A) Genetic cassettes for the monobody CAR constructs. Monobody variants were incorporated as receptor domains in a 3rd generation CAR design and introduced into Jurkat cells by lentivirus. **(B)** PD-L1 binding of monobody CARs. 10 nM, 100 nM, and 1 µM biotinylated PD-L1 and streptavidin-phycoerythrin were used to stain Jurkat-displayed monobody CARs in pH 7.4 PBS buffer.

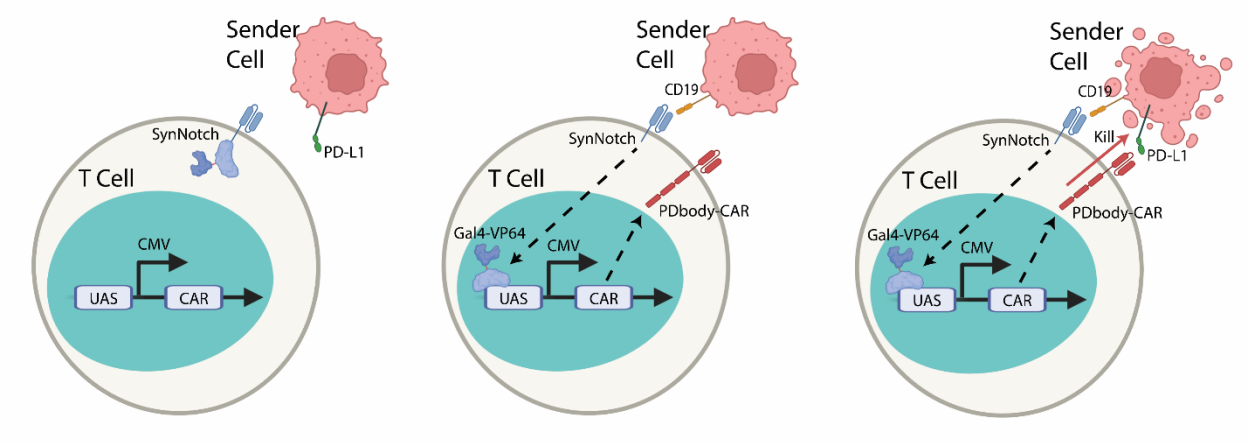

Figure 3.2: Schematic of CD19-SynNotch PDbody-CAR T cell killing

Schematic showing the AND-gate functionality of CD19-SynNotch PDbody-CAR. Only upon the expression of both antigens CD19 and PD-L1 is the tumor cell killed.

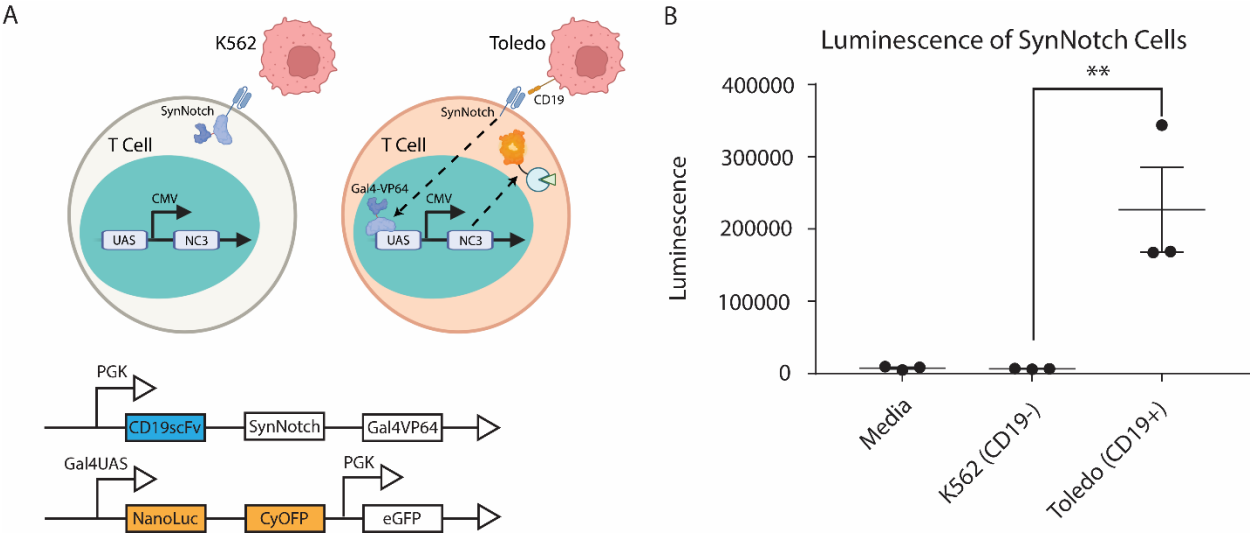

Figure 3.3: SynNotch construct verification

(A) αCD19 SynNotch receptor is used in combination with BRET luminescence in the reporter construct. Target cells used for verification are Toledo cells (CD19+) and K562 cells (CD19-). **(B)** Luminescence measurements of co-cultured SynNotch cells.

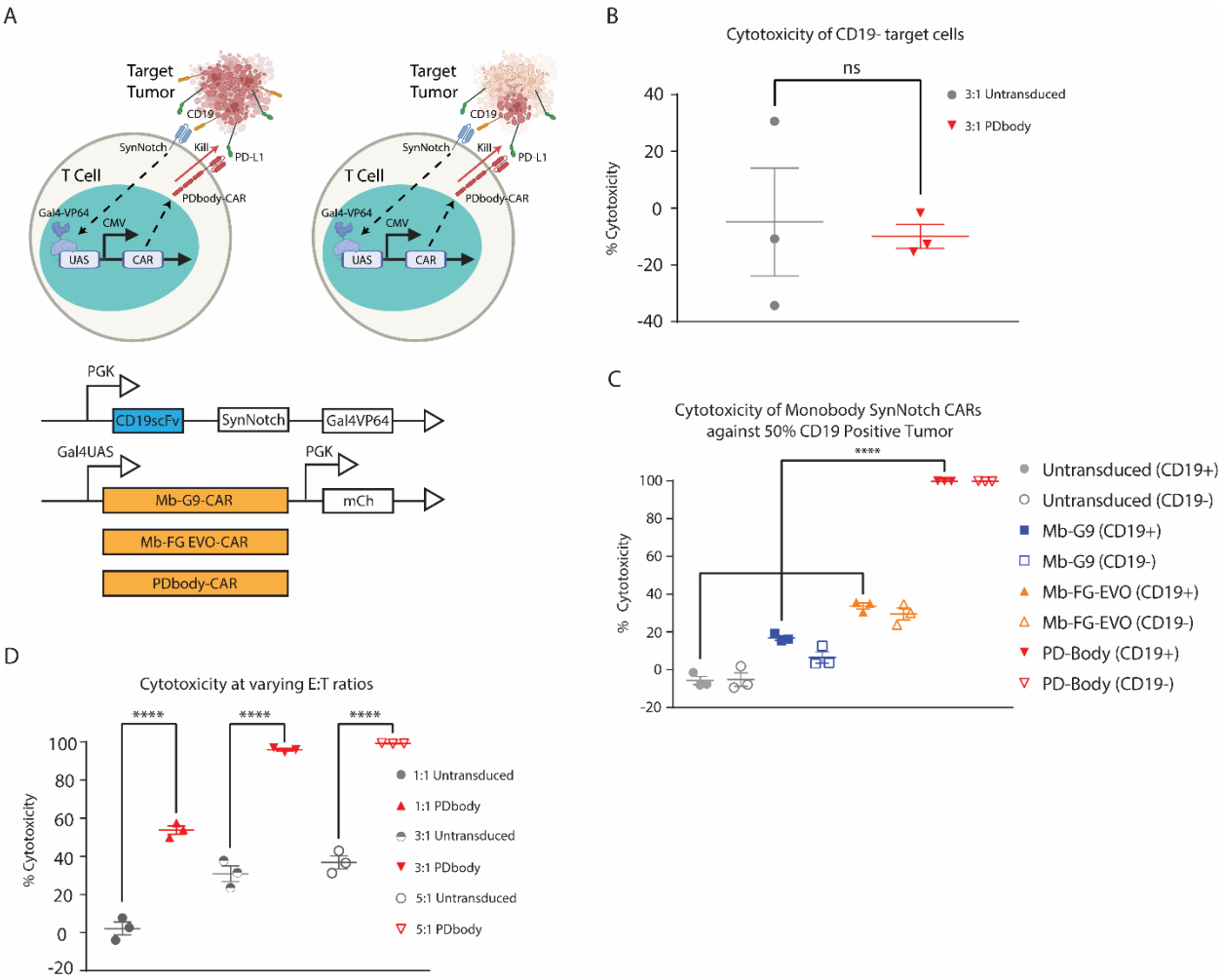

Figure 3.4: CD19-SynNotch PDbody-CAR *in vitro* killing assays

(A) Genetic cassettes used for killing assays. Monobody CARs were cloned into the SynNotch reporter construct. Co-cultures were performed with CD19+ MDA cells and CD19- MDA cells. **(B)** Killing assay of CD19-SynNotch PDbody-CAR T cells against CD19- MDA cells. Untransduced and CD19-SynNotch PDbody-CAR T cells were co-cultured with CD19- MDA cells in a 3:1 E:T ratio. Cytotoxicity of untransduced T cells is shown in light gray, cytotoxicity of CD19-SynNotch PDbody-CAR T cells is shown in red. **(C)** Cytotoxicity of CD19-SynNotch monobody-CARs. T cells were co-cultured for 24 hrs in a 3:1 ratio with a 1:1 mixture of CD19+ MDA cells and CD19- MDA cells. Cytotoxicity of untransduced cells, Mb-G9 CAR, Mb-FG-EVO CAR, and PDbody-CAR are shown in light gray, blue, orange, and red, respectively. **(D)** Cytotoxicity of CD19-SynNotch PDbody-CAR T cells at varying E:T ratios. Untransduced and CD19-SynNotch PDbody-CAR T cells were co-cultured with 100% CD19+ MDA cells at 1:1, 3:1, and 5:1 E:T ratios. Cytotoxicity of untransduced and CD19-SynNotch PDbody-CAR T cells is shown in light gray and red, respectively.

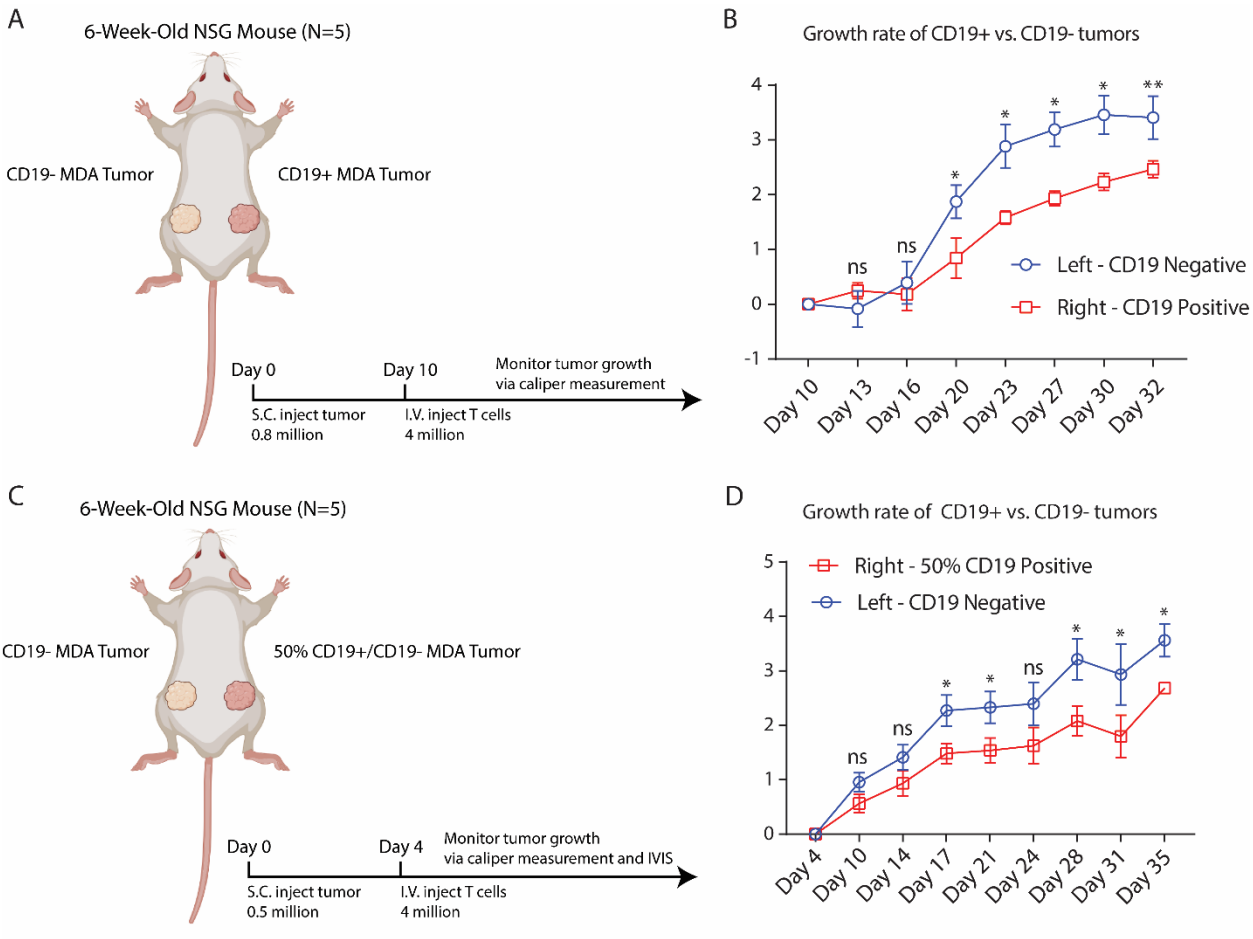

Figure 3.5: CD19-SynNotch PDbody-CAR suppresses tumor growth *in vivo*

(A) Experimental design for *in vivo* bilateral tumor mouse model. MDA-MB-231 tumor cells were injected into mice and were allowed to grow for 10 days at which point CD19-SynNotch PDbody-CAR T cells were injected intravenously. Tumor growth was monitored via caliper measurement. **(B)** Tumor growth rate as a function of time. Average tumor growth rate was monitored via caliper measurement (N=5). CD19- and CD19+ tumor growth rates are represented as lines in blue and red, respectively. **(C)** Experimental design for *in vivo* bilateral tumor mouse model with 1:1 CD19+/CD19- tumor mixtures. MDA-MB-231 tumor cells (Left: CD19- only; Right: 1:1 CD19+/CD19- mixture) were injected into mice and were allowed to grow for 4 days at which point CD19-SynNotch PDbody-CAR T cells were injected intravenously. Tumor growth was monitored via IVIS and caliper measurement. **(D)** Tumor growth rate as a function of time. Average tumor growth rate was monitored via caliper measurement (N=5). The growth curves of CD19- tumor cells on both sides are represented as lines in blue and red, respectively.

3.6: SUPPLEMENTARY FIGURES

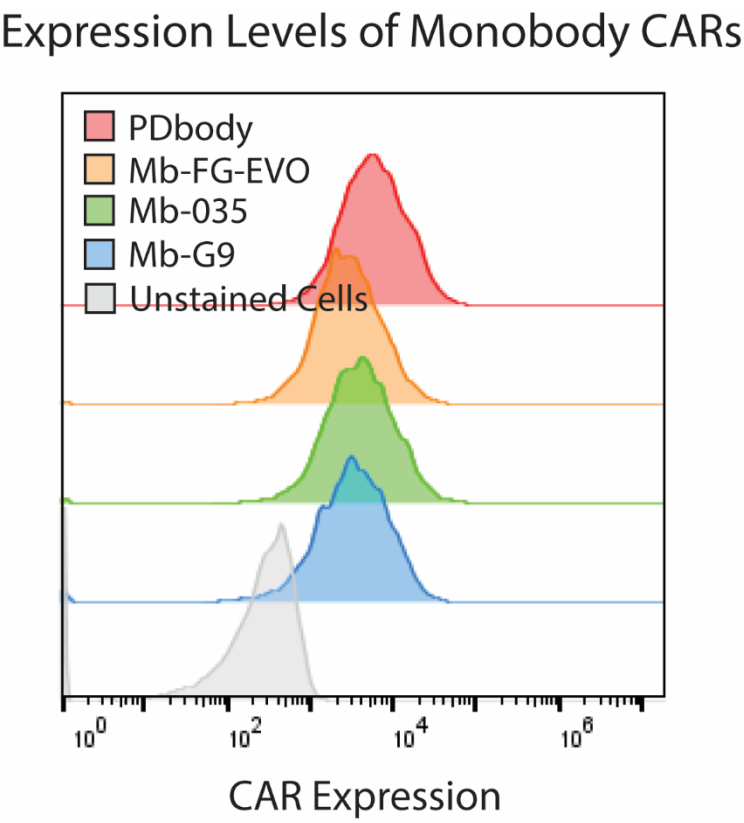

Figure S3.1: Expression levels of monobody CARs

FACS-sorted Jurkat cells expressing monobody CARs were labeled with anti-myc Alexa Fluor 647. CAR expression level of Mb-G9-CAR is shown in blue, CAR expression level of Mb-035 CAR is shown in green, CAR expression level of Mb-FG-EVO-CAR is shown in orange, and CAR expression level of PDbody-CAR is shown in red.

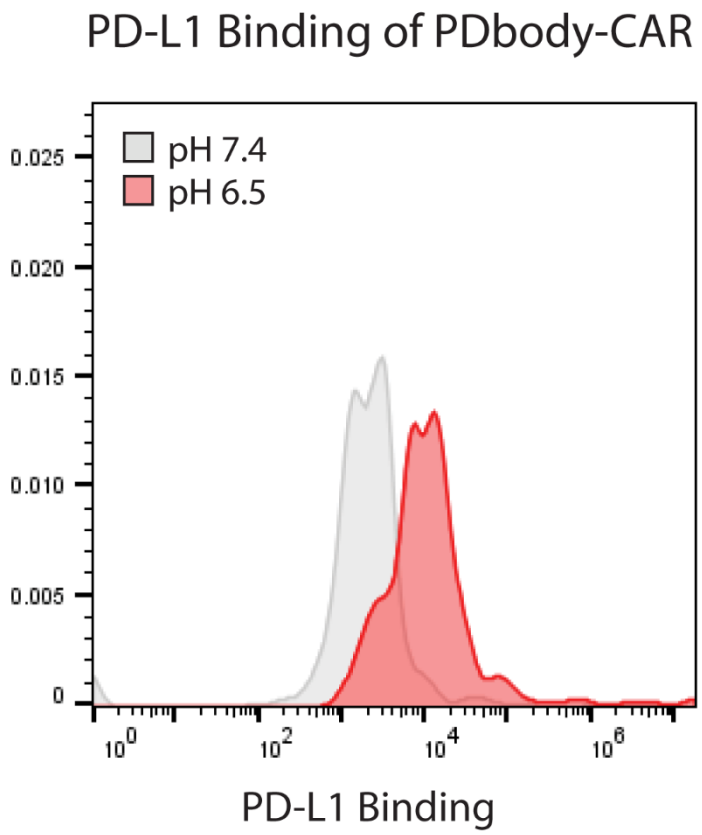

Figure S3.2: PD-L1 staining of PDbody-CAR-expressing Jurkat cells

Equal numbers of PDbody-CAR cells were stained with 1.675 µM PD-L1 and SA-PE and washed in either pH 7.4 PBS or pH 6.5 PBS (30 mL PBS acidified with 14 µL 10M HCl).

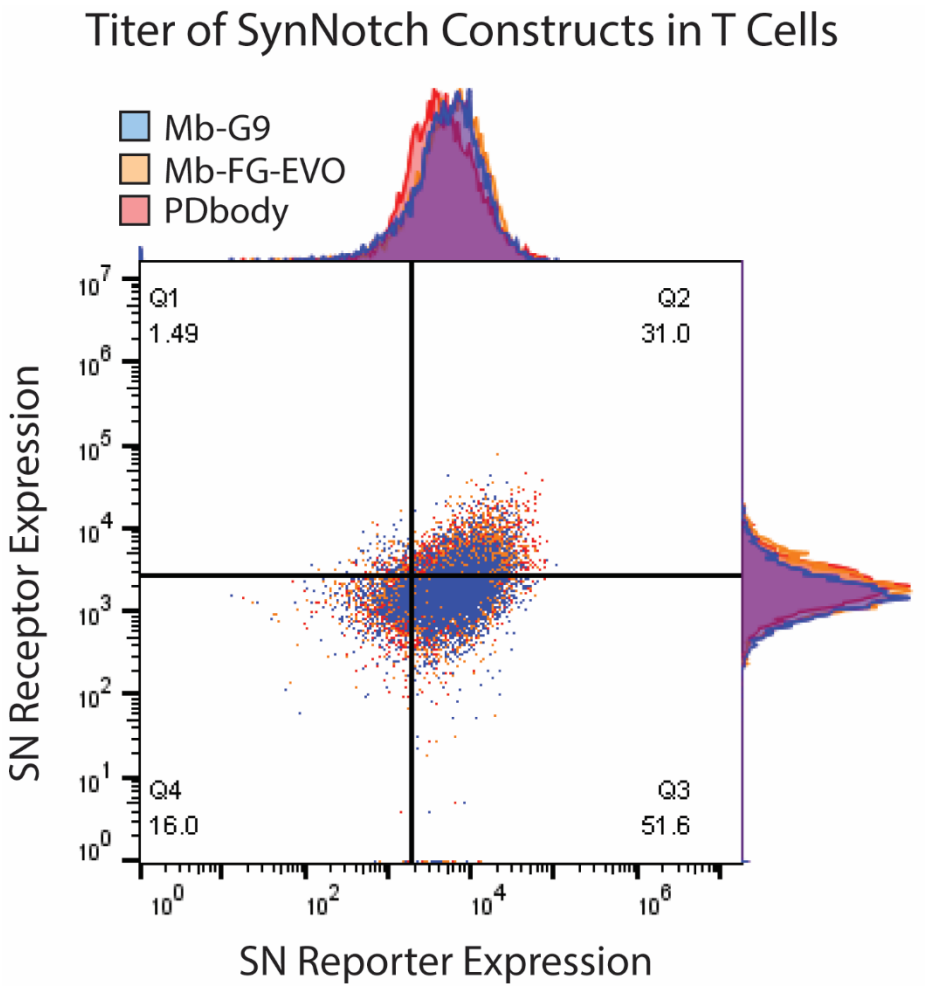

Figure S3.3: Expression levels of SynNotch constructs in T cells

αCD19 SynNotch monobody CAR constructs were detected via anti-myc Alexa Fluor 647 staining for the SynNotch receptor and mCherry expression for the SynNotch reporter.

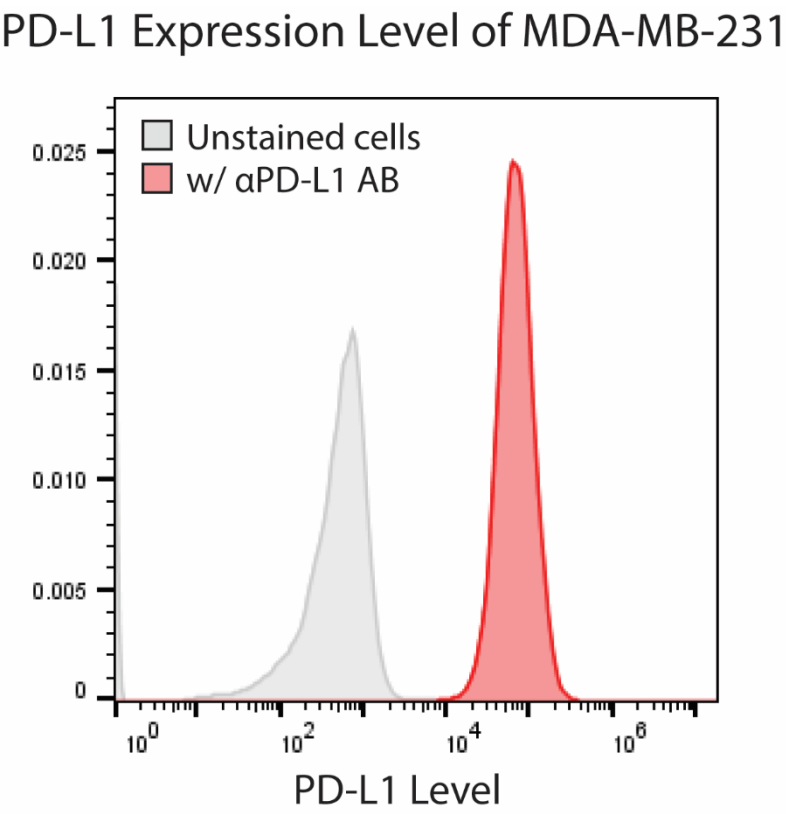

Figure S3.4: Measurement of PD-L1 expression in MDA-MB-231 cells

MDA-MB-231 cells were stained with anti-PD-L1 APC antibody to verify PD-L1 expression levels.

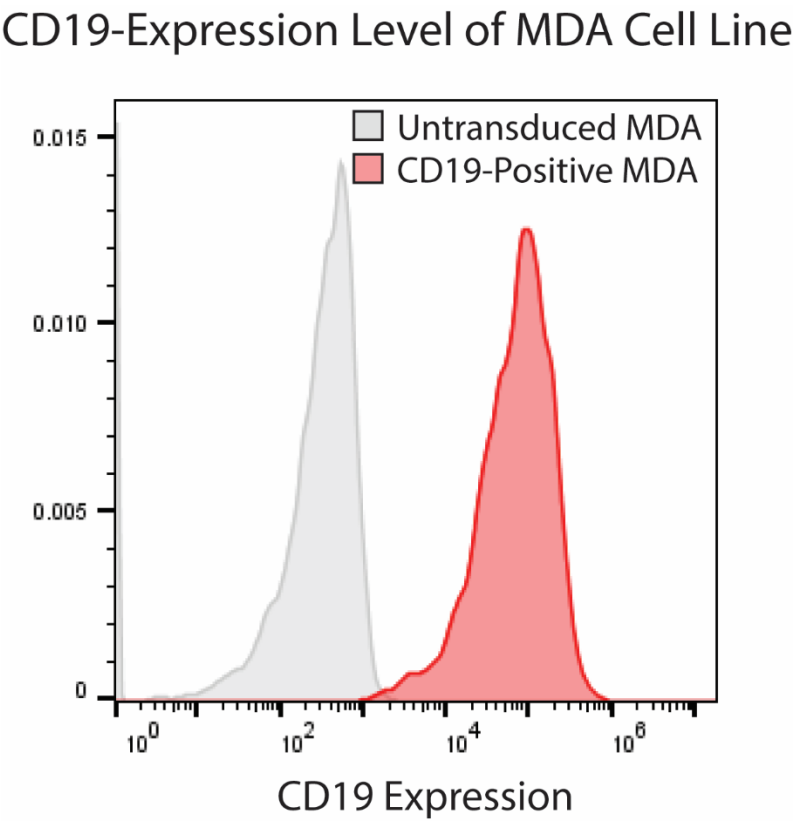

Figure S3.5: Measurement of CD19 expression level in MDA cell line

Lentivirally transduced and FACS-sorted MDA cells were stained with anti-CD19 Alexa Fluor 647 antibody to determine CD19 levels.

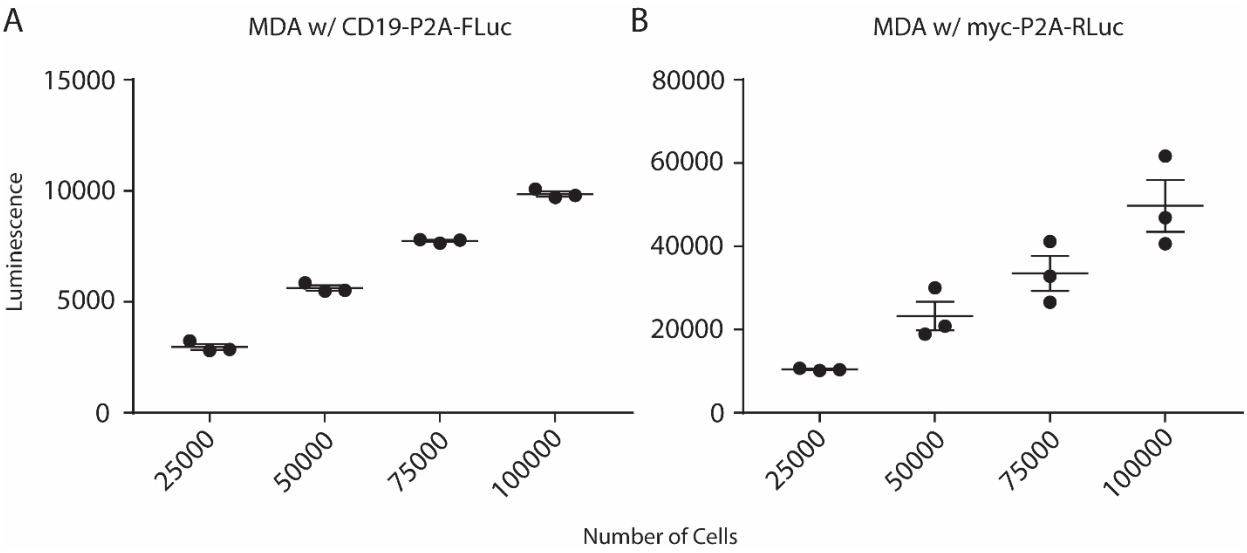

Figure S3.6: Bioluminescence standard measurement of MDA target cell lines

Luminescence of standard numbers of MDA cells were measured using **(A)** firefly luciferase substrate for the CD19+ cell line (MDA w/ CD19-P2A-FLuc) and **(B)** Renila luciferase substrate for the CD19- cell line (MDA w/ myc-P2A-RLuc).

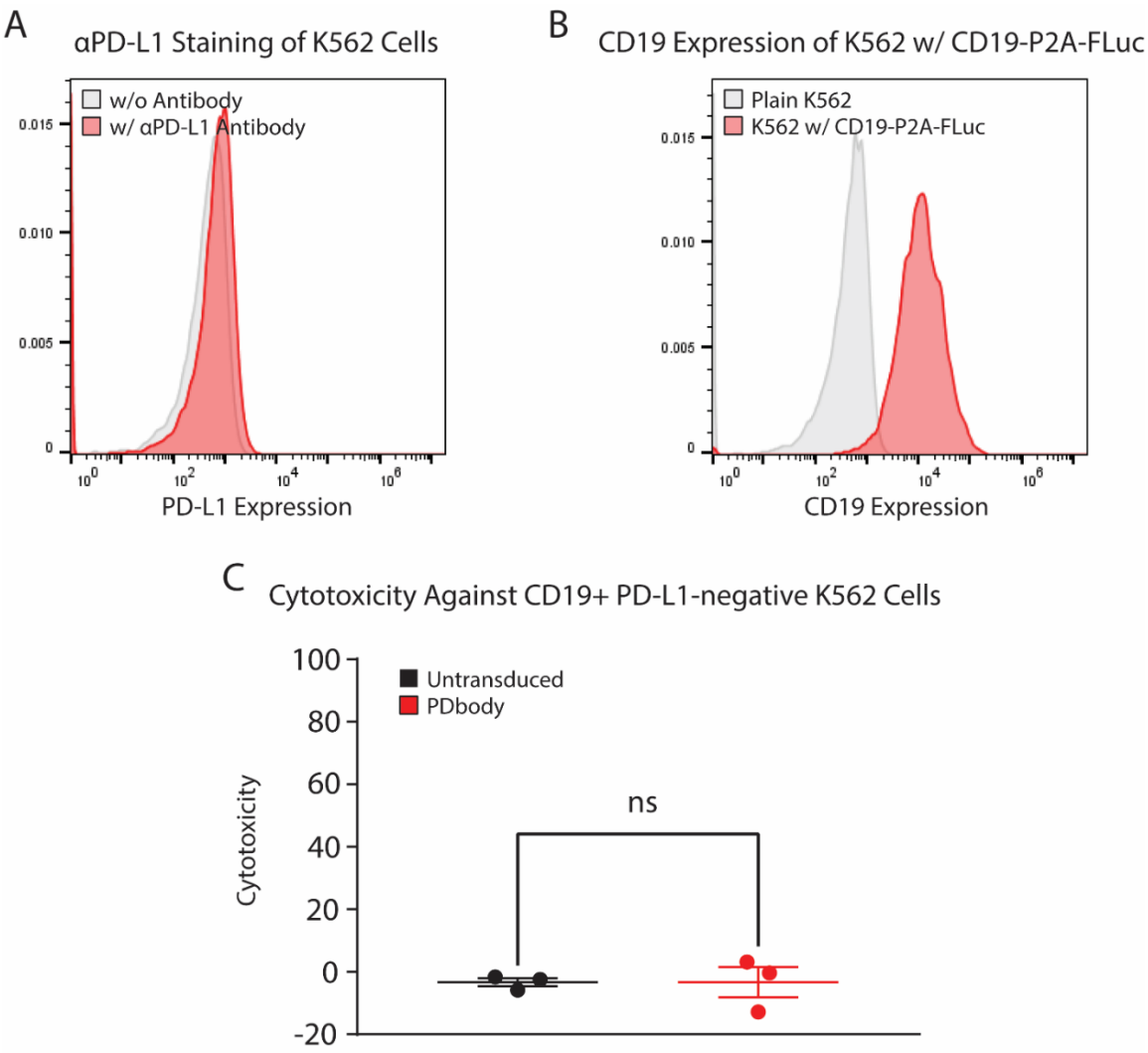

Figure S3.7. Control experiment demonstrating that there is no CD19-SynNotch PDbody-CAR cytotoxicity against CD19-positive but PD-L1-negative K562 cells

(A) PD-L1 expression level was measured in K562 cells with anti-PD-L1 APC antibody staining. **(B)** CD19 expression of CD19+ K562 cell line was measured via anti-CD19 Alexa Fluor 647 antibody staining. **(C)** Killing assay was performed against CD19+ PD-L1- K562 cells at a 1:1 E:T ratio. Cytotoxicity of untransduced T cells is shown in black, and cytotoxicity of CD19-SynNotch PDbody-CAR T cells is shown in red.

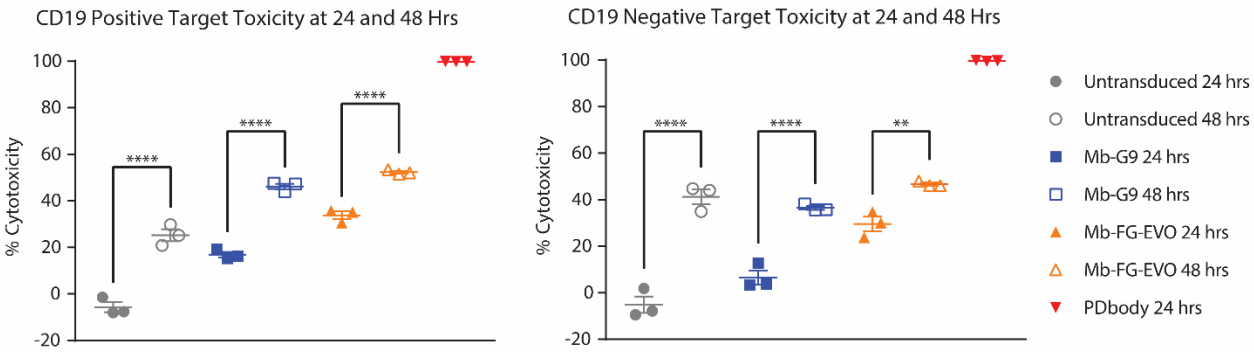

Figure S3.8: Killing assay of CD19-SynNotch monobody-CARs at 24 and 48 hrs

Luminescence was measured 24 and 48 hrs after co-culture for each of the different groups. Measurements were performed in triplicate. Cytotoxicity of untransduced T cells is shown in light gray, cytotoxicity of CD19-SynNotch Mb-G9-CAR T cells is shown in blue, cytotoxicity of CD19-SynNotch Mb-FG-EVO-CAR T cells is shown in orange, and cytotoxicity of CD19-SynNotch PDbody-CAR T cells is show in red.

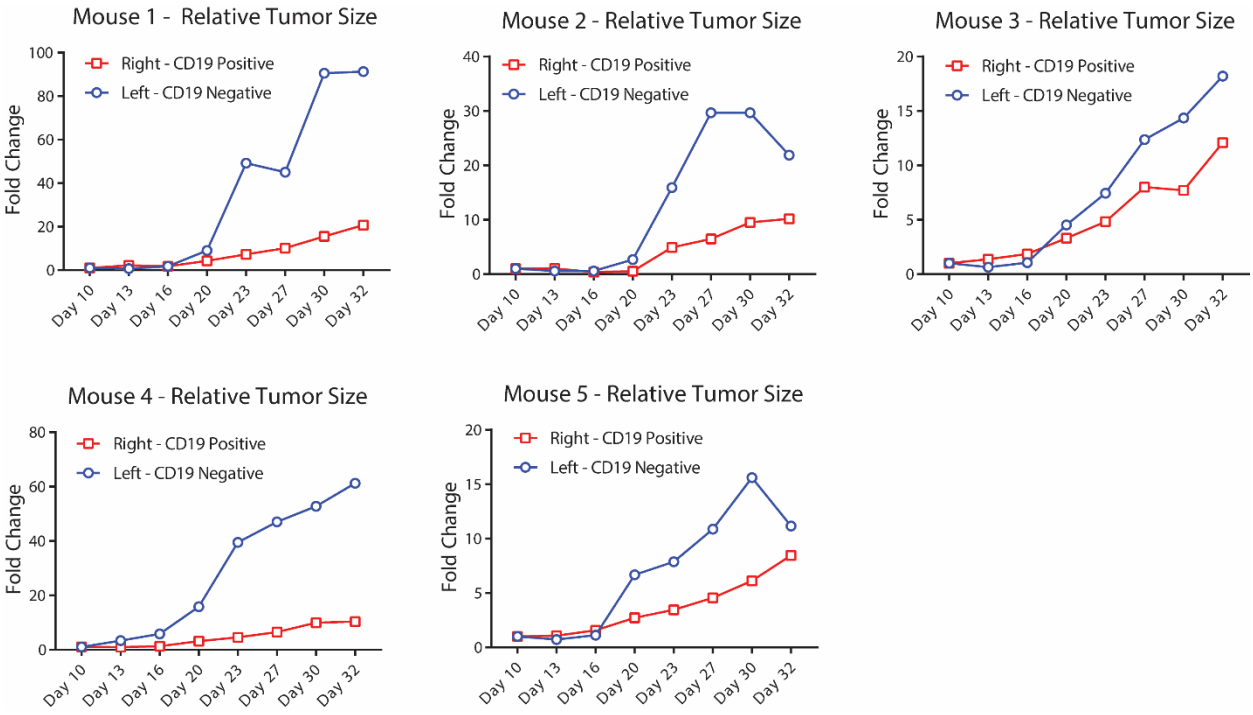

Figure S3.9: Relative tumor size measurements for individual mice in *in vivo* bilateral tumor model

CD19- tumors are shown in blue, and CD19+ tumors are shown in red.

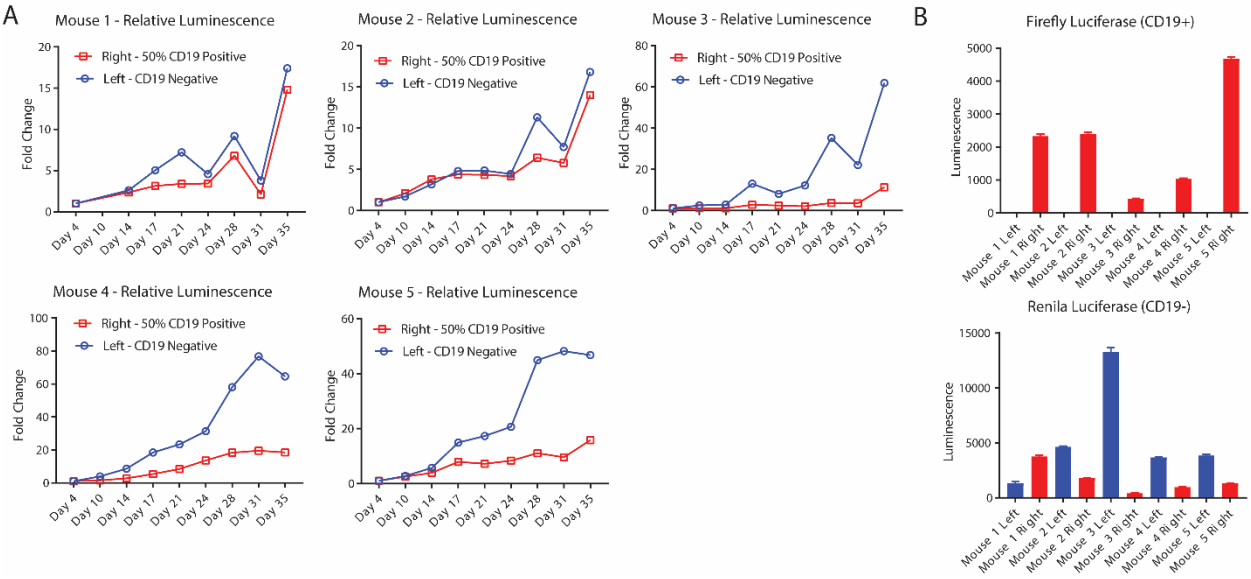

Figure S3.10: Measurements for 50% CD19+ in vivo experiment

(A) Relative luminescence of individual mice. Renila luciferase readings were normalized with Day 4 measurements. **(B)** Platereader measurements for extracted tumor cells at Day 35 after tumor injection. Tumor cells underwent DNAse and collagenase digestion and red blood cell lysis. Luciferase measurements were taken using the Dual Glo kit on 0.2 million cells in triplicate from each tumor.

ACKNOWLEDGEMENTS

Chapter 3, in part has been submitted for publication of the material as it may appear in ACS Central Science. Man, Chi-Wei; Zhu, Linshan; Harrison, Reed; Peng, Qin; Limsakul, Praopim; Hashimoto, Matthew; Mamaril, Anthony; Xu, Hongquan; Wang, Yingxiao. "Engineering a PD-L1-targeting Monobody via Directed Evolution for SynNotch-Gated Cancer Immunotherapy". The dissertation author was the primary researcher and author of this paper.

Figures 3.2, 3.3A, 3.4A, 3.5A, and 3.5C were created with Biorender.com.

This work was supported in part by grants from NIH R01 CA262815, EB029122, R35 GM140929, R01 HL121365, and HD107206 (Y.W.).

REFERENCES

1. Brentjens, R. J., Davila, M. L., Riviere, I., Park, J., Wang, X., Cowell, L. G., Bartido, S., Stefanski, J., Taylor, C., Olszewska, M., Borquez-Ojeda, O., Qu, J., Wasielewska, T., He, Q., Bernal, Y., Rijo, I. V., Hedvat, C., Kobos, R., Curran, K., *et al.* CD19-targeted T cells rapidly induce molecular remissions in adults with chemotherapy-refractory acute lymphoblastic leukemia. *Sci. Transl. Med.* **5**, (2013).

2. Mullard, A. FDA approves first CAR T therapy. *Nat. Rev. Drug Discov.* **16**, 669 (2017).

3. Pulè, M. A., Straathof, K. C., Dotti, G., Heslop, H. E., Rooney, C. M. & Brenner, M. K. A chimeric T cell antigen receptor that augments cytokine release and supports clonal expansion of primary human T cells. *Mol. Ther.* **12**, 933–941 (2005).

4. Sadelain, M., Brentjens, R. & Rivière, I. The basic principles of chimeric antigen receptor design. *Cancer Discov.* **3**, 388–398 (2013).

5. Feucht, J., Sun, J., Eyquem, J., Ho, Y. J., Zhao, Z., Leibold, J., Dobrin, A., Cabriolu, A., Hamieh, M. & Sadelain, M. Calibration of CAR activation potential directs alternative T cell fates and therapeutic potency. *Nat. Med.* **25**, 82–88 (2019).

6. Ramello, M. C., Benzaïd, I., Kuenzi, B. M., Lienlaf-Moreno, M., Kandell, W. M., Santiago, D. N., Pabón-Saldaña, M., Darville, L., Fang, B., Rix, U., Yoder, S., Berglund, A., Koomen, J. M., Haura, E. B. & Abate-Daga, D. An immunoproteomic approach to characterize the CAR interactome and signalosome. *Sci. Signal.* **12**, 1–16 (2019).

7. Hou, A. J., Chen, L. C. & Chen, Y. Y. Navigating CAR-T cells through the solid-tumour microenvironment. *Nat. Rev. Drug Discov.* **20**, 531–550 (2021).

8. Quail, D. F. & Joyce, J. A. Microenvironmental regulation of tumor progression and metastasis. *Nat. Med.* **19**, 1423–1437 (2013).

9. Binnewies, M., Roberts, E. W., Kersten, K., Chan, V., Fearon, D. F., Merad, M., Coussens, L. M., Gabrilovich, D. I., Ostrand-Rosenberg, S., Hedrick, C. C., Vonderheide, R. H., Pittet, M. J., Jain, R. K., Zou, W., Howcroft, T. K., Woodhouse, E. C., Weinberg, R. A. & Krummel, M. F. Understanding the tumor immune microenvironment (TIME) for effective therapy. *Nat. Med.* **24**, 541–550 (2018).

10. Sharpe, A. H. & Pauken, K. E. The diverse functions of the PD1 inhibitory pathway. *Nat. Rev. Immunol.* **18**, 153–167 (2018).

11. Sun, C., Mezzadra, R. & Schumacher, T. N. Regulation and Function of the PD-L1 Checkpoint. *Immunity* vol. 48 434–452 at https://doi.org/10.1016/j.immuni.2018.03.014 (2018).

12. Cercek, A., Lumish, M., Sinopoli, J., Weiss, J., Shia, J., Lamendola-Essel, M., El Dika, I. H., Segal, N., Shcherba, M., Sugarman, R., Stadler, Z., Yaeger, R., Smith, J. J., Rousseau, B., Argiles, G., Patel, M., Desai, A., Saltz, L. B., Widmar, M., *et al.* PD-1 Blockade in Mismatch Repair-Deficient, Locally Advanced Rectal Cancer. *N. Engl. J. Med.* 2363–2376 (2022) doi:10.1056/NEJMoa2201445.

13. Topalian, S. L., Drake, C. G. & Pardoll, D. M. Targeting the PD-1/B7-H1(PD-L1) pathway to activate anti-tumor immunity. *Curr. Opin. Immunol.* **24**, 207–212 (2012).

14. Cherkassky, L., Morello, A., Villena-Vargas, J., Feng, Y., Dimitrov, D. S., Jones, D. R., Sadelain, M. & Adusumilli, P. S. Human CAR T cells with cell-intrinsic PD-1 checkpoint blockade resist tumor-mediated inhibition. *J. Clin. Invest.* **126**, 3130–3144 (2016).

15. Chong, E. A., Svoboda, J., Dwivedy Nasta, S., Landsburg, D. J., Winchell, N., Napier, E., Mato, A. R., Melenhorst, J. J., Ruella, M., Lacey, S. F., June, C. H. & Schuster, S. J. Sequential Anti-CD19 Directed Chimeric Antigen Receptor Modified T-Cell Therapy (CART19) and PD-1 Blockade with Pembrolizumab in Patients with Relapsed or Refractory B-Cell Non-Hodgkin Lymphomas. *Blood* **132**, 4198–4198 (2018).

16. Hirayama, A. V., Gauthier, J., Hay, K. A., Sheih, A., Cherian, S., Chen, X., Pender, B. S., Hawkins, R. M., Vakil, A., Steinmetz, R. N., Phi, T.-D., Chapuis, A. G., Till, B. G., Kiem, H.-P., Shadman, M., Cassaday, R. D., Acharya, U. H., Riddell, S. R., Maloney, D. G., *et al.* Efficacy and Toxicity of JCAR014 in Combination with Durvalumab for the Treatment of Patients with Relapsed/Refractory Aggressive B-Cell Non-Hodgkin Lymphoma. *Blood* **132**, 1680–1680 (2018).

17. Neelapu, S. S., Tummala, S., Kebriaei, P., Wierda, W., Gutierrez, C., Locke, F. L., Komanduri, K. V., Lin, Y., Jain, N., Daver, N., Westin, J., Gulbis, A. M., Loghin, M. E., De Groot, J. F., Adkins, S., Davis, S. E., Rezvani, K., Hwu, P. & Shpall, E. J. Chimeric antigen receptor T-cell therapy-assessment and management of toxicities. *Nat. Rev. Clin. Oncol.* **15**, 47–62 (2018).

18. Hay, K. A., Hanafi, L. A., Li, D., Gust, J., Liles, W. C., Wurfel, M. M., López, J. A., Chen, J., Chung, D., Harju-Baker, S., Cherian, S., Chen, X., Riddell, S. R., Maloney, D. G. & Turtle, C. J. Kinetics and biomarkers of severe cytokine release syndrome after CD19 chimeric antigen receptor–modified T-cell therapy. *Blood* **130**, 2295–2306 (2017).

19. Gust, J., Taraseviciute, A. & Turtle, C. J. Neurotoxicity Associated with CD19-Targeted CAR-T Cell Therapies. *CNS Drugs* **32**, 1091–1101 (2018).

20. Parker, K. R., Migliorini, D., Perkey, E., Yost, K. E., Bhaduri, A., Bagga, P., Haris, M., Wilson, N. E., Liu, F., Gabunia, K., Scholler, J., Montine, T. J., Bhoj, V. G., Reddy, R., Mohan, S., Maillard, I., Kriegstein, A. R., June, C. H., Chang, H. Y., *et al.* Single-Cell Analyses Identify Brain Mural Cells Expressing CD19 as Potential Off-Tumor Targets for CAR-T Immunotherapies. *Cell* **183**, 126-142.e17 (2020).

21. Morgan, R. A., Yang, J. C., Kitano, M., Dudley, M. E., Laurencot, C. M. & Rosenberg, S. A. Case report of a serious adverse event following the administration of t cells transduced with a chimeric antigen receptor recognizing ERBB2. *Mol. Ther.* **18**, 843–851 (2010).

22. Xie, Y. J., Dougan, M., Jailkhani, N., Ingram, J., Fang, T., Kummer, L., Momin, N., Pishesha, N., Rickelt, S., Hynes, R. O. & Ploegh, H. Nanobody-based CAR T cells that target the tumor microenvironment inhibit the growth of solid tumors in immunocompetent mice. *Proc. Natl. Acad. Sci. U. S. A.* **116**, 7624–7631 (2019).

23. Boedtkjer, E. & Pedersen, S. F. The Acidic Tumor Microenvironment as a Driver of Cancer. *Annu. Rev. Physiol.* **82**, 103–126 (2020).

24. Koide, a, Bailey, C. W., Huang, X. & Koide, S. The fibronectin type III domain as a scaffold for novel binding proteins. *J. Mol. Biol.* **284**, 1141–51 (1998).

25. Koide, S., Koide, A. & Lipovšek, D. Target-binding proteins based on the 10th human fibronectin type III domain (10 Fn3). *Methods Enzymol.* **503**, 135–156 (2012).

26. Koide, A., Wojcik, J., Gilbreth, R. N., Hoey, R. J. & Koide, S. Teaching an old scaffold new tricks: Monobodies constructed using alternative surfaces of the FN3 scaffold. *J. Mol. Biol.* **415**, 393–405 (2012).

27. Bos, T. J., De Bruyne, E., Van Lint, S., Heirman, C. & Vanderkerken, K. Large double copy vectors are functional but show a size-dependent decline in transduction efficiency. *J. Biotechnol.* **150**, 37–40 (2010).

28. Ajina, A. & Maher, J. *Strategies to address chimeric antigen receptor tonic signalling*. vol. 17 (2019).

29. Lerner, R. A. Combinatorial antibody libraries: New advances, new immunological insights. *Nat. Rev. Immunol.* **16**, 498–508 (2016).

30. Wörn, A. & Plückthun, A. Stability engineering of antibody single-chain Fv fragments. *J. Mol. Biol.* **305**, 989–1010 (2001).

31. Sun, W., Xie, J., Lin, H., Mi, S., Li, Z., Hua, F. & Hu, Z. A combined strategy improves the solubility of aggregation-prone single-chain variable fragment antibodies. *Protein Expr. Purif.* **83**, 21–29 (2012).

32. Wörn, A. & Plückthun, A. Different equilibrium stability behavior of scFv fragments: Identification, classification, and improvement by protein engineering. *Biochemistry* **38**, 8739–8750 (1999).

33. Han, X., Cinay, G. E., Zhao, Y., Guo, Y., Zhang, X. & Wang, P. Adnectin-Based Design of Chimeric Antigen Receptor for T Cell Engineering. *Mol. Ther.* **25**, 2466–2476 (2017).

34. Park, S., Shevlin, E., Vedvyas, Y., Zaman, M., Park, S., Hsu, Y. M. S., Min, I. M. & Jin, M. M. Micromolar affinity CAR T cells to ICAM-1 achieves rapid tumor elimination while avoiding systemic toxicity. *Sci. Rep.* **7**, 1–15 (2017).

35. Ghorashian, S., Kramer, A. M., Onuoha, S., Wright, G., Bartram, J., Richardson, R., Albon, S. J., Casanovas-Company, J., Castro, F., Popova, B., Villanueva, K., Yeung, J., Vetharoy, W., Guvenel, A., Wawrzyniecka, P. A., Mekkaoui, L., Cheung, G. W. K., Pinner, D., Chu, J., *et al.* Enhanced CAR T cell expansion and prolonged persistence in pediatric patients with ALL treated with a low-affinity CD19 CAR. *Nat. Med.* **25**, 1408–1414 (2019).

36. Liu, X., Jiang, S., Fang, C., Yang, S., Olalere, D., Pequignot, E. C., Cogdill, A. P., Li, N., Ramones, M., Granda, B., Zhou, L., Loew, A., Young, R. M., June, C. H. & Zhao, Y. Affinity-tuned ErbB2 or EGFR chimeric antigen receptor T cells exhibit an increased therapeutic index against tumors in mice. *Cancer Res.* **75**, 3596–3607 (2015).

37. Caruso, H. G., Hurton, L. V., Najjar, A., Rushworth, D., Ang, S., Olivares, S., Mi, T., Switzer, K., Singh, H., Huls, H., Lee, D. A., Heimberger, A. B., Champlin, R. E. & Cooper, L. J. N. Tuning sensitivity of CAR to EGFR density limits recognition of normal tissue while maintaining potent antitumor activity. *Cancer Res.* **75**, 3505–3518 (2015).

38. Wu, R., Wang, C., Li, Z., Xiao, J., Li, C., Wang, X., Kong, P., Cao, J., Huang, F., Li, Z., Huang, Y., Chen, Y., Li, X., Yang, D., Zhang, H., Mai, J., Feng, G., Deng, R. & Zhu, X. SOX2 promotes resistance of melanoma with PD-L1 high expression to T-cell-mediated cytotoxicity that can be reversed by SAHA. *J. Immunother. cancer* **8**, e001037 (2020).

39. Morsut, L., Roybal, K. T., Xiong, X., Gordley, R. M., Coyle, S. M., Thomson, M. & Lim, W. A. Engineering Customized Cell Sensing and Response Behaviors Using Synthetic Notch Receptors. *Cell* **164**, 780–791 (2016).

40. Roybal, K. T., Rupp, L. J., Morsut, L., Walker, W. J., McNally, K. A., Park, J. S. & Lim, W. A. Precision Tumor Recognition by T Cells with Combinatorial Antigen-Sensing Circuits. *Cell* **164**, 770–779 (2016).

41. Roybal, K. T., Williams, J. Z., Morsut, L., Rupp, L. J., Kolinko, I., Choe, J. H., Walker, W. J., McNally, K. A. & Lim, W. A. Engineering T Cells with Customized Therapeutic Response Programs Using Synthetic Notch Receptors. *Cell* **167**, 419-432.e16 (2016).

42. O'Donoghue, G. P., Bugaj, L. J., Anderson, W., Daniels, K. G., Rawlings, D. J. & Lim, W. A. T cells selectively filter oscillatory signals on the minutes timescale. *Proc. Natl. Acad. Sci. U. S. A.* **118**, (2021).

43. Hernandez-Lopez, R. A., Yu, W., Cabral, K. A., Creasey, O. A., del Pilar Lopez Pazmino, M., Tonai, Y., de Guzman, A., Mäkelä, A., Saksela, K., Gartner, Z. J. & Lim, W. A. T cell circuits that sense antigen density with an ultrasensitive threshold. *Science (80-.).* **371**, 1166–1171 (2021).

44. Hyrenius-Wittsten, A., Su, Y., Park, M., Garcia, J. M., Alavi, J., Perry, N., Montgomery, G., Liu, B. & Roybal, K. T. SynNotch CAR circuits enhance solid tumor recognition and promote persistent antitumor activity in mouse models. *Sci. Transl. Med.* **13**, (2021).

45. Choe, J. H., Watchmaker, P. B., Simic, M. S., Gilbert, R. D., Li, A. W., Krasnow, N. A., Downey, K. M., Yu, W., Carrera, D. A., Celli, A., Cho, J., Briones, J. D., Duecker, J. M., Goretsky, Y. E., Dannenfelser, R., Cardarelli, L., Troyanskaya, O., Sidhu, S. S., Roybal, K. T., *et al. SynNotch-CAR T cells overcome challenges of specificity, heterogeneity, and persistence in treating glioblastoma*. *Sci. Transl. Med* vol. 13 www.humanproteomemap.org (2021).

46. Chu, J., Oh, Y., Sens, A., Ataie, N., Dana, H., Macklin, J. J., Laviv, T., Welf, E. S., Dean, K. M., Zhang, F., Kim, B. B., Tang, C. T., Hu, M., Baird, M. A., Davidson, M. W., Kay, M. A., Fiolka, R., Yasuda, R., Kim, D. S., *et al.* A bright cyan-excitable orange fluorescent protein facilitates dual-emission microscopy and enhances bioluminescence imaging in vivo. *Nat. Biotechnol.* **34**, 760–767 (2016).

47. Liu, H., Zang, C., Fenner, M. H., Possinger, K. & Elstner, E. PPARgamma ligands and ATRA inhibit the invasion of human breast cancer cells in vitro. *Breast Cancer Res. Treat.* **79**, 63–74 (2003).

48. Chavez, K. J., Garimella, S. V & Lipkowitz, S. Triple negative breast cancer cell lines: one tool in the search for better treatment of triple negative breast cancer. *Breast Dis.* **32**, 35–48 (2010).

49. Zak, K. M., Kitel, R., Przetocka, S., Golik, P., Guzik, K., Musielak, B., Dömling, A., Dubin, G. & Holak, T. A. Structure of the Complex of Human Programmed Death 1, PD-1, and Its Ligand PD-L1. *Structure* **23**, 2341–2348 (2015).

50. Maute, R. L., Gordon, S. R., Mayer, A. T., McCracken, M. N., Natarajan, A., Ring, N. G., Kimura, R., Tsai, J. M., Manglik, A., Kruse, A. C., Gambhir, S. S., Weissman, I. L. & Ring, A. M. Engineering high-affinity PD-1 variants for optimized immunotherapy and immuno-PET imaging. *Proc. Natl. Acad. Sci. U. S. A.* **112**, E6506–E6514 (2015).

51. Liu, Y., Chen, X., Han, W. & Zhang, Y. Tisagenlecleucel, an approved anti-CD19 chimeric antigen receptor T-cell therapy for the treatment of leukemia. *Drugs Today (Barc).* **53**, 597–608 (2017).

52. Sharma, P., King, G. T., Shinde, S. S., Purev, E. & Jimeno, A. Axicabtagene ciloleucel for

the treatment of relapsed/refractory B-cell non-Hodgkin's lymphomas. *Drugs Today (Barc).* **54**, 187–198 (2018).

CHAPTER 4

INDUCIBLE CIS ACTIVATION DRIVES CAR T CELL FUNCTION AGAINST HETEROGENEOUS AND ANTIGEN NEGATIVE TUMORS

4.1: INTRODUCTION

Chimeric Antigen Receptor T cells (CAR T cells) are recent and novel therapeutics that have demonstrated efficacy in treating hematological cancers[1]. Comprising an extracellular antigen recognition domain, a hinge domain, a transmembrane domain, a co-stimulatory domain, and a signaling domain, CAR T cells recognize and target tumor cells expressing a specific antigen of interest[2,3]. CAR T cells targeting CD19 were the first to be FDA approved[4], and to this date, CD19 CARs have been the most widely and successfully used. Despite this widespread success, CAR T cell therapy is still susceptible to failure due to tumor antigen escape, in which tumor cells re-propagate absent of the antigen of interest[5]. Thus, different engineering strategies are necessary to circumvent tumor antigen escape.

Currently, various engineering strategies exist to work around the problem of antigen loss. Tandem CAR's (TanCAR's) target two different antigens, so if one is lost, the tumor can still be targeted via the second[6,7]. T cells have been engineered to express immune stimulatory molecules, so they can elicit cytotoxicity even in absence of antigen of interest, a strategy known as "armored CAR"[8]. Also, antigen expression levels can be increased in the tumor cells of interest via combination therapy with oncolytic viruses[9].

Here, we present a more universally applicable and controllable way to mitigate tumor antigen loss: heat-inducible cis-activated CAR (CisCAR). In this novel strategy, heat is used to activate CAR by driving expression of CD19 antigen in the CD19scFv CAR itself[10]. Compared to the TanCAR strategy, CisCAR is more universally applicable, compared to the armored CAR

strategy, CisCAR can be more locally targeted, and compared to the tumor engineering strategy, CisCAR is simpler to implement. Overall, heat-inducible CisCAR should provide a useful tool for CAR T cell therapy to combat antigen loss.

4.2: MATERIALS AND METHODS

4.2.1: Molecular cloning

Plasmids were generated using Gibson Assembly (NEB, E2611L), T4 ligation (NEB, M0202L), and golden gate assembly (Thermo Scientific, FERER0452). PCR was performed using Q5 DNA polymerase (NEB, M0491) and synthesized primers (Integrated DNA Technologies). Constructs were verified by Sanger sequencing (Azenta).

4.2.2: General mammalian cell culture

Human embryonic kidney (HEK293T) and MDA-MB-231 cells were cultured in Dulbecco's Modified Eagle Medium (DMEM) (Gibco, 11995115) with 10% fetal bovine serum (FBS) (Gibco, 10438026) and 1% penicillin-streptomycin (P/S) (Gibco, 15140122). Jurkat and K562 cells were cultured in Roswell Park Memorial Institute Medium (RPMI 1640) (Gibco, 22400105) with 10% FBS and 1% P/S. Primary human T cells were cultured in complete RPMI 1640 supplemented with 100 U mL^{-1} recombinant human IL-2 (PeproTech, 200-02). All cell types were cultured at 37˚C in a humidified 5% CO_2 incubator.

4.2.3: SynNotch bioluminescence assays

$2*10^5$ SynNotch Jurkat cells were cultured with $2*10^5$ sender cells in 150 μL RPMI. Cells were spun down at 400g for one min and incubated together for 24 hrs. After co-culture, Nano-Glo Luciferase Assay (Promega, 1110) was used to measure NC3 reporter expression using detection by platereader.

4.2.4: Microscopy, image acquisition, and analysis

Virally transduced HEK293T cells were cultured on 20 μg/mL fibronectin coated glass bottom dishes (Ningbo, DISH1315) and imaged with a Nikon Eclipse Ti inverted microscope. For the heat shock experiment, cells were heated for 15 mins at 42˚C via heating stage (Instec). Images were acquired in real time under the same conditions to normalize fluorescence readings. Data was analyzed in ImageJ.

4.2.5: Quantification of CD69 levels in Jurkat cell cultures

Jurkat cells expressing CAR and CisCAR constructs were created via lentiviral transduction. $2*10^5$ CAR-expressing Jurkat cells were heat shocked for 42˚C for 15 mins and cultured at 2.5, 5.0, or $7.5*10^6$ cells per mL for 24 hrs in 150 μL RPMI. Cells were stained with αCD69 APC (BioLegend, 310910) for 30 mins then analyzed with BD Accuri flow analyzer.

4.2.6: Isolation and transduction of primary human T cells

Human peripheral blood mononuclear cells were isolated from buffy coats from the San Diego Blood Bank with lymphocyte separation medium (Corning, 25-072-CV). Primary human T cells were isolated using a Pan T Cell Isolation Kit (Milteenyi, 130-096-535). Following isolation, T cells were stimulated with Dynabeads Human T-Expander CD3/CD28 (ThermoFisher, 11141D) at a ratio of 1:1 Dynabeads per T cell. 48 hrs after Dynabead stimulation, cells were transduced on Retronectin-coated (Takara, T100B) plates with concentrated Lentivirus at a multiplicity of infection 5 per construct. 6 days after infection Dynabeads were magnetically removed, T cells were stained with αmouse IgG,$F(ab')_2$ fragment specific antibody (Jackson ImmunoResearch,115-606-072) and FACS sorted with a Sony SH800.

4.2.7: Cytotoxicity assay

K562 and MDA-MB-231 target cell lines were generated through Lentiviral transduction and subsequent sorting with Sony SH800. For cytotoxicity assays, $5.0*10^4$ target cells were co-cultured with T-cells in 150 µL RPMI for 24 hrs. Bioluminescence measurements were taken using the Dual Glo Luciferase Assay kit (Promega, E2920). Cytotoxicity was calculated by taking the percent difference in luminescence of T cells-cultured wells versus luminescence of target cells only.

4.2.8: Statistical analysis

Statistical analysis was performed in Graphpad Prism. P-values were calculated using unpaired one-way ANOVA.

4.3: RESULTS

4.3.1: CD19scFv SynNotch was used to elucidate trends of ligand co-expression

CD19scFv SynNotch (SN) was first used as a tool to quantify and elucidate trends in cis-ligand expression. First, a CD19scFv SynNotch cell line was created in Jurkat cells (Figure 4.1A). Two genetic cassettes were introduced to Jurkat cells: a CD19scFv SynNotch receptor construct and a Nanoluciferase-Cyan Orange Fluorescent Protein (NC3) reporter construct[11]. Upon recognition of CD19 on sender cells, the SN transmembrane domain is cleaved by ADAM metalloprotease and γ-secretase enzymes, releasing a fusion protein of Gal4 DNA-binding domain and VP64 transcriptional activator[12]. The fusion protein then translocates into the cell nucleus and inducibly expresses the NC3 BRET reporter. Compared to a conventional fluorescent reporter, the BRET reporter has the advantage of being detectable via microscopy and luminescence detection assays. Furthermore, this specific BRET reporter is more suitable for in vivo studies for two reasons: it can be chemically induced via Furimizine versus light

stimulation, which has shallow penetration. Also, its long-shifted emission makes it more easily detectable than its constituent Nanoluciferase.

First, SN functionality was verified without any cis-co-expression of CD19 ligand. SN- cells were co-cultured in three conditions: without sender cells, with CD19-negative K562 cells, and with CD19-positive Toledo cells in a 1:1 ratio. After co-culture for 24 hrs, cells were analyzed via microscopy (Figure 4.1B). Quantification of imaging data showed that co-culture with Toledo cells showed significantly higher fluorescence intensity compared to co-cultures with no sender cells and K562 cells (Figure 4.1C). Quantification of co-cultures via bioluminescence readings also produced the same results (Figure 4.1D), demonstrating that the reporter system is robust and quantifiable.

Next, CD19scFv SN cell lines were co-cultured with co-expressed CD19 ligand to explore the effect of ligand co-expression. Truncated CD19 (tCD19) construct was generated, consisting of a constitutive PGK promoter driving expression of CD19 ectodomain and transmembrane domain (minus signaling domain). Cell lines were generated by infecting CD19scFv SN cells with titered amounts of tCD19 lentivirus to create low-tCD19, med-tCD19, and high-tCD19 groups (Figure 4.2A). Anti-CD19 antibody staining verified that these cell lines expressed tCD19 at detectably different levels.

SN cells were then co-cultured with the same groups of sender cells as those in Figure 4.1 and measured via bioluminescence assay. Cis-inhibition was observed in the CD19-positive Toledo cell co-culture (Figure 4.2B). Compared to the no-tCD19 SN control group, med-tCD19 and high-tCD19 SN cells showed significantly diminished SN activation. Similar decreases in activation were also observed in the K562 and no sender co-cultures for the med-tCD19 and high-tCD19 SN cells (Figure 4.2C-D). Surprisingly, the low-tCD19 SN cells displayed

significant activation compared to the rest of the groups. To explore why this might be the case, SN receptor expression was measured in these cells (Figure 4.2E). Compared to the baseline level of SN receptor expression, low-tCD19 group showed much lower levels of receptor expression. Furthermore, med-tCD19 and high-tCD19 groups showed no detectable levels of SN receptor expression. Taken together, these results suggest that co-expression of tCD19 either has the effect of masking SN receptor detection or has already cleaved the receptor prior to co-culture. Also, these results suggest that there is a narrow range of ligand co-expression where cis-activation occurs. Once this range of ligand co-expression is exceeded, cis-inhibition effects take over.

4.3.2: CD19 cis-activation is observed in CAR T cells

The results of the SN experiments suggested that CD19scFv and tCD19 could interact in cis and either activate or inhibit receptor signaling based on tCD19 levels. If this mechanism were to be translated to CAR T cells, significant therapeutic controls could be attained. Thus, we wanted to see whether cis-activation could also be observed in CD19scFv CAR T cells. To explore this question, constitutively expressed tCD19-eGFP and constitutively expressed CD19scFv CAR-mCherry were co-expressed in HEK293T cells via lentiviral transduction (Figure 4.3A). Co-localization was observed between tCD19 and CD19scFv CAR in microscope images (Figure 4.3B). The amount of co-localization clusters also seemed to increase with increasing levels of tCD19 expression. Similar to the SN system, co-localization was also observed in CAR, suggesting that CAR T cells can self-activate via ligand co-expression.

Having established that constitutive tCD19 can interact with CAR and potentially drive activation, adding inducibility to tCD19 expression could help control cytotoxicity and keep CAR activation localized to the tumor. To achieve this, constitutive PGK promoter was replaced

with heat-shock promoter (HSP) (Figure 4.3C). HSP-tCD19 was expressed in Jurkat cells via lentiviral transduction, and cells were heated for 15 mins at 42˚C. tCD19 expression was measured at 0, 1, 3, 6, and 24 hrs after heat shock. (Figure 4.3D). tCD19 expression was maximal at 3 and 6 hrs after heat shock. After 24 hrs, expression level decreased almost back to pre-heat-shock levels. With the kinetics of HSP-tCD19 expression established, interaction with CAR was again imaged in HEK293T cells. Cells were heat-shocked using a heating stage and fluorescence was monitored (Figure 4.3E). Consistent with flow cytometry data, tCD19 was observed three hrs after heat shock. Furthermore, co-localization between tCD19 and CD19scFv CAR was also observed.

To test whether inducible tCD19 could activate CAR, a CD69 assay was performed. A comparison was made between two cell lines, one containing only the CD19scFv CAR, hence dubbed CAR only, and one containing both CD19scFv CAR and heat-inducible CAR construct, hence dubbed CisCAR (Figure 4.3F). To test whether these cells could be activated and whether activation was concentration dependent, they were cultured overnight at different concentrations (0.25 million cells/mL, 0.5 million cells/mL, and 0.75 million cells per mL) (Figure 4.3G). CisCAR shows heat-inducible expression of CD69, indicating that CAR activation is driven by heat shock. As a control, no increase in CD69 expression is observed in the CAR only group between heat-shock and non-heat-shock groups. Also, CD69 levels of CisCAR are the same at each cell concentration, suggesting that CisCAR activation occurs in a concentration-independent manner.

4.3.3: CisCAR can inducibly kill heterogeneous and CAR antigen-less tumors

After establishing that CisCAR can become activated in Jurkat cells, killing assays were performed in T cells. Killing assays were performed against mixtures of antigen positive and

antigen negative tumors and antigen negative only tumors (Figure 4.4A). Construct expression levels were verified in T cells for CAR only and CisCAR groups (Figure 4.4B). Antigen positive and antigen negative cell lines were established in K562 and MDA-MB-2321 cells, by infecting them with tCD19-P2A-FLuc and myc-P2A-RLuc constructs respectively. The orthogonal luciferases allowed for differential detection between antigen positive cytotoxicity and antigen negative cytotoxicity.

First, CisCAR cytotoxicity was tested against a mixture of 10%/90% antigen negative/antigen positive cells. Heat-shocked CisCAR only, 75%/25% CisCAR/CAR, and CAR only groups were tested (Figure 4.4C). Results showed that the mixture of 75% CisCAR/25% CAR was able to significantly kill more antigen negative cells than the 100% CAR only group while still clearing all of the antigen positive cells. Next, CisCAR cytotoxicity was tested against completely antigen negative K562 tumors (Figure 4.4D). Results showed that CisCAR displayed significantly more cytotoxicity than CAR only and was furthermore able to demonstrate heat-inducible killing. CisCAR killing was also tested against MDA-MB-231 cells to test whether inducible killing could be carried over to different cell types (Figure 4.4E). Results indicated that CisCAR cytotoxicity was significantly higher than that of CAR by itself.

4.4: DISCUSSION

Here, we present a novel method to self-activate CD19 CAR through heat-inducible cis-ligand expression. This method is advantageous because it can be universally applied to target any tumor-associated antigen. In addition to demonstrating tumor-specific cytotoxicity, this technology should be safe from an immunogenicity standpoint because it makes use of the already clinically-proven CD19 CAR. Also, the heat-inducibility of cis-activation adds a second layer of control to mitigate off-tumor cytotoxicity. Furthermore, we demonstrate that this method

can be applied across different cell types as well, including hematological K562 cancer cell line and the triple-negative MDA-MB-231 solid tumor breast cancer cell line.

Heat-inducible CisCAR represents a first generation proof of principle design. Although CisCAR T cells were able to demonstrate significantly higher killing compared to that of standard CD19 CAR T-cells, they were still unable to fully eradicate tumors, which precluded further *in vivo* studies. Incomplete killing could be for several reasons. The first is that cis-expression of tCD19 led to T cell-mediated fratricide by either T cells killing tCD19-expressing CisCAR cells in trans or by CisCAR T cells becoming activated and indiscriminately killing tumor cells and other T cells. Another reason could be that T cells were not chemically bound to tumor cells. Although T cells and tumor cells were spun down during co-culture to promote cell-cell contact, lack of target antigen on tumor cells could have prevented the proper formation of immunological synapse. Next generation CisCAR could incorporate additional binding motifs to enhance cell adhesion and cytotoxicity. Although lack of proper adhesion could lead to homing issues for completely antigen negative cells, this should not be an issue for heterogeneous tumors which express both antigen positive and antigen negative cells.

In addition to its clinical potential, the CisCAR system provides valuable scientific insights as well. Cis-inhibition and recently cis-activation have been well-reported in the context of Notch receptors[13–15]. Here, we quantitatively explored how cis-ligand expression functioned in CD19 SynNotch receptors. Those studies clearly demonstrated that both cis-activation and cis-inhibition occurred at different levels of tCD19 expression. We then translated this application from SynNotch to CAR where similar interactions were observed, suggesting that we could couple CAR activation with cis-ligand control. In CAR T cells, microscopy data confirmed that ligand interactions were predominantly occurring in cis rather than trans. Microscopy data also validated the heat-shock promoter induced expression of tCD19 which was later shown to drive T cell activation, confirmed by CD69 assays.

As a relatively new cancer therapeutic, our knowledge of CAR T-cell therapy is constantly expanding, and paradigms are shifting. Previously, the boundary between CAR T-

cells and tumors was understood to be quite rigid; however, we now understand that the boundary is actually quite fluid. Through the process of trogocytosis, CAR T-cells are able to absorb target antigens, which decreases target cell antigen expression and has implications for tumor antigen escape[16]. Furthermore, tumor cells have been reported to absorb CAR receptors, masking their own antigen expression and expanding uncontrollably to fatal outcomes[17]. Thus, CisCAR can act not only as a beneficial clinical tool but also as a model to understand the ever-evolving immune environment.

4.5: FIGURES

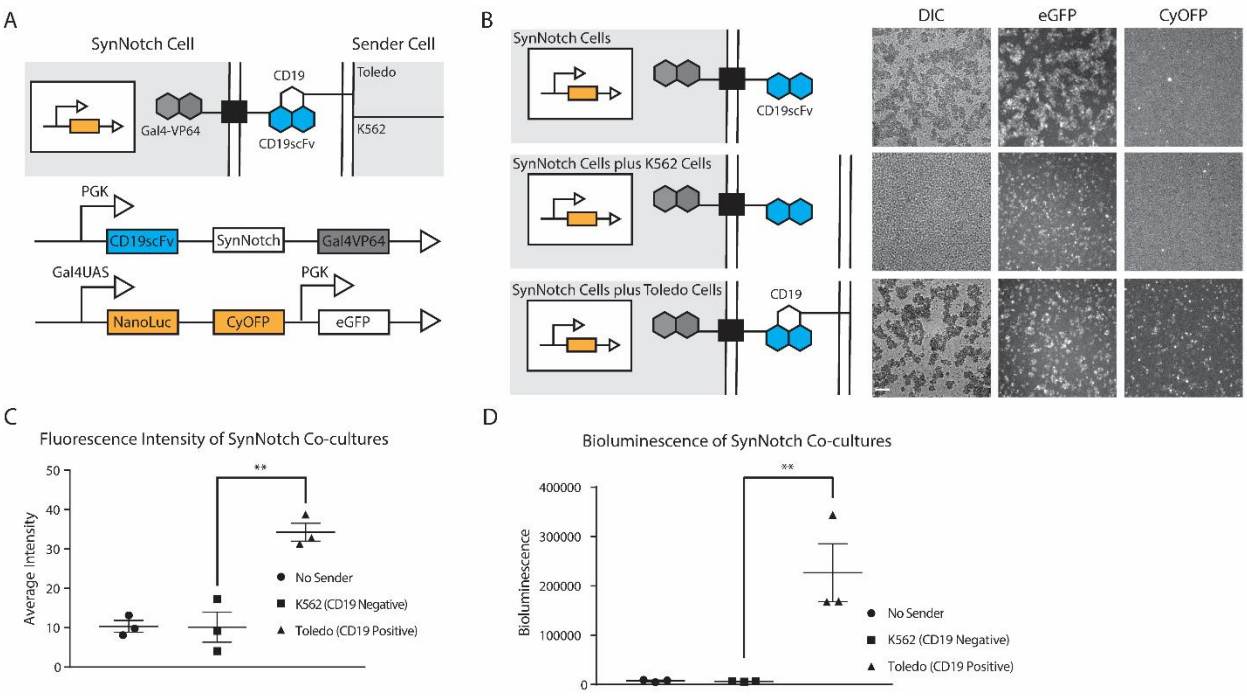

Figure 4.1: CD19-SynNotch expresses reporter on recognition of CD19 on antigen presenting cells

(A) Schematic of SynNotch system with NC3 BRET reporter inserted into the inducible cassette. SynNotch cells recognize CD19 expression of sender cells and express NC3. **(B)** Representative microscopy images demonstrating the functionality of SynNotch in Jurkat cells. Inducible CyOFP is most highly expressed when SynNotch cells were co-cultured with CD19 endogenously expressing Toledo cells. Scale bar is 100 μm. **(C)** Quantification of fluorescence intensity from Figure 4.1B. Toledo co-culture is highest, indicating that SynNotch is functioning properly. **(D)** Bioluminescence measured by nanoluciferase assay. Toledo co-culture is highest, indicating that SynNotch is functioning properly.

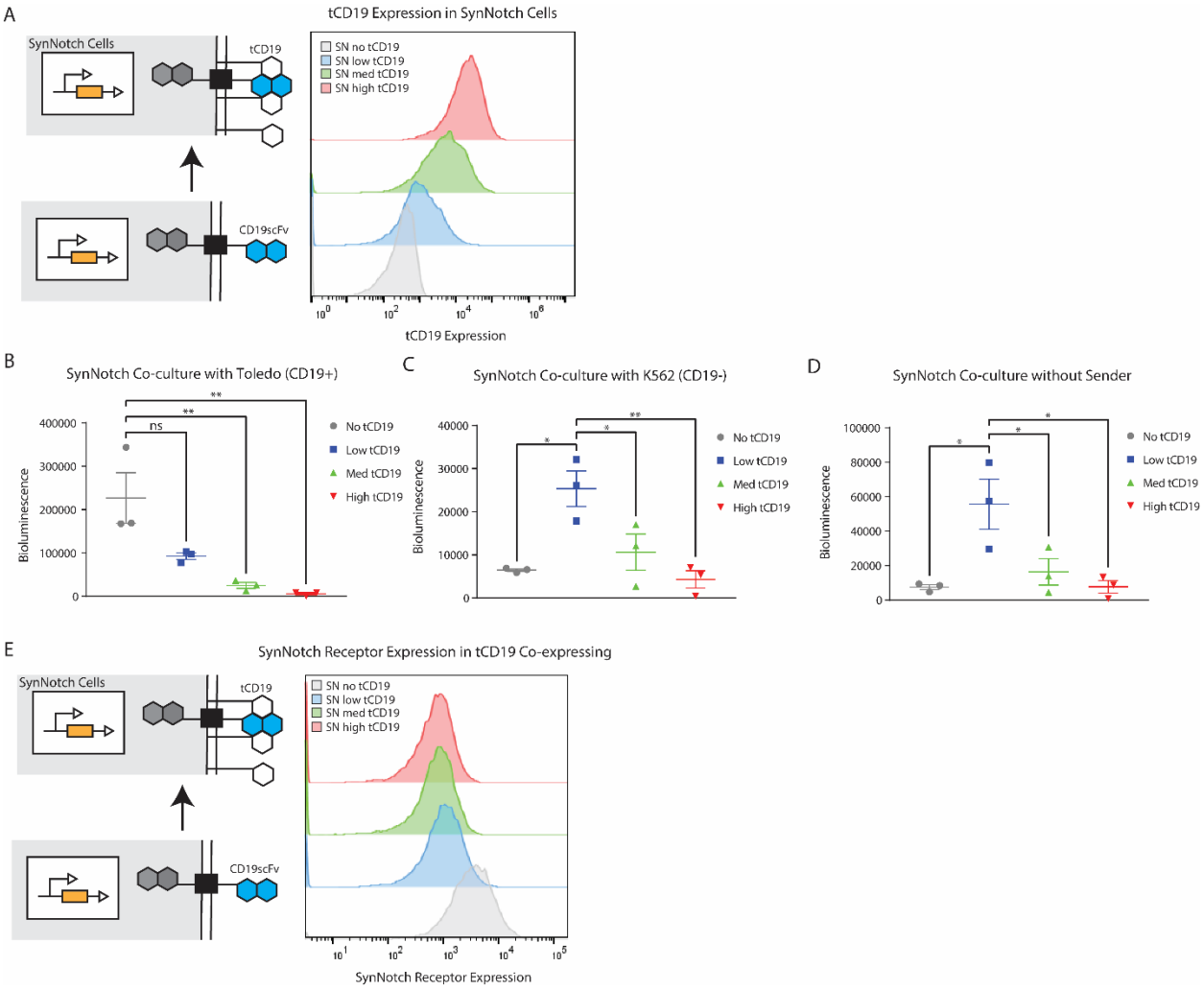

Figure 4.2: SynNotch usage to study tCD19 co-expression in Jurkat cells

(A) Jurkat SynNotch cell lines co-expressing titered amounts of tCD19. **(B)** SynNotch co-culture results with CD19-expressing Toledo cells. **(C)** SynNotch co-culture results with CD19-negative Toledo cells. **(D)** SynNotch co-culture results with no sender cells. **(E)** SynNotch receptor expression in tCD19-expressing cells.

Figure 4.3: tCD19 co-localizes with CD19scFv receptor and activates receptor signaling

(A) Genetic cassettes for co-expression of tCD19 with CD19scFv CAR. **(B)** Imaging results in HEK293T cells. Scale bar is 10 μm. **(C)** Genetic cassette of CD19scFv CAR and heat shock inducible tCD19 constructs. **(D)** Heat shock inducible tCD19 in Jurkat cells. **(E)** Microscopy time-course in HEK293T cells. Scale bar is 10 μm. **(F)** Genetic cassettes for CD19scFv CAR and HSP-inducible tCD19. **(G)** CD69 activation assay in Jurkat cells comparing CisCAR and CAR only cells at different cell concentrations.

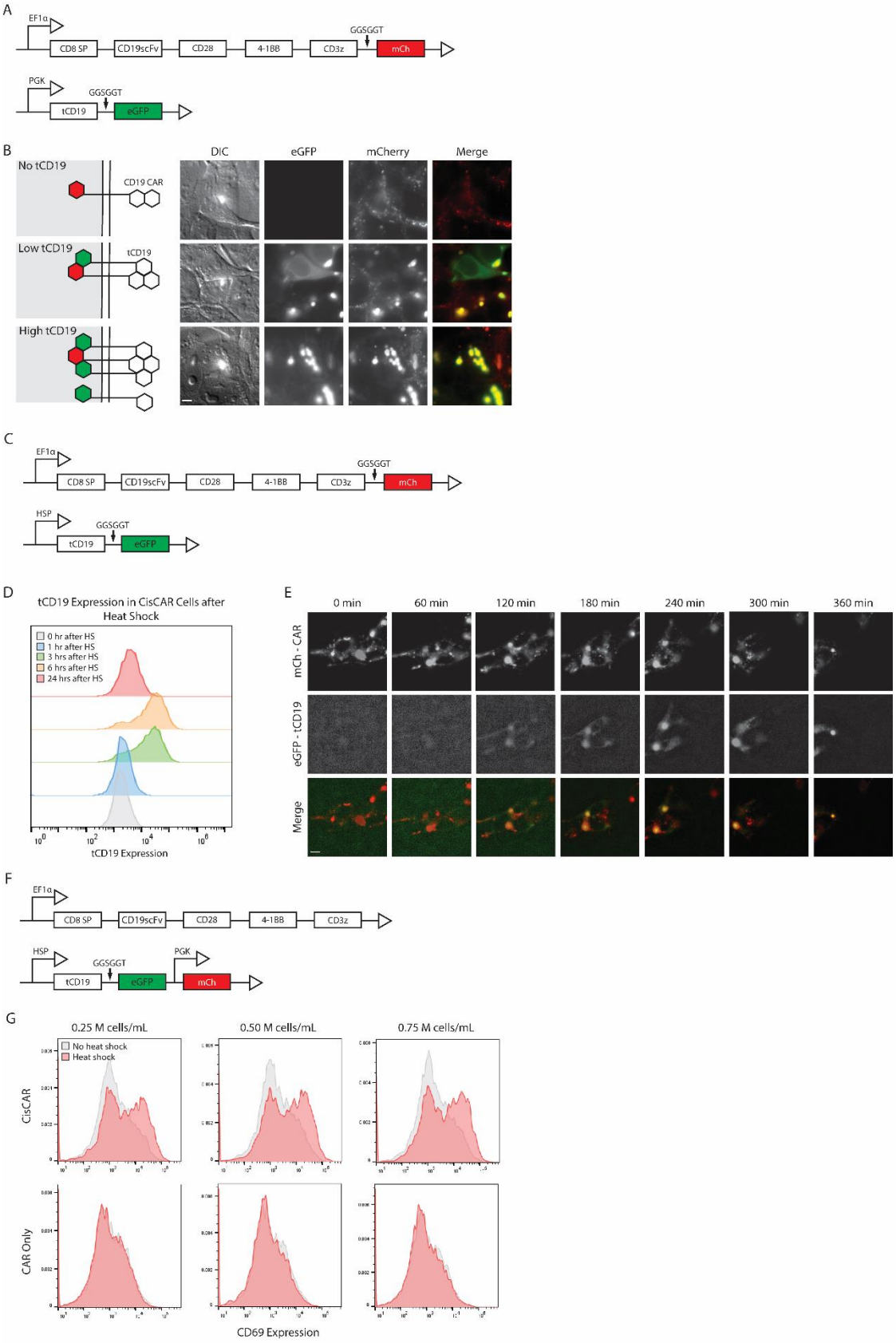
A
EF1α
CD8 SP
CD19scFv
CD28
4-1BB
CD3z
GGSGGT
mCh
PGK
GGSGGT
tCD19
eGFP
B
DIC
eGFP
mCherry
Merge
No tCD19
CD19 CAR
Low tCD19
tCD19
High tCD19
C
EF1α
CD8 SP
CD19scFv
CD28
4-1BB
CD3z
GGSGGT
mCh
HSP
GGSGGT
tCD19
eGFP
D
tCD19 Expression in CisCAR Cells after Heat Shock
0 hr after HS
1 hr after HS
3 hrs after HS
6 hrs after HS
24 hrs after HS
tCD19 Expression
E
0 min
60 min
120 min
180 min
240 min
300 min
360 min
mCh - CAR
eGFP - tCD19
Merge
F
EF1α
CD8 SP
CD19scFv
CD28
4-1BB
CD3z
HSP
GGSGGT
PGK
tCD19
eGFP
mCh
G
0.25 M cells/mL
0.50 M cells/mL
0.75 M cells/mL
No heat shock
Heat shock
CisCAR
CAR Only
CD69 Expression

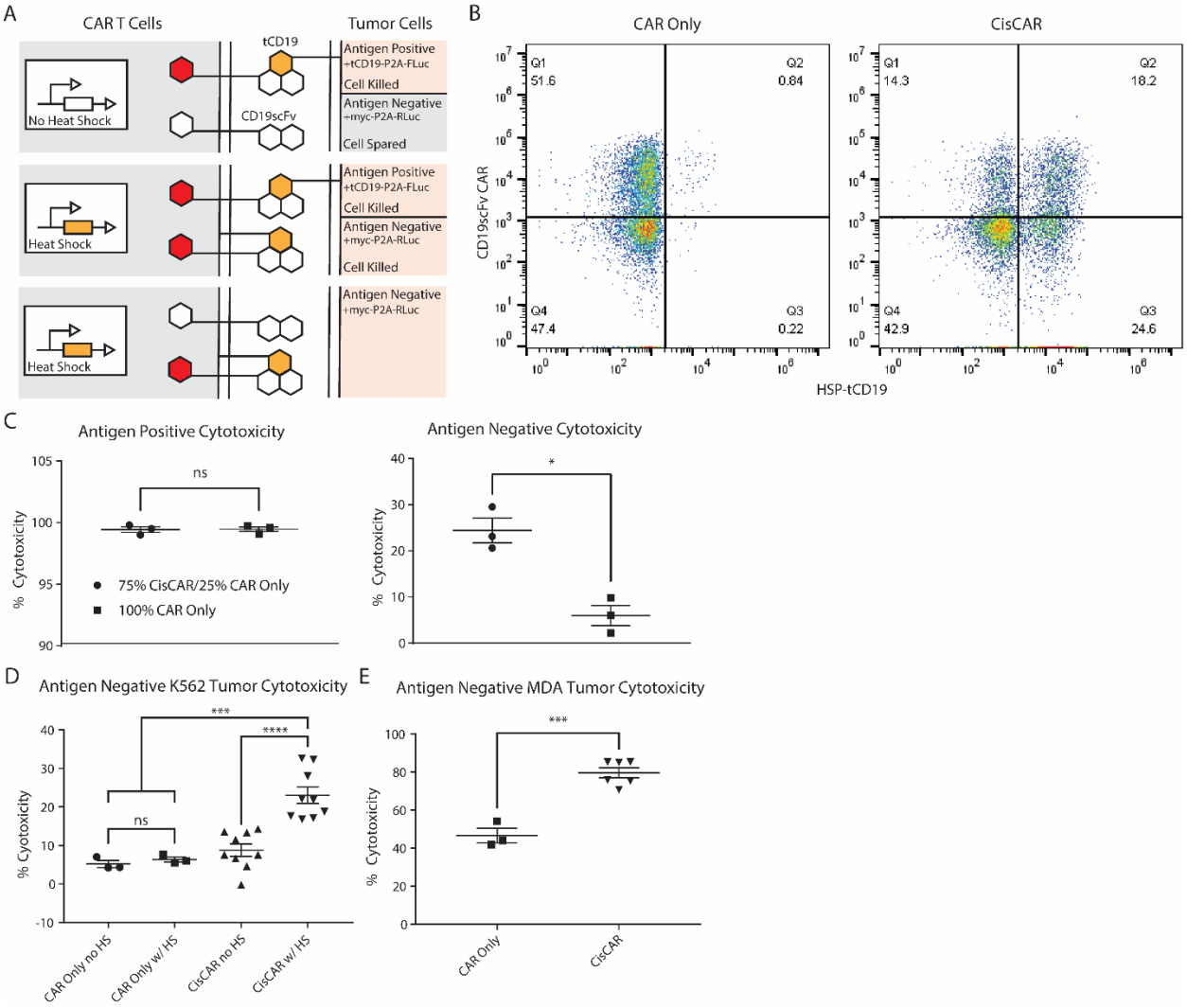

Figure 4.4: Heat-shock inducible CisCAR cytotoxicity assays in primary human T cells

(A) Schematic illustrating how heat-driven expression of tCD19 can inducibly eradicate heterogeneous tumors or completely antigen-negative tumors. **(B)** Expression levels of CD19scFv CAR and HSP-tCD19 constructs in T cells. **(C)** Cytotoxicity assay of CisCAR co-cultured with K562 cells (90% antigen negative/10% antigen positive). E:T ratio is 5:1. Heat shock is performed at 42˚C for 15 min. **(D)** Cytotoxicity assay of CisCAR co-cultured with antigen negative K562 cells. E:T ratio is 5:1. Heat shock is performed at 42˚C for 15 min. **(E)** Cytotoxicity assay of CisCAR co-cultured with antigen negative MDA-MB-231 cells. E:T ratio is 5:1. Heat shock is performed at 42˚C for 15 min.

ACKNOWLEDGEMENTS

Chapter 4, in full is currently being prepared for submission of the material. Man, Chi-Wei; Wu, Yiqian; Liu, Longwei; Hashimoto, Matthew; Mamaril, Anthony; Wang, Yingxiao. "Inducible cis activation drives CAR T cell function against heterogeneous and antigen negative tumors". The dissertation author was the primary researcher and author of this paper.

This work was supported in part by grants from NIH R01 CA262815, EB029122, R35 GM140929, R01 HL121365, and HD107206 (Y.W.).

REFERENCES

1. Brentjens, R. J., Davila, M. L., Riviere, I., Park, J., Wang, X., Cowell, L. G., Bartido, S., Stefanski, J., Taylor, C., Olszewska, M., Borquez-Ojeda, O., Qu, J., Wasielewska, T., He, Q., Bernal, Y., Rijo, I. V., Hedvat, C., Kobos, R., Curran, K., *et al.* CD19-targeted T cells rapidly induce molecular remissions in adults with chemotherapy-refractory acute lymphoblastic leukemia. *Sci. Transl. Med.* **5**, (2013).

2. Sadelain, M., Brentjens, R. & Rivière, I. The basic principles of chimeric antigen receptor design. *Cancer Discov.* **3**, 388–398 (2013).

3. Pulè, M. A., Straathof, K. C., Dotti, G., Heslop, H. E., Rooney, C. M. & Brenner, M. K. A chimeric T cell antigen receptor that augments cytokine release and supports clonal expansion of primary human T cells. *Mol. Ther.* **12**, 933–941 (2005).

4. Mullard, A. FDA approves first CAR T therapy. *Nat. Rev. Drug Discov.* **16**, 669 (2017).

5. Orlando, E. J., Han, X., Tribouley, C., Wood, P. A., Leary, R. J., Riester, M., Levine, J. E., Qayed, M., Grupp, S. A., Boyer, M., De Moerloose, B., Nemecek, E. R., Bittencourt, H., Hiramatsu, H., Buechner, J., Davies, S. M., Verneris, M. R., Nguyen, K., Brogdon, J. L., *et al.* Genetic mechanisms of target antigen loss in CAR19 therapy of acute lymphoblastic leukemia. *Nat. Med.* **24**, 1504–1506 (2018).

6. Zhang, W. Y., Wang, Y., Guo, Y. L., Dai, H. R., Yang, Q. M., Zhang, Y. J., Zhang, Y., Chen, M. X., Wang, C. M., Feng, K. C., Li, S. X., Liu, Y., Shi, F. X., Luo, C. & Han, W. D. Treatment of cd20-directed chimeric antigen receptor-modified t cells in patients with relapsed or refractory b-cell non-hodgkin lymphoma: An early phase iia trial report. *Signal Transduct. Target. Ther.* **1**, 1–9 (2016).

7. Fry, T. J., Shah, N. N., Orentas, R. J., Stetler-Stevenson, M., Yuan, C. M., Ramakrishna, S., Wolters, P., Martin, S., Delbrook, C., Yates, B., Shalabi, H., Fountaine, T. J., Shern, J. F., Majzner, R. G., Stroncek, D. F., Sabatino, M., Feng, Y., Dimitrov, D. S., Zhang, L., *et*

al. CD22-targeted CAR T cells induce remission in B-ALL that is naive or resistant to CD19-targeted CAR immunotherapy. *Nat. Med.* **24**, 20–28 (2018).

8. Hawkins, E. R., D'souza, R. R. & Klampatsa, A. Armored CAR T-cells: The next chapter in T-cell cancer immunotherapy. *Biol. Targets Ther.* **15**, 95–105 (2021).

9. Park, A. K., Fong, Y., Kim, S. I., Yang, J., Murad, J. P., Lu, J., Jeang, B., Chang, W. C., Chen, N. G., Thomas, S. H., Forman, S. J. & Priceman, S. J. Effective combination immunotherapy using oncolytic viruses to deliver CAR targets to solid tumors. *Sci. Transl. Med.* **12**, (2020).

10. Wu, Y., Liu, Y., Huang, Z., Wang, X., Jin, Z., Li, J., Limsakul, P., Zhu, L., Allen, M., Pan, Y., Bussell, R., Jacobson, A., Liu, T., Chien, S. & Wang, Y. Control of the activity of CAR-T cells within tumours via focused ultrasound. *Nat. Biomed. Eng.* **5**, 1336–1347 (2021).

11. Chu, J., Oh, Y., Sens, A., Ataie, N., Dana, H., Macklin, J. J., Laviv, T., Welf, E. S., Dean, K. M., Zhang, F., Kim, B. B., Tang, C. T., Hu, M., Baird, M. A., Davidson, M. W., Kay, M. A., Fiolka, R., Yasuda, R., Kim, D. S., *et al.* A bright cyan-excitable orange fluorescent protein facilitates dual-emission microscopy and enhances bioluminescence imaging in vivo. *Nat. Biotechnol.* **34**, 760–767 (2016).

12. Morsut, L., Roybal, K. T., Xiong, X., Gordley, R. M., Coyle, S. M., Thomson, M. & Lim, W. A. Engineering Customized Cell Sensing and Response Behaviors Using Synthetic Notch Receptors. *Cell* **164**, 780–791 (2016).

13. Nandagopal, N., Santat, L. A. & Elowitz, M. B. Cis-activation in the Notch signaling pathway. *Elife* **8**, 1–34 (2019).

14. Del Álamo, D., Rouault, H. & Schweisguth, F. Mechanism and significance of cis-inhibition in notch signalling. *Curr. Biol.* **21**, 40–47 (2011).

15. Benjamin Purow. *Notch Signaling in Embryology and Cancer*. *Adv Exp Med Biol* vol. 727 (2012).

16. Hamieh, M., Dobrin, A., Cabriolu, A., van der Stegen, S. J. C., Giavridis, T., Mansilla-Soto, J., Eyquem, J., Zhao, Z., Whitlock, B. M., Miele, M. M., Li, Z., Cunanan, K. M., Huse, M., Hendrickson, R. C., Wang, X., Rivière, I. & Sadelain, M. CAR T cell trogocytosis and cooperative killing regulate tumour antigen escape. *Nature* **568**, 112–116 (2019).

17. Ruella, M., Xu, J., Barrett, D. M., Fraietta, J. A., Reich, T. J., Ambrose, D. E., Klichinsky, M., Shestova, O., Patel, P. R., Kulikovskaya, I., Nazimuddin, F., Bhoj, V. G., Orlando, E. J., Fry, T. J., Bitter, H., Maude, S. L., Levine, B. L., Nobles, C. L., Bushman, F. D., *et al.* Induction of resistance to chimeric antigen receptor T cell therapy by transduction of a single leukemic B cell. *Nat. Med.* **24**, 1499–1503 (2018).

CHAPTER 5

CONCLUSION

5.1: SUMMARY OF DISSERTATION

The overarching theme of this dissertation was to utilize molecular and cellular engineering to expand the application of CAR T cell therapy. Though extremely effective in treating hematological malignances, CAR T cell therapy has struggled to translate its success to other cancer types, especially solid tumors. Accordingly, this dissertation sought to add tools to the CAR arsenal to help it overcome resistance to treatment. More specifically, CD19-SynNotch PDbody-CAR tackled the problem of PD-L1-mediated immune checkpoint inhibition, and heat-inducible CisCAR tackled the problem of antigen escape.

In Chapter 2 (Directed Evolution of PDbody, a Programmed Death-Ligand 1-Targeting Monobody), directed evolution was used to engineer PDbody from Mb-G9. First, the monobody display platform was established in EBY100 yeast cells. Next, a PD-L1 binding nanobody loop was inserted into the FG loop of Mb-G9 to increase baseline PD-L1 binding and create Mb-035. Molecular dynamics simulations were then performed on the FG loop of Mb-035 to determine which residues were the most “optimizable” for PD-L1 binding. Based off of these molecular dynamics simulations, site saturated mutagenesis was performed on the predicted residues to create a library. FACS was then used to screen this library, resulting in isolation of the Mb-FG-EVO clone. Another subsequent round of site-saturated mutagenesis and FACS screening was then performed on the BC loop of Mb-FG-EVO to further improve PD-L1 binding. PDbody was the result of this round of screening. Finally, yeast staining verified the improved PD-L1 binding of PDbody, approving it for further application as a CAR.

Having generated PDbody via directed evolution, Chapter 3 (Application of CD19-SynNotch PDbody-CAR) sought to utilize it as a CAR to target PD-L1 for cancer treatment. First, PDbody was subcloned into a 3rd generation CAR to create PDbody-CAR, and its PD-L1 binding was verified. Next, PDbody-CAR was combined with CD19-SynNotch to make its expression inducible and mitigate off-tumor toxicity. This combined system was called CD19-SynNotch PDbody-CAR. This system was then transduced into primary human T cells which demonstrated complete eradication of a PD-L1 positive triple negative breast cancer model. Following the *in vitro* success of CD19-SynNotch PDbody-CAR T cells, it was tested *in vivo* in bilateral tumor mouse models. In two separate experiments, CD19-SynNotch PDbody-CAR T cells demonstrated that they could significantly slow tumor growth compared to appropriate tumor controls.

In Chapter 4 (Inducible Cis Activation Drives CAR T Cell Function Against Heterogeneous and Antigen Negative Tumors), a heat-inducible CisCAR system was generated to help CAR T cells overcome tumor antigen escape. First, CD19-SynNotch was used to probe the effects of cis-ligand (tCD19) expression in Jurkat cells. Results of these experiments demonstrated that at low tCD19 levels, SynNotch activation was elevated, suggesting a mechanism of cis activation. Next, cis-ligand and receptor co-localization were observed in CAR T cells via microscopy. tCD19 expression was then made heat shock inducible by subcloning an upstream heat shock promoter. A CD69 assay then proved that CAR activation could be coupled to heat shock. The combination of CD19-CAR with heat shock driven tCD19 was subsequently dubbed heat-inducible CisCAR, which was then transduced into primary human T cells and tested against tumor antigen escape models with varying levels of antigen negativity. These killing assays revealed a significant improvement in tumor killing compared to CAR only cells.

5.2: FUTURE WORK

In Chapters 2 and 3, PDbody was engineered to bind to PD-L1 and then applied as a PD-L1 targeting CAR. Interestingly during the engineering of PDbody, its PD-L1 binding was observed to be improved in acidic pH's. In the context of CAR T cell therapy, this could make the PDbody-CAR more specific to the local tumor microenvironment because it is well reported that the local tumor microenvironment is more acidic. While briefly touched upon in this dissertation, the acidic-targeting nature of PDbody-CAR could certainly be further studied in future tumor models. An acid-favoring CAR binder has the potential to help CAR T cells target solid tumors.

During *in vivo* tests, CD19-SynNotch PDbody-CAR was able to suppress tumor growth in mouse models but unable to fully eliminate tumors. Likely, this is due to the moderate affinity of PDbody (4.75 μM) for PD-L1. While moderate affinity has proven beneficial to reduce off-target toxicity, the tradeoff is that efficacy can be harmed. Future studies could focus on improving the binding affinity of PDbody towards PD-L1 or even changing the 3rd generation CAR into a 4th generation "armored" CAR to help improve efficacy. These could both make PDbody-CAR more effective at combating the immunosuppressive tumor microenvironment.

In Chapter 4, a novel CAR design was developed to help combat tumor antigen escape: heat-inducible CisCAR. Although efficacy was demonstrated *in vitro* with primary human T cells, the difference was not large enough to be carried on to *in vivo* studies. Future studies could focus on improving the killing efficiency of heat-inducible CisCAR by perhaps introducing additional adhesion molecules. This could improve cell-cell interaction from a molecular standpoint and as a result improve killing. Once complete *in vitro* killing has been achieved, *in*

vivo studies can be performed using high intensity focused ultrasound to generate heat and expand heat-inducible CisCAR to more clinically relevant models.